2018

Modeling Alzheimer's Disease in Induced Pluripotent Stem Cells

Andrew Gregg

MODELING ALZHEIMER'S DISEASE IN INDUCED PLURIPOTENT STEM CELLS

A Thesis Presented to the Faculty of

The Rockefeller University

in Partial Fulfillment of the Requirements for

The degree of Doctor of Philosophy

by

Andrew Gregg

June 2018

MODELING ALZHEIMER'S DISEASE IN INDUCED PLURIPOTENT STEM CELLS

Andrew Gregg, Ph.D.

The Rockefeller University 2018

Alzheimer's disease (AD) is the most common cause of dementia worldwide, and is now the 5th leading cause of death in the United States. The pathologic hallmarks of AD include the deposition of extracellular plaques of aggregated amyloid-β (Aβ) and intracellular neurofibrillary tangles of tau aggregates (NFTs). Autosomal dominant inheritance of AD has been attributed to genetic mutations in three key genes: amyloid precursor protein (*APP*), presenilin-1 (*PSEN1*), and presenilin-2 (*PSEN-2*). Together, these pathologic findings and genetics provided the framework for the amyloid cascade hypothesis, which states that Aβ deposition is a necessary, early event that is upstream of the formation of NFTs, and is causative of AD.

Despite this seminal work, the mechanisms underlying the clinical progression of AD is still poorly understood. This gap in our knowledge is due, in large part, to the lack of appropriate AD disease models. Specifically, rodent models of human neurodegenerative disease fail to completely recapitulate disease phenotypes. In the body of work that follows, we utilized recent advances in induced pluripotent stem cell (iPSC) and genome editing technologies to investigate two

separate AD disease mechanisms: tau spreading and Aβ production in familial AD (FAD) *PSEN*1 mutants.

Using TALENs, we generated a transgenic donor iPSC line that harbors a transgene for inducing the expression of fluorescently tagged tau protein and a recipient iPSC line that expresses membrane anchored YFP. These cell lines, when differentiated into human cortical neurons and cultured together, demonstrated that tau is transferred between neurons. However, similar protein spreading was observed for the control cell line expressing only mCherry, suggesting that tau did not transfer by a unique mechanism in this culture system.

With the hope of revealing new insights into AD mechanisms, we next used CRISPR/Cas9 to produce a series of isogenic iPSC lines that harbor discrete FAD *PSEN1* mutations. These mutations in *PSEN1* alter the relative amount of Aβ peptides, specifically increasing the ratio of Aβ 42:40 and Aβ 42:38. Our results demonstrate that each mutation causes a reduction in the levels of both Aβ40 and Aβ38, as well as an increase in Aβ42. These results support the model that FAD *PSEN1* mutations cause a loss of protein function, in that PSEN1 cannot properly process Aβ42 into smaller, less aggregation prone peptides. Consistent with this, we found that C-terminal fragments of APP (β-CTF) accumulate in neurons with homozygous FAD mutations in PSEN1. Additionally, we also observed defects in the processing of other γ-secretase substrates such as N-Cadherin. Intriguingly, the Aβ 42:40 ratio and Aβ40 levels correlated with disease onset in heterozygous mutants,

while Aβ42 levels correlated with disease onset in homozygous mutants, suggesting that these values could be predictive of disease progression in culture.

These results are all consistent with a partial loss in PSEN1 function, extending our current understanding of how FAD *PSEN1* mutations affect PSEN1 function, and, perhaps more importantly, identifying a mechanistic perturbation that is common to the tested FAD mutations. Taken together, PSEN1 dysfunction results in production of larger, aggregation prone Aβ peptides, as well as CTFs. These insights may be important for ultimately understanding how these mutations cause FAD, which will be critical for developing effective therapeutics that slow or prevent progression of this devastating disease

To my wife and family for constant support and always believing in me.

Acknowledgements

There are many people that need to be thanked, but first and foremost is Marc for his guidance and mentorship throughout the course of my thesis work. In fact, Marc's support began well before my graduate studies when I was an intern in his lab at Genentech and during the transition to Rockefeller. During that time, it became apparent that his lab was a special place, due in large part to his tremendous intellect and scientific rigor. As a result, I found myself drawn back to his lab as a medical student, and eventually decided to continue to pursue my research in his lab as an MD-PhD student. All along the way, Marc was completely supportive of me and my endeavors, and I will always be grateful for everything he has done for me, both scientifically and personally.

One of Marc's many talents' is the ability to attract and hire amazing people. The people in Marc's lab are truly phenomenal, and made coming to work every day joyful. I especially want to thank Olav Olsen for not only helping set up an amazing culture and environment, but also for his guidance in the later stages of my thesis work. I would also like to thank Kim, Dave, Zhuhao, Nick, Yuya, Nico, and Jing for their help and advice over the last four years. Thank you to my fellow graduate students, Jason, Deanna, Shaun, Eliza and Ross, for always listening, advising, and commiserating when necessary.

I have to give a special thank you to the iPS team in the lab. Thank you, Dominik, for your leadership and guidance. Without your rigorous and detailed

establishment of the iPS system in the lab, and amazing teaching, my thesis research would not have been possible. Dylan, thank you so much for being such an amazing fellow graduate student to work with. The iPS system is difficult, fickle, and sometimes downright cruel, but I'm glad I had you to help me through it. And towards the end of my thesis when our projects began to collide, I couldn't have asked for a better colleague. To Mike and Antonia, without your help none of this would have come to fruition. Thank you for your tireless work.

I would also like to thank the Tri-Institutional MD-PhD Program, especially Olaf, Jochen, and Ruthie. Thank you for accepting me as a transfer student from the medical school into the program. Your guidance and endless support has been invaluable, and I look forward to the years ahead.

Thank you to my committee, David Eliezer, Shai Shaham, and Sandy Simon, for all of your insight and advice as my projects evolved over the last four years. I could not have asked for a better group of scientists to help me along the way.

I would also like to thank my family, David, Lee, and Sarah for their endless support and love over the last four years. It has been a long and winding path to where I am now, and you never ceased supporting me.

Finally, I would like to thank my wife, Ashley. The ups and downs of graduate school are a shared experience between husband and wife, and I couldn't have asked for a better partner to go through it with. Thank you for helping me keep things

in perspective. I could not have done any of this without your love and support, and I cannot wait to see what the next chapter in our lives has in store.

Table of Contents

List of Figures

List of Tables

List of Abbreviations

3x-Tg	Triple-transgenic mouse
AAVS1	Adeno-associated virus integration site 1
Ab	Amyloid-b
AD	Alzheimer's disease
AICD	APP intracellular domain
Aph1	Anterior Pharynx 1
APOE	Apolipoprotein E
APP	Amyloid Precursor Protein
APPswe	APP Swedish mutation
attP	Phage attachment site
α-CTF	α-C-terminal fragment of APP
b-CTF	β-C-terminal fragment of APP
BACE	β-secretase
CFP	Cerulean Fluorescent Protein
CJD	Crutzfeld-Jacob disease
CNV	Copy-number variant
CRISPR	Clustered regularly interspaced short palindromic repeat
DICE	Dual cassette integrase exchange
DIV	Day in vitro
DRG	Dorsal root ganglion
DS	Downs Syndrome
DSB	Double stranded break
ECL	Electrochemiluminescent
EIPA	5-N-ethyl-N-isopropyl-amiloride
FACS	Fluorescence activated cell sorting
FAD	Familial Alzheimer's disease
FRET	Fluorescence resonance energy transfer
FTD	Frontotemporal dementia
gDNA	Genomic DNA
GFP	Green Fluorescent Protein
gRNA	Guide RNA
GWAS	Genome-wide association studies
HDR	Homology directed repair

HEK293T	Human Embryonic Kidney 293T cell line
HSPG	Heparan sulfate proteoglycan
I-CLiP	Intramembrane cleaving protease
Indel	Insertion or deletion
iPSC	Induced pluripotent stem cell
MAP	Microtubule Associated Proteins
MAPT	Microtubule Associated Protein Tau
MEF	Mouse embryonic fibroblast
memYFP	Membrane anchored YFP
MOI	Multiplicity of infection
NCT	Nicastrin
NEHJ	Non-homologus end joining
NFT	Neurofibrillary tangles
NICD	Notch intracellular domain
NPC	Neural precursor cell
NTF	N-terminal fragment
PAM	Proto-spacer adjacent motif
PCR	Polymerase chain reaction
PEN2	Presenilin Enhancer 2
PrP	Prion Protein
PSEN-2	Presenilin-2
PSEN1	Presenilin-1
RD	Repeat domains
RFLP	Restriction fragment length polymorphism
SA	Splice acceptor
sAPPβ	Soluble APPβ
sAPPα	Soluble APPα
ssODN	Single stranded oligo DNA nucleotide
TALEN	Transcription activator-like effector nuclease
TRE	Tetracycline response element
YFP	Yellow Fluorescent Protein

CHAPTER 1: INTRODUCTION

Rationale for the following studies

In 1907, German psychiatrist and neuropathologist, Alois Alzheimer, detailed the case of a 51 year-old woman in a Frankfurt mental health institution experiencing rapid memory loss and behavioral disturbances (Alzheimer, 1907; Stelzmann et al., 1995). Upon autopsy, he noted that there were numerous “minute miliary foci” throughout the cortex caused by the “deposition of a special substance” (Alzheimer, 1907). More than a century later, our understanding of Alzheimer’s disease (AD) has seen immense progress. However, AD remains puzzling, as its etiology, pathogenesis, and cure are still avidly pursued.

AD is the most common form of neurodegenerative dementia worldwide. For several decades we have understood that AD is defined by the presence of extracellular plaques consisting primarily of amyloid-beta (Aβ) (Tanzi et al., 1987), and intracellular neurofibrillary tangles (NFTs) consisting of hyperphosphorylated tau protein (Grundke-Iqbal et al., 1986; Wischik et al., 1988). While the vast majority of AD is sporadic, with no underlying genetic cause, families have been identified that carry autosomal dominant mutations in one of three genes, amyloid precursor protein (*APP*) (Goate et al., 1991; Hendriks et al., 1992; Janssen et al., 2003; Mullan et al., 1992; Peacock et al., 1993), Presenilin-1 (*PSEN1*) (George-Hyslop et al., 1992; Schellenberg et al., 1992; Van Broeckhoven et al., 1992), and Presenilin-2

(*PSEN2*) (Rogaev et al., 1995), that cause FAD. These mutations are all involved in the accumulation of Aβ, highlighting the central role of APP processing in the pathogenesis of AD.

There are many models of AD, including rodents, invertebrates, and *in vitro* cell culture (Götz and Ittner, 2008; Weggen and Beher, 2012). However, all of these models fail to completely recapitulate disease phenotypes. Even the best *in vivo* models that come close to mimicking the disease still require massive overexpression of transgenes, and expression of multiple transgenes, in order to obtain measurable results. The failures of these models are likely attributed to the fact that AD is a disease of aging, and restricted to humans, making it difficult to model in other species that don't develop the disease *de novo* or live long enough for the disease to develop (age of onset is over 20 years for even the most aggressive FAD mutations). Unfortunately, cell lines of human cortical neurons, the cells primarily affected by AD, simply do not exist as they are post-mitotic, making the disease difficult to replicate *in vitro*.

Fortunately, the advent of the induced pluripotent stem cell (iPSC) system brought with it the possibility to generate better models of AD (Takahashi and Yamanaka, 2006). iPSCs are self-renewing stem cells derived from somatic cells, such as human fibroblasts, that can differentiate into any type of cell or tissue. Thus, iPSCs hold the potential of providing an inexhaustible source of human cortical neurons. Together with the discovery and application of recent advances in genome

editing, namely the transcription activator-like effector nuclease (TALEN) system and the clustered regularly interspaced short palindromic repeat (CRISPR) system, IPSCs provide an opportunity to generate transgenic, knock-in, and knock-out human neurons in a systematic way. As such, the focus of this work was centered around generating AD models in iPSCs to study two different mechanisms of AD pathogenesis: tau propagation and aggregation, and the mechanism of APP processing in isogenic FAD mutants.

AD epidemiology and clinical presentation

Dementia is classified as a syndrome with many causes, including AD, frontotemporal dementia (FTD), vascular or multi-infarct dementia, Parkinson's disease, vitamin deficiency, and many more. The symptoms of dementia often involve loss of memory, language, problem solving, and personal independence. As the most common form of dementia, AD affects 5.5 million Americans and some 40 million people worldwide (Alzheimer's Association, 2017; Scheltens et al., 2016). Age is the biggest risk factor for AD, as it affects one in 10 people over the age of 65, and one in three over the age of 85 years old (Alzheimer's Association, 2017). As modern medicine continues to advance, human longevity concomitantly increases. As such, the proportion of our population over the age of 65 is steadily increasing, and is expected to rapidly expand in the coming decades as the first members of the baby boom generation turned 70 in 2016 (Alzheimer's Association,

2017). As a result, it is estimated that the number of people with AD will roughly triple by 2050 to almost 14 million Americans (Alzheimer's Association, 2017). Importantly, AD is the only disease in the list of top 10 causes of death that cannot be prevented or even slowed, as no disease modifying therapies have been approved to date, and perhaps more importantly, no clinical trials have shown even a hint of beneficial clinical effects. Therefore the financial burden of AD will continue to rise, from an estimated $259 billion in 2017, to an estimated $1.1 trillion in 2050, if effective therapies are not discovered (Alzheimer's Association, 2017).

The clinical manifestations of AD are numerous and can vary from patient to patient. The typical presentation of AD is the insidious onset of memory loss in elderly patients over the age of 65, usually described as deficits in the ability to learn and make new memories. The disease then progresses, without pause, to impair executive function, language, and visuoconstructive abilities (i.e. the ability to organize spatial information), impairing activities of daily living and requiring round the clock care (American Psychiatric Association, 2013). In the final stages of the disease, motor control is also impaired, resulting in gait disturbances, dysphagia and incontinence, leaving the patient bedbound and completely incapable of taking care of themselves. Finally, the most common cause of death in these patients is due to aspiration and subsequent pneumonia.

Unfortunately, many of the symptoms of AD are shared among other neurocognitive disorders, such as Lewy body dementia and FTD. In addition, vitamin

B12 deficiency can present with similar symptoms. Therefore, an AD diagnosis requires a careful recounting of the patient's medical history obtained from the patient, family and/or care givers to first rule out all other etiologies, making AD a diagnosis of exclusion (American Psychiatric Association, 2013). But even with history, physical and neurologic exams, AD can only be diagnosed as "probable" or "possible" in the clinical setting; post-mortem analysis is required to definitively diagnose AD based on the presence of distinct neuropathological features.

Neuropathology of AD: Aβ and tau

AD is defined by the presence of key neuropathological findings, namely global brain atrophy, synapse loss, extracellular plaques composed of Aβ (Tanzi et al., 1987), and intracellular tangles of tau (Grundke-Iqbal et al., 1986; Wischik et al., 1988). Aβ is derived from a series of cleavages of its precursor protein, APP (**Figure 1.1**). APP is a ubiquitously expressed, single pass transmembrane protein that is initially cleaved by either the metalloprotease α-secretase, or the aspartyl protease β-secretase (BACE). Initial ectodomain shedding of APP by α-secretase commits APP towards the non-amyloidogenic pathway, as the ultimate products are soluble APPα (sAPPα) and P3, a soluble non-toxic byproduct of γ-secretase cleavage of the α-C-terminal fragment (α-CTF). On the other hand, initial cleavage by BACE commits APP to the generation of Aβ.

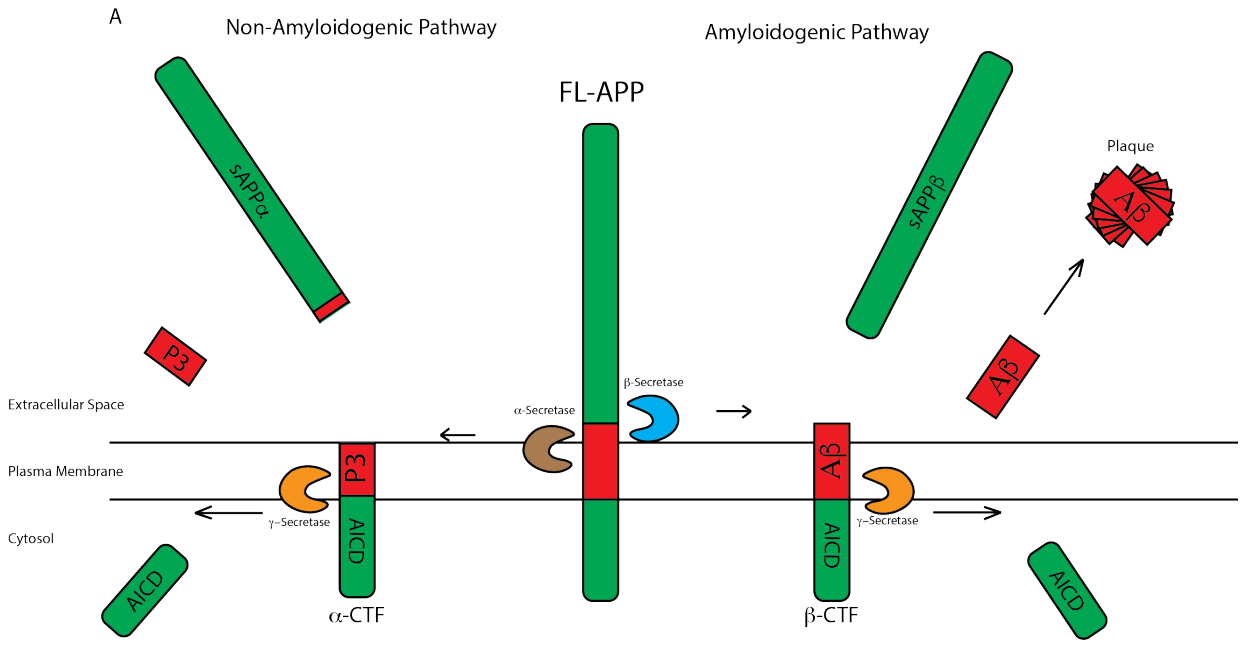

Figure 1.1 Processing of APP. APP is a single pass transmembrane protein that undergoes a series of catalytic cleavages. In the non-amyloidogenic pathway, APP is initially cleaved by α-secretase, yielding sAPPα and α-CTF. γ-secretase then cleaves the α-CTF to release the AICD and the soluble P3 fragment. The amyloidogenic pathway is initiated by cleavage of APP by BACE, producing sAPPβ and β-CTF. γ-secretase then utilizes the same mechanism used in the non-amyloidogenic pathway to produce the AICD and Aβ, which under pathogenic conditions aggregates and deposits as Aβ plaques.

Cleavage of APP by BACE generates soluble APP-β (sAPPβ) and a β-C-terminal fragment (β-CTF). Similar to α-CTF, β-CTF subsequently undergoes intramembranous proteolytic cleavage by γ-secretase to release the APP intracellular domain (AICD) within the cell, and Aβ fragments of various lengths into the extracellular space (**Figure 1.2**). γ-secretase is a tetrameric protein complex

composed of a 1:1:1:1 ratio of the catalytic subunit, PSEN1 or PSEN2, nicastrin (NCT), anterior pharynx 1 (Aph1), and presenilin enhancer 2 (PEN2). γ-secretase normally cleaves β-CTF with an initial endopeptidase cleavage between amino acids 50/49 or amino acids 49/48, releasing an AICD of two different lengths. γ-secretase then performs several successive tri- or tetra-peptide carboxypeptidase cleavages of the Aβ protein fragment to ultimately yield either Aβ of 38 (Aβ38) or 40 (Aβ40) amino acids (Takami et al., 2009). Normally, Aβ is released as these shorter, soluble fragments, with Aβ40 being the most predominant (Rogaev et al., 1995; Scheuner et al., 1996; Selkoe, 1996). Longer forms of Aβ, like the 42 amino acid form (Aβ42), are more prone to aggregation (Jarrett et al., 1993), and are the most abundant forms found in AD plaques (Iwatsubo et al., 1995), suggesting that Aβ42 is more pathogenic.

Under homeostatic conditions, Aβ peptides are regularly cleared from the brain parenchyma (Castellano et al., 2011; Paresce et al., 1996; Selkoe, 2000; Wyss-Coray et al., 2003). However, under conditions where the production of longer Aβ species is increased, or the clearance of Aβ is reduced, there is an increase in the concentration of Aβ, which facilitates oligomerization and fibrillization of Aβ into plaques (Selkoe, 2000; Selkoe and Hardy, 2016). Nevertheless, three decades of research have failed to reveal the mechanism by which Aβ promotes neurodegeneration, as well as its contribution to the clinical presentation of AD.

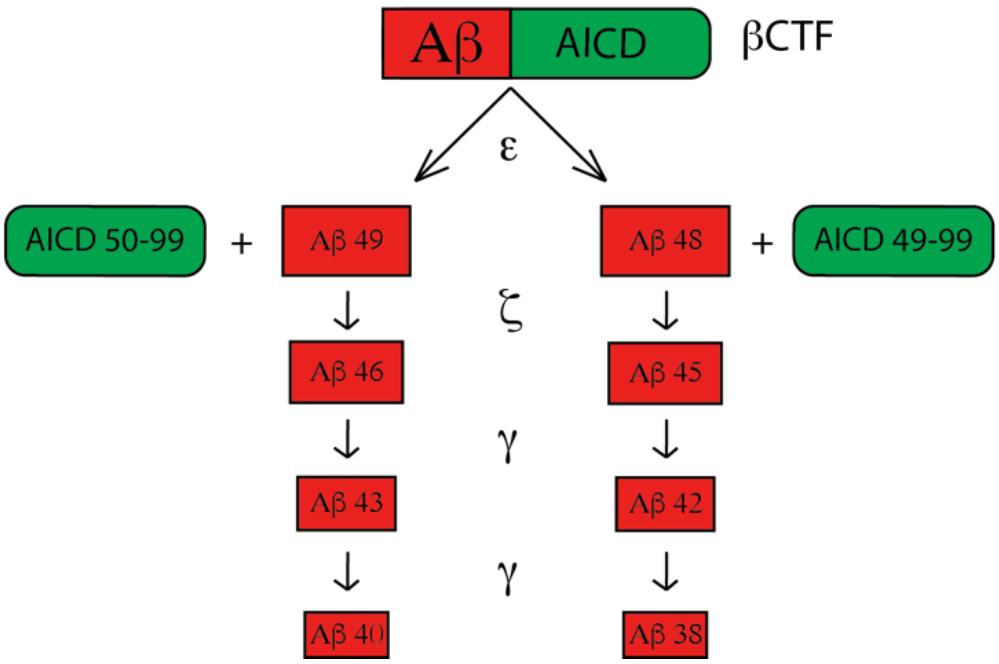

Figure 1.2 Processing of β-CTF by γ-secretase. β-CTF is recognized and cleaved intramembraneously by the γ-secretase complex. The catalytic component, PSEN1 or PSEN2, cleaves β-CTF initially between amino acids 50/49 or 49/48. This endopeptidase activity commits β-CTF to the production of either Aβ40 or Aβ38 respectively through a series of carboxypeptidase cleavages, removing 3 or 4 amino acids at a time.

The second clinical hallmark of AD is the aggregation and hyperphosphorylation of the microtubule associated protein tau (Grundke-Iqbal et al., 1986). Importantly, it was observed that the degree of NFT burden, not Aβ, correlated with disease severity, implying a causal role for tau in the pathogenesis of AD (Braak and Braak, 1991). Tau is a cytosolic protein that binds to microtubules

and helps to facilitate their assembly (Weingarten et al., 1975). Microtubules are the major structural component of neuronal axons, serving as molecular highways on which many proteins and vesicles are trafficked, from cell body to synapse and vice versa. Tau helps to stabilize these microtubules and facilitate the transport of cargo along microtubules (Ebneth et al., 1998; Millecamps and Julien, 2013; Spires-Jones and Hyman, 2014). Tau is therefore normally distributed throughout axons of the central and peripheral nervous systems, with more limited expression in the cell bodies and dendrites. However, tau becomes hyperphosphorylated in AD, causing it to dissociate from microtubules, mislocalize to somatodendritic compartments, and aggregate intracellularly into fibrils and NFTs (**Figure 1.3**) (Götz and Ittner, 2008). Intracellular aggregation of hyperphosphorylated tau jeopardizes normal neuronal function by recruiting and sequestering functional tau, as well as other microtubule associated proteins (e.g. MAP1 and MAP2 (Alonso et al., 1997)), into these aggregates, thereby compromising normal microtubule function. The impaired function of microtubules disrupts the axonal integrity, leading to the degeneration of synapses, and ultimately of the neuron itself. However, the exact cellular mechanisms of how intracellular aggregation of tau causes neuronal degeneration remain unclear (Iqbal et al., 2015).

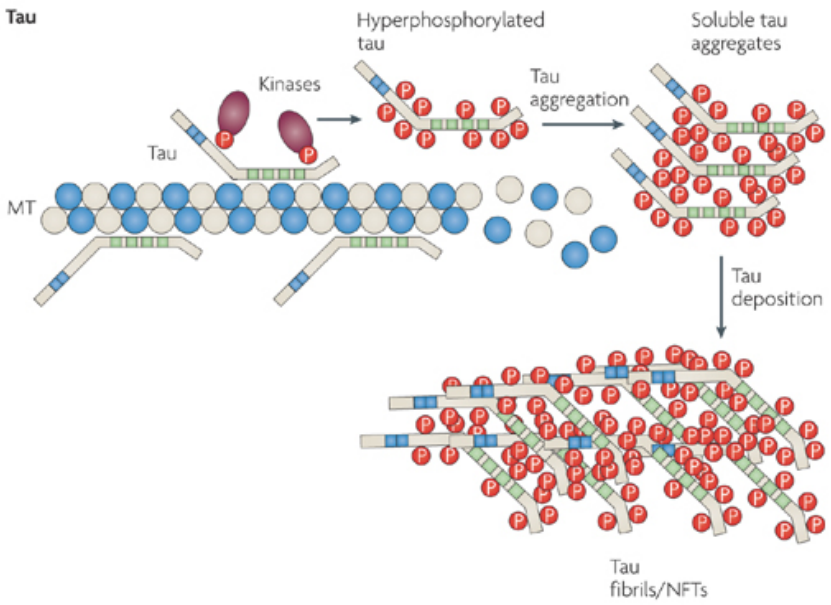

Figure 1.3 Tau pathology in AD. Tau normally binds and stabilizes microtubules in axons. In AD, tau becomes abnormally hyperphosphorylated. This facilitates dissociation from microtubules, oligomerization and aggregation of tau in the somatodendritic compartment. (Reprinted with permission from (Götz and Ittner, 2008))

Genetics of AD and the Amyloid Cascade Hypothesis

In 99% of AD cases, the disease occurs sporadically. This form of AD typically occurs late in life, with the earliest symptoms occurring almost always after the age of 65. The remaining 1% of AD patients inherit the disease in an autosomal dominant fashion. It was first suspected that AD could be inherited when it was recognized that patients with trisomy 21, or Downs Syndrome (DS), that survived into their fourth and fifth decades of life frequently developed AD (Masters et al., 1985). In the years following, it was discovered that the major component of the

extracellular plaques in AD brains consisted of Aβ, a degradation product of APP, which, interestingly, maps to chromosome 21 (Goldgaber et al., 1987; Kang et al., 1987; Robakis et al., 1987; Roher et al., 1986; St George-Hyslop et al., 1987; Tanzi et al., 1987). Thus, genetic triplication of chromosome 21 in Downs Syndrome leads to over-production of APP and its byproducts, including Aβ. It is thought that these elevated Aβ levels cause an earlier age of onset in FAD than in their sporadic counterparts. Shortly thereafter, two families were reported to have a high incidence of an aggressive, AD like illness that occurred earlier in life, with an autosomal dominant pattern of inheritance (Goate et al., 1991). In these families, a missense mutation was mapped to APP on chromosome 21, providing the first direct link between *APP* and AD.

These genetic findings, coupled with the characteristic histopathology of AD, gave APP processing a central role in the cause of both sporadic and familial AD. This view was reinforced with the discovery of mutations in two other genes, mapping to chromosome 14 and chromosome 1, that also caused FAD (Clark et al., 1995; George-Hyslop et al., 1992; Levy-Lahad et al., 1995; Rogaev et al., 1995; Schellenberg et al., 1992; Van Broeckhoven et al., 1992). Though the function of these proteins were not initially known, it was soon shown that both genes were involved in the production of Aβ (Citron et al., 1996; 1997; Klafki et al., 1996; Levitan et al., 1996; Li and Greenwald, 1996; Scheuner et al., 1996; Tischer and Cordell, 1996). The genes, *PSEN1* and *PSEN2,* encode the transmembrane proteins PSEN1

and PSEN2 (De Strooper et al., 1997), which are the catalytic components of the γ-secretase complex responsible for cleaving β-CTF to produce Aβ (**Figure 1.2**) (De Strooper et al., 1998). In seminal work, these researchers were the first to demonstrate the disproportionate overproduction of Aβ42 relative to Aβ40 in these families. Further, it focused the field's attention on the importance of APP processing in AD and, more specifically, on the production of longer Aβ fragments. These genetic findings bolstered support for Aβ, specifically the overproduction of Aβ, as a causal agent in the pathogenesis of FAD.

In contrast to FAD, sporadic AD is much more common and presents later in life. Many risk factors for developing sporadic AD have been identified. The most important, and perhaps the most obvious risk factor for AD is age (American Psychiatric Association, 2013). There are, however, many other genetic risk factors that can potentially be used as targets for AD therapies. The greatest genetic risk factor that has been identified is the apolipoprotein E (APOE) genotype, with the APOE ε4 allele conferring a 50% lifetime risk for developing AD in homozygotes, while the APOE ε2 allele is considered to be protective against AD (Corder et al., 1994; 1993; Scheltens et al., 2016; Strittmatter et al., 1993). APOE has several disparate roles, functioning in both the systemic circulation as well as in the brain. As it relates to AD, APOE has been shown to function in the clearance of Aβ, with the APOE4 allele being less efficient in clearing Aβ (Castellano et al., 2011). In addition to APOE, genome-wide association studies (GWAS) have identified several other

loci that are risk factors for the development of AD (Guerreiro and Hardy, 2014; Guerreiro et al., 2013). Many of the genes identified by these studies are involved in the clearance or metabolism of APP products (Guerreiro and Hardy, 2014), suggesting that sporadic AD may be a disease of reduced Aβ clearance, rather than an increase in Aβ production as in FAD (Mawuenyega et al., 2010). Importantly, both mechanisms result in a shared phenotype, specifically increased Aβ levels in the brain.

The finding that both sporadic and familial AD result in elevated Aβ levels in the brain led to, and support, the "amyloid cascade hypothesis," which postulates that a chronic imbalance between production and clearance of Aβ leads to the deposition and accumulation of Aβ plaques in the brain, and this gradual accumulation of plaques over many years ultimately leads to the pathologic changes that are characteristic of AD (Hardy and Higgins, 1992). Importantly, the hypothesis states that Aβ is the initiating factor of AD, with all other pathological changes, including tau hyperphosphorylation and aggregation, occurring downstream of Aβ. Evidence to support that Aβ can induce toxicity upstream of tau was demonstrated when Aβ oligomers induced neurodegeneration of mouse primary neuronal cultures, but failed to do so in neuronal cultures from tau knock-out mice (Rapoport et al., 2002; Roberson et al., 2007). Aβ has also been shown to induce tau phosphorylation (Jin et al., 2011) and promote synapse loss (Koffie et al., 2009), two major phenotypes observed in AD patients. Further, plaques of Aβ induce microgliosis and

astrocytosis in their immediate area, tying Aβ toxicity to inflammatory processes that have also been confirmed by GWAS studies.

While the amyloid cascade hypothesis is supported by a large body of data, there are other pieces of evidence that bring the hypothesis into question. Perhaps the most compelling and intriguing evidence that argues against the amyloid cascade hypothesis is the regular observation of cognitively normal individuals that have a substantial amyloid plaque burden in the brain post-mortem (Davis et al., 1999). This suggests that Aβ deposits may not always be toxic and that AD is much more complex than a linear sequence of events that begins and ends with aberrant Aβ homeostasis. Furthermore, patients with other forms of dementia, such as FTD, present with similar clinical symptoms, including NFTs and neurodegeneration, but have no evidence of Aβ plaques in their brains (Dumanchin et al., 1998; Hong et al., 1998; Hutton et al., 1998). As mutations in *MAPT*, the locus encoding the tau protein, are causal in FTD, it suggests that tau is sufficient induce neurodegeneration on its own, without an Aβ trigger. These observations further highlight the complexity and our incomplete understanding of the underlying etiology of AD.

Models of AD

Since the discovery of familial mutations that cause AD and FTD, numerous animal and cell culture models have been developed to study these diseases.

Because there is no identifiable cause of sporadic AD, researchers have relied on these familial mutations to reveal mechanistic insights into these diseases in the hope that their findings will also be relevant for understanding and treating sporadic cases of AD. The most prominent, and perhaps most useful, models have been animal disease models, with transgenic mice leading the way. The study of transgenic mice has helped elucidate important disease mechanisms, including the role of PSEN1 in Aβ production (De Strooper et al., 1998; Qian et al., 1998; Thinakaran et al., 1996). However, these animal models also have some major drawbacks.

In order to be an effective tool for understanding disease mechanisms, it is imperative that the animals share the same, or similar, symptoms and pathologies to those observed in human patients. In the case of AD mouse models, the hallmarks of the disease that mice should exhibit include age-dependent deposition of Aβ plaques and NFTs in the brain, neurodegeneration and impaired cognition. Because heterozygous carriers of mutations in *APP, PSEN1* and *PSEN2* are sufficient to cause AD, it is reasonable to expect that mice expressing a transgene of one of these disease-causing alleles would be sufficient to induce hallmarks of AD. However, this has not been the case for any FAD allele that has been expressed as a transgene in mice to date. For example, mice overexpressing mutant human *APP* (e.g. the APP Swedish mutation (APPswe)), develop age related Aβ plaques, exhibit neuronal loss and cognitive impairment, but do not develop NTFs (Hall and

Roberson, 2012; Hsiao et al., 1996; Sturchler-Pierrat et al., 1997; Weggen and Beher, 2012). Similarly, in mice overexpressing mutant *PSEN1* (e.g. *M146V* mutation), Aβ levels in brain are elevated, specifically Aβ42, however the mice do not develop plaques, NFTs or show cognitive deficits (Duff et al., 1996; Hall and Roberson, 2012; Holcomb et al., 1999). These shortcomings of mouse models may be attributable to differences between human and mouse genetics. In the case of PSEN1 models, human PSEN1 may process human APP differently than mouse APP, which differs by 17 amino acids, three of which are in the N-terminus of Aβ (Hall and Roberson, 2012). Examples like this highlight the difficulties in modeling a uniquely human disease in an animal that fails to develop the disease on its own.

Nevertheless, researchers eventually prevailed in developing a mouse model that recapitulates all the characteristics of AD. This required the expression of separate mutations in *APP*, *PSEN1* and *MAPT*, and is known as the triple-transgenic mouse (3x-Tg) (Oddo et al., 2003). Notably, this mouse required the expression of a *MAPT* mutation that does not result in AD, but instead causes FTD (Hutton et al., 1998). Furthermore, the 3x-Tg, as well as other AD mouse models with disease pathology, requires the massive overexpression of transgenes to observe relevant phenotypes. However, this is significantly different from the human condition, in which physiological expression of a single diseased allele is sufficient to cause the pathology and the disease. This illustrates not only the difficulties in establishing

animal models of AD, but also serves as a warning against using these animals to make concrete conclusions about the mechanisms that cause AD in humans.

In addition to animal models, there has been considerable effort to generate cell culture models of AD. While these models cannot be used to study the complex behavioral deficits associated with AD, they have been instrumental in defining the mechanisms of Aβ production and γ-secretase function. Studies examining the function of γ-secretase have been particularly insightful. Many of these models utilize stable overexpression of a FAD-causing *PSEN1* mutation in non-neuronal cell lines (**Figure 1.4**). Often, these cell lines are in a background of a *PSEN1/PSEN2-/-* double-knockout, thereby conferring the ability to study the FAD mutant in isolation (Bentahir et al., 2006; Thinakaran et al., 1997; Walker et al., 2005; Weggen and Beher, 2012). However, this is another example of a departure from the diseased patient. FAD patients are heterozygous for the mutant allele, and therefore express WT and mutant PSEN1 at roughly equal levels, whereas these *in vitro* models only express the mutant allele. Furthermore, the diseased patient also expresses WT PSEN2, whereas the cell culture double-knockout model does not express PSEN2 at all. While these models are extremely useful in understanding the mechanisms of action of WT and mutant PSENs in isolation, they may not reflect the true disease phenotypes experienced in a patient.

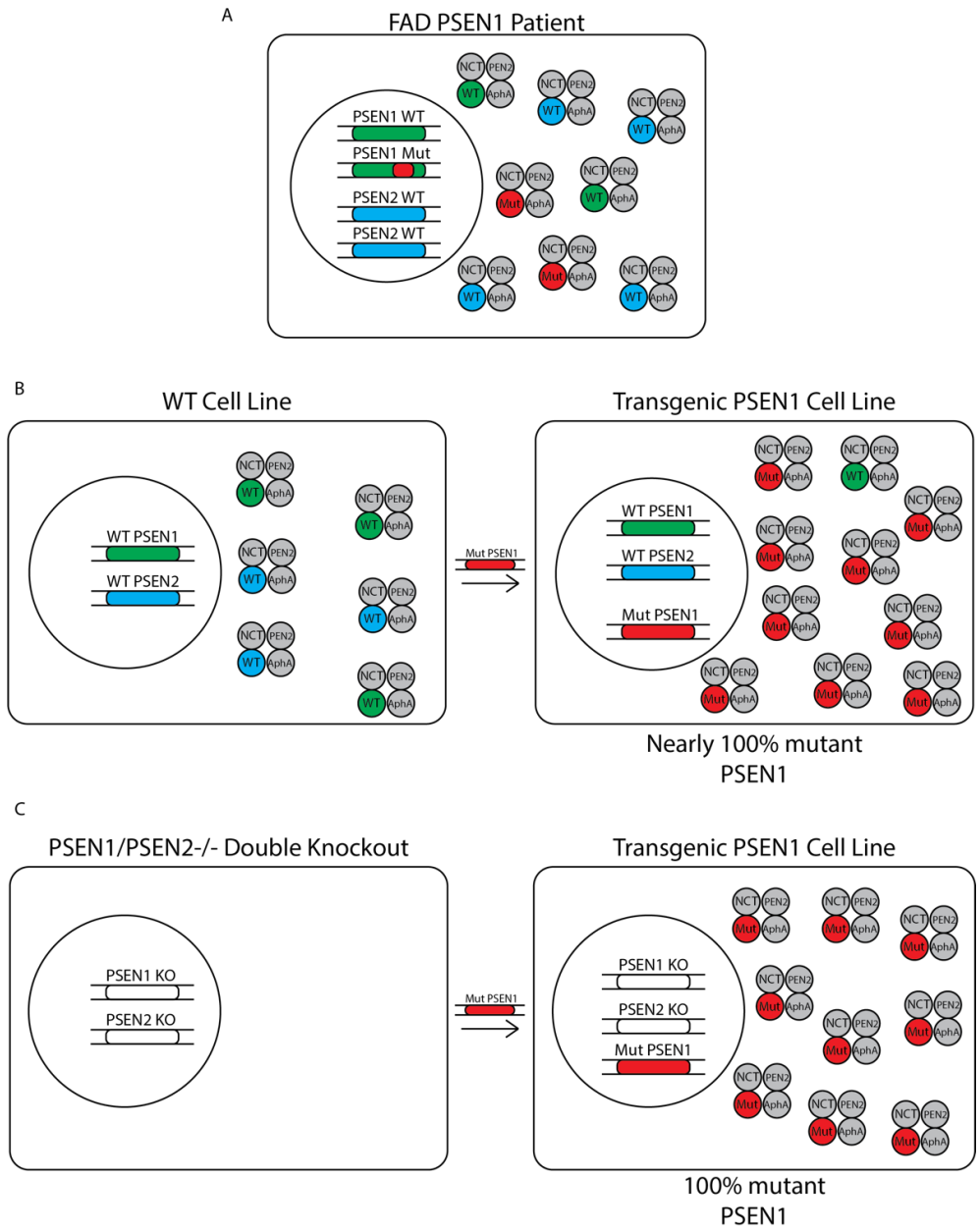

Figure 1.4 Cell culture models of *PSEN1* mutations. A) FAD patients are heterozygous for *PSEN1* (green) or *PSEN2* (blue), expressing equal ratios of WT and mutant alleles (red). In most cell culture models, however, mutant *PSEN1* transgenes are B) stably overexpressed and are therefore express almost 100% mutant PSEN1, or C) in the case of the *PSEN1/PSEN2* double knockout, 100% mutant PSEN1.

These shortcomings in disease models, however, do not call into question previous findings. Many of the observations from these models have been confirmed across numerous systems, and the mechanisms that have been elucidated and widely accepted as true. Instead, they simply call for the generation of newer models that better represent the physiologic conditions in diseased patients. This is especially critical as newer technologies are developed, such as the iPSC system, and genome editing techniques (TALEN and CRISPR).

Induced pluripotent stem cells

In 2006, Shinya Yamanaka and colleagues demonstrated that somatic cells, such as fibroblasts, could be reprogramed to an embryonic stem cell like state (Takahashi and Yamanaka, 2006). All that was required for this transformation was the introduction of four transcription factors, Oct4, Klf4, Sox2 and C-Myc, and the cell would express genes that promoted the dedifferentiation of somatic cells, and therefore resemble a stem cell. Like embryonic stem cells, these iPSCs are capable of limitless self-renewal, and importantly, can differentiate into all three germ layers: ectoderm, mesoderm and endoderm. These qualities earned these cells the title of induced pluripotent stem cells, capable of generating any cell type with the exception of placental and extraplacental tissue. This extraordinary technology earned Dr. Yamanaka a share of the 2012 Nobel Prize in Medicine.

With the advent of iPSC technology came many promises for the scientific community, including a better approach for modeling monogenetic diseases. Patients with disease causing mutations could now provide a skin biopsy that can be used to dedifferentiate their fibroblasts into iPSCs, thereby generating a cell repository for numerous patient iPSC lines that harbor various diseases-causing mutations. These lines could then be differentiated into their disease relevant cell types (e.g. human cortical neurons in FAD), studied for disease mechanisms, and used for pharmacological screens to identify drugs that may eventually be used to treat the diseased patient (**Figure 1.5**). Based on work in embryonic stem cells, cortical neuron differentiation protocols were quickly established for iPSCs, allowing for the reliable generation of human cortical neurons of both upper and lower cortical layers (Chambers et al., 2009) (**Figure 1.6**).

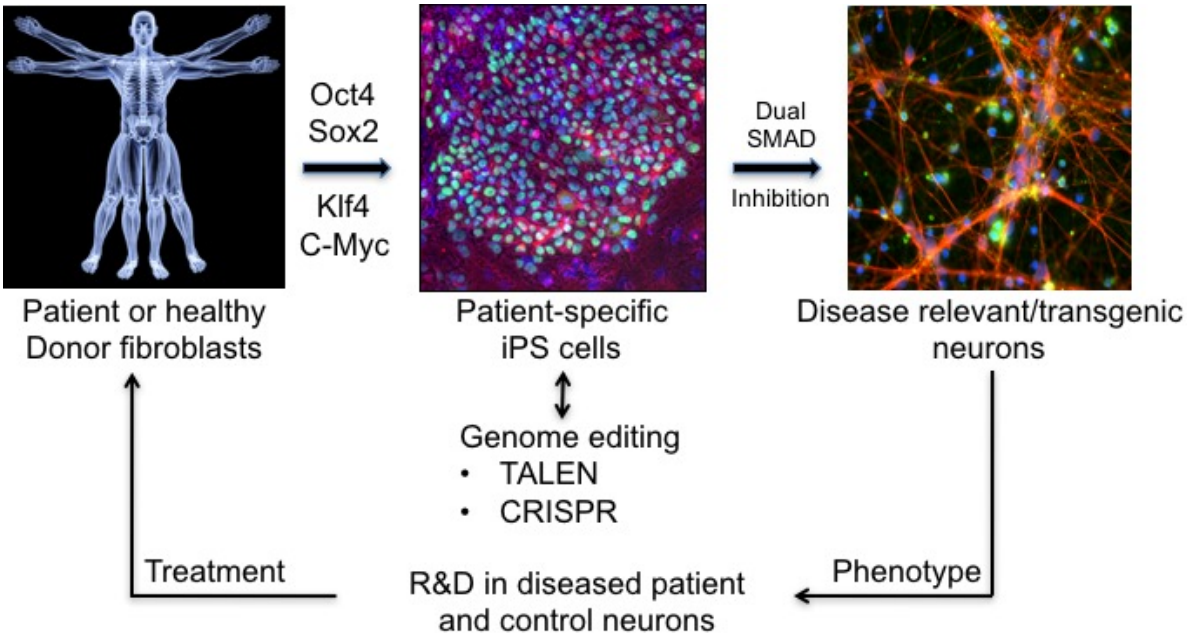

Figure 1.5 iPSC disease modeling. The introduction of four transcription factors, Oct4, Sox2, Klf4, and C-Myc, into any somatic cell of a human patient or healthy control, will convert it to an iPSC. This then allows for the generation of disease relevant cell types, such as cortical neurons in FAD, for the study of disease phenotypes *in vitro*. Discoveries made *in vitro* can then be translated into therapeutic strategies for patients affected by the disease.

As a result, many different iPSC models for FAD models have been generated (Koch et al., 2012; Kondo et al., 2013; Muratore et al., 2014; Shi et al., 2012a; Woodruff et al., 2013; Yagi et al., 2011; Yahata et al., 2011; Zhang et al., 2014). However, the vast majority of these studies have compared phenotypes of patient derived iPSC lines to related or unrelated WT iPSC lines. While these can be considered appropriate control cell lines, differences in genetic heterogeneity and dedifferentiation can confound the interpretation of the data when comparing cell

lines from different people and therefore from different iPSC clones. This is crucially important when comparing subtle phenotypes, as slight differences in genetic background could potentially lead to false-positive, or false-negative interpretations of results. This highlights the need for isogenic control iPSC lines when comparing the effects of a single mutation. Fortunately, the advent of modern genome editing technology has made it possible to rapidly generate isogenic iPSCs.

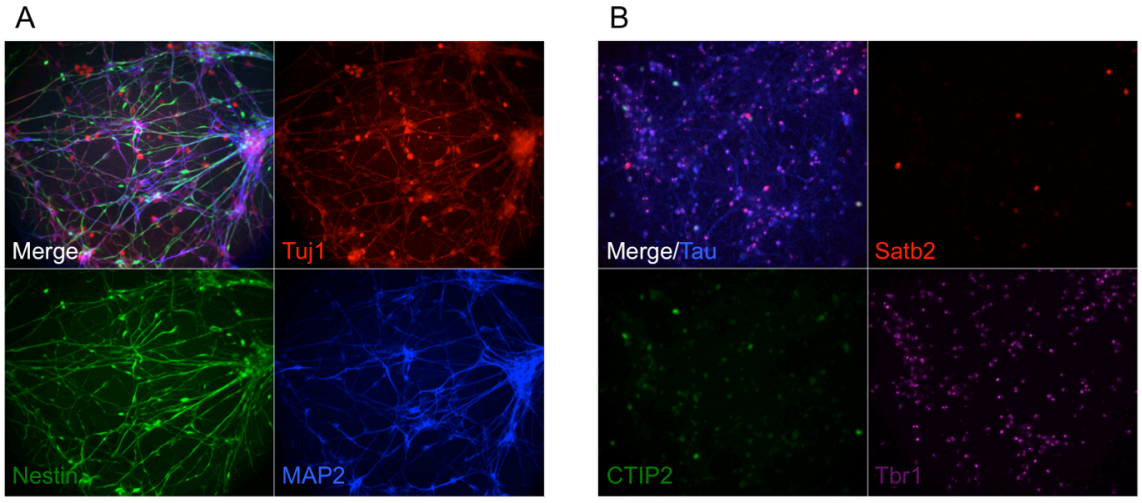

Figure 1.6: **Differentiation of iPSCs into cortical neurons**. **A**) Neurons derived from WT iPSCs and cultured until DIV64 express axonal markers of β-III tubulin (Tuj1) and the dendritic marker MAP2, as well as Nestin, an NPC marker. **B**) Longer maturation of neurons until DIV103 reveals neurons expressing upper (Satb2) and lower (CTIP2 and Tbr1) cortical layer markers, along with an extensive tau-positive axonal network.

Genome editing with TALENs and CRISPR

In the last decade, there have been major advances in the ability to efficiently edit the genome of human cells. Two of the tools commonly used for genome editing

are TALENs and CRISPR/Cas9. TALENs are naturally occurring proteins produced by the plant pathogen *Xanthomonas spp.* (Römer et al., 2007). These proteins are formed with a string of amino acid repeats that are engineered to specifically bind DNA sequences of the plant host in order to enhance the pathogen's virulence (DeFrancesco, 2011). Once the amino acid code of TALENs was deduced (Boch et al., 2009; Moscou and Bogdanove, 2009), it was clear that these proteins could be engineered to target any DNA sequence in the genome by fusing TALENs to a DNA nuclease, such as FokI, to create a precisely targeted double stranded break (DSB) (**Figure 1.7A**). In fact, it wasn't long before this system was adapted to human iPSCs (Hockemeyer et al., 2011), allowing for the generation of transgenic, knockout, or knock-in iPSCs by taking advantage of the host cell's DNA repair system (**Figure 1.7A and B**).

At around the same time, the CRISPR/Cas9 genome editing technology was being developed from the bacterial and archaeal adaptive immune system (Horvath and Barrangou, 2010). The CRISPR/Cas9 system uses a strand of RNA to bind to a complementary strand of DNA from an invading pathogen, such as a bacteriophage, to guide the Cas9 complex, a large protein complex that typically has endonuclease activity, to silence the invading organism and protect the host. Like TALENs, this system was quickly adapted for mammalian cells to perform RNA guided (gRNA) DNA repair or gene editing using the endogenous DNA DSB repair machinery (Hsu et al., 2014; Jinek et al., 2012; Mali et al., 2013). Typically, DSBs generated by

CRISPR/Cas9 are repaired by non-homologous end joining (**Figure 1.7B**) (NHEJ), which repairs the break by the insertion or deletion (indel) of random nucleotides, often resulting in frameshift mutations (Hsu et al., 2014). This provides an easy and efficient way of generating knockouts of a target gene, but generating knock-in mutations pose a more difficult task.

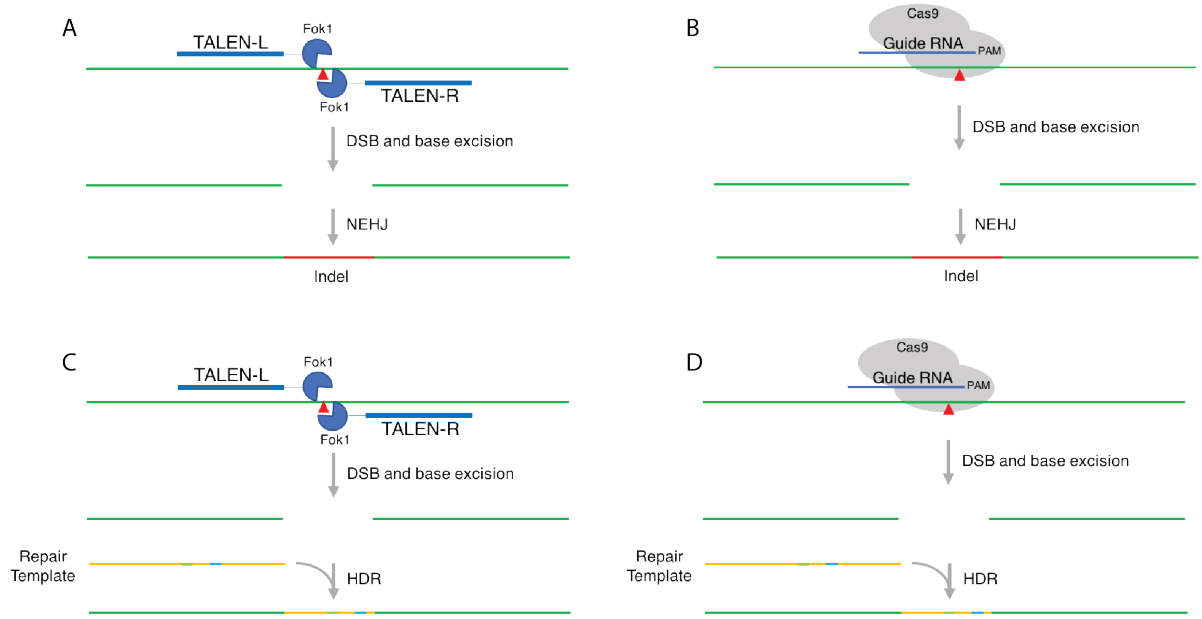

Figure 1.7. Genome editing with TALENs and CRISPR/Cas9. Schematics representing the mechanisms of genome editing by TALENs (A and C) and CRISPR/Cas9 (B and D). Both techniques generate a DSB at the targeted locus, which is predominantly edited by the random insertion or deletions of nucleotides via NHEJ (A and B). In rare instances, a repair template is used to facilitate HDR of the locus.

In order to generate knock-in mutations, a cell must undergo homology directed repair (HDR), which utilizes a DNA template to guide the accurate repair

(**Figure 1.7B and D**) (Mali et al., 2013). However, this process is very inefficient and imprecise (Canver et al., 2014; Cong et al., 2013; Dow et al., 2015; Platt et al., 2014; Yang et al., 2013). Fortunately, our laboratory developed a system that enhances both the efficiency and accuracy of HDR to introduce the knock-in of specific point mutations using a single stranded oligo DNA nucleotide (ssODN) (Kwart et al., 2017; Paquet et al., 2016). The method takes advantage of silent mutations that block the proto-spacer adjacent motif (PAM), which consists of a three base-pair (bp) NGG sequence, to increase the accuracy of editing by preventing Cas9 from re-cutting a locus that has already been targeted and repaired. Thus, our method reduces the rate of NHEJ, thereby increasing the accuracy of editing and facilitating the rapid generation of isogenic mutant iPSC lines for modeling of human diseases.

Perspective and overview of thesis project

The work presented in this thesis project originally began with the goal of elucidating the mechanism of tau spreading in iPSC-derived human cortical neurons. Previous studies had shown that tau could move from neuron to neuron along anatomically connected pathways in transgenic mice. These mice regionally expressed a human tau transgene in the entorhinal cortex, and demonstrated age-dependent dissemination of human tau throughout the cortex along the perforant pathway, suggesting trans-synaptic spreading (Liu et al., 2012). While these *in vivo* data are compelling, it was still unclear whether tau was moving from inside one cell

to inside another, as some studies suggested that the promoter used to restrict localization of tau to the entorhinal cortex was leaky (Yetman et al., 2015). In addition, it has been shown *in vitro* that aggregates of tau can induce normal soluble tau to misfold, a mechanism similar to that seen in prion disease (Crutzfeld-Jacob disease) (Guo and Lee, 2011; Kfoury et al., 2012; Sanders et al., 2014). This provides an important link between spreading of tau and disease progression, as aggregates of tau that gain access to a previously healthy neuron can induce aggregation and disease in distant regions of the brain. As such, we aimed to develop an *in vitro* model to not only faithfully track tau as it moved from donor to recipient neurons, but also to aid in elucidating the mechanism of tau transfer. Importantly, this model system would be the first to use human cortical neurons, the disease relevant cell type in AD, and understanding this disease mechanism in a physiologically relevant context would potentially identify targets for novel drug development.

In addition to the tau spreading project I originally proposed, I also undertook a second project in the last year of my thesis work. As will be discussed in more detail below, we found that tau does in fact spread, however to no greater extent than the cytosolic fluorophore of our control cell line. This suggested that cellular transfer tau was mediated by a mechanism that is not specific to tau. Seeing as this result would require the generation of numerous additional control cell lines expressing proteins of various size, conformation, charge or polarity, and therefore

many more years than was possible, we decided to investigate a second AD disease mechanism that had previously been demonstrated in the lab by Dylan Kwart. Dylan had shown that introducing the FAD *PSEN1* mutation, *M146V*, into iPSCs via CRISPR/Cas9 genome editing results in an increase in the ratio of Aβ42:40 when differentiated into cortical neurons, a finding that has been repeatedly observed *in vivo* and *in vitro*. Since there has been significant debate in the field surrounding whether *PSEN1* FAD mutations are gain-of-function or loss-of-function, we decided to focus on PSEN1 and its role in Aβ production by knocking in several different FAD mutations into WT iPSCs to create a series of isogenic lines. Importantly, doing this in iPSCs via knock-in mutation of the endogenous locus allowed us to study the effects of these mutations in clinically relevant human cell types, and at physiological levels of expression, therefore establishing a system that is much more closely relatable to the disease in humans.

I have completed two fairly unrelated projects; both required a significant amount of cell line generation via genome editing, so I will devote all of Chapter 2 describing the generation of the various iPSC lines for both projects. For the tau spreading project, TALENs were used to target the genomic safe harbor locus, AAVS1, where I inserted a doxycycline inducible promoter transgenic system to control the expression of various fluorescently labeled tau transgenes. To generate recipient cell lines, a second genomic safe harbor was targeted with TALENs, the H11 locus, and a constitutively expressed membrane anchored YFP (memYFP) was

inserted. For the PSEN1 project, CRISPR/Cas9 was used to knock-in four separate FAD mutations, *M146V, L166P, M233L* and *A246E*, in either heterozygous or homozygous form.

In Chapter 3, I will focus on the tau spreading project. In contrast to previous studies, I will show that tau does in fact spread from cell to cell in this system, however it does not spread in a manner specific to tau, as the donor control cell line, expressing just the mCherry fluorophore, spread just as efficiently as the tau donor. I then wanted to ask what the consequence of spreading is in human iPSC-derived cortical neurons. Namely, can tau induce aggregation of normal tau in human cortical neurons? To answer this, I generated recombinant tau aggregates with the assistance of my Committee Member, Dr. David Eliezer. These aggregates were able to induce the aggregation of tau in a HEK293T biosensor system designed to measure the seeding activity of tau aggregates using immunofluorescence or fluorescence resonance energy transfer (FRET) (Holmes et al., 2014). However, when these aggregates were added to our human cortical neurons, we observed no ability to seed and induce aggregation of healthy tau.

Chapter 4 will focus on the PSEN1 project, which aimed to describe the changes in Aβ production resulting from FAD mutations in *PSEN1*. I found that mutations in *PSEN1* resulted in a decrease in Aβ40 and Aβ38, and an increase in Aβ42. Importantly, in heterozygous mutants, the total Aβ remained relatively unchanged, while in homozygous mutants, Aβ was decreased. These data suggest

that *PSEN1* mutations are partial loss of function, specifically altering the last cleavage of Aβ.

In Chapter 5, I will conclude this thesis with a general discussion of the implications of the results from each of these projects. In addition, I will provide suggestions for future work for both of these projects.

CHAPTER II: GENOME EDITING AND CELL LINE GENERATION

Donor and recipient cell lines for tau spreading

Rationale

In order to study the mechanisms that mediate spreading of tau between human neurons, we set forth to establish an *in vitro* system with two main features: 1) the transfer of tau would readily and reproducibly propagate from neuron to neuron, and 2) propagated tau is distinguishable from endogenous tau in recipient neurons. Such a model would provide a system to quantitatively assess the spreading of tau between cells as well as probe and manipulate the cellular pathways that mediate tau transmissions. To distinguish between endogenous and transmitted tau, the cells expressing tau designated to spread, or “donor” cell lines, must express a unique species of tau from the “recipient” cell lines. This can be accomplished in a variety of ways, including tagging tau with either a fluorophore, like mCherry or GFP, or with a small polypeptide protein tag, like a FLAG-tag or His-tag. Another possibility is to utilize tau knockout recipient cells lines, such that only the donor cell line only express tau. With these considerations in mind, we decided to establish a system in which the donor cells expressed tau with an N-terminal mCherry tag. Because tau is only expressed in neurons, we thought it necessary that the mCherry tagged tau be under the control of an inducible promotor, namely the Tet-On 3G inducible expression system so that tau was not improperly

expressed in iPSCs or neural precursors (NPCs) (González et al., 2014; Gossen and Bujard, 1992). For the recipient cell lines, we generated a cell line that constitutively expressed a membrane anchored YFP (memYFP).

Recipient Cell Line

Our initial efforts of genome editing utilized a method that was previously reported to faithfully insert transgenes of interest into iPSCs at a safe, intergenic, and transcriptionally active locus on chromosome 22 (H11 locus) (Zhu et al., 2013). This method was originally developed for introducing transgenes into iPSCs utilizing TALEN mediated HDR. Specifically, the cassette, or "landing pad" consists of a neomycin resistance and memYFP gene, and is flanked by two attachment sites (attP) for the integrases phiC31 and Bxb1. These integrase attachment sites allow for the introduction of a second donor cassette expressing a gene of interest, thereby facilitating the exchange by way of dual cassette integrase exchange (DICE) (**Figure 2.1A**). For the purposes of this work, we only used the landing pad to express memYFP in order to generate the recipient cell line (**Table 2.1**).

To generate our iPSC lines, WT iPSCs were co-electroporated with the landing pad and TALEN pair, then allowed to recover. Next, electroporated iPSCs were serially diluted to plate them as single cells, and neomycin (G418) was introduced for one week to select for clonal cell lines that successfully integrated the landing pad into the H11 locus. Surviving clonal colonies were expanded and then were manually picked into individual wells of a 96-well plate lined with MEFs. Clones

that had irregular or low expression of memYFP were excluded. The clones were then analyzed for the correct incorporation of the landing pad into the H11 locus by PCR (**Figure 2.1B**). Southern blot was used to confirm a single incorporation of the landing pad (**Figure 2.1C**). Cell lines were next analyzed by karyotyping, confirming that they lacked any chromosomal abnormalities (**Figure 2.1D**). Finally, these lines were also analyzed for pluripotency by immunocytochemistry using the pluripotency markers, Oct4, Tra-1-60, SSEA4 and Nanog (**Figure 2.1E**).

Table 2.1: **Tau spreading cell lines**. List of donor and recipient cell lines generated for studying tau spreading

Donor Cell Lines						
#	**Transgene**	**Promoter**	**Tag**	**Selection**	**Locus**	**Parental Cell line**
1	mCherry	TRE	mCherry	Puro/Neo	AAVS1	Tau Knock-out
2	FL - WT					
3	FL – P301L					
4	RD - WT					
5	RD – P301L					
Recipient Cell Lines						
6	memYFP	CAG	None	Neo	H11	WT

Figure 2.1: **Generation of recipient cell line**. **A**) Schematic of targeting and integration of the landing pad to generate recipient cell lines. **B**) PCR of genomic DNA to screen for heterozygous integration of the landing pad. Each genomic DNA PCR was amplified twice for the endogenous allele (WT-594bp) and the allele containing the integrated landing pad (LP-617bp) in control (CTL) and WT. **C**) Southern Blot of HindIII digested genomic DNAs with probe targeting the memYFP transgene. Arrow indicates expected band of 9.8kb. **D**) Karyotypye of clone E3 selected for further analysis. **E**) Assessment of pluripotency markers Oct4, Tra-1-60, SSEA4 and Nanog by immunofluorescence.

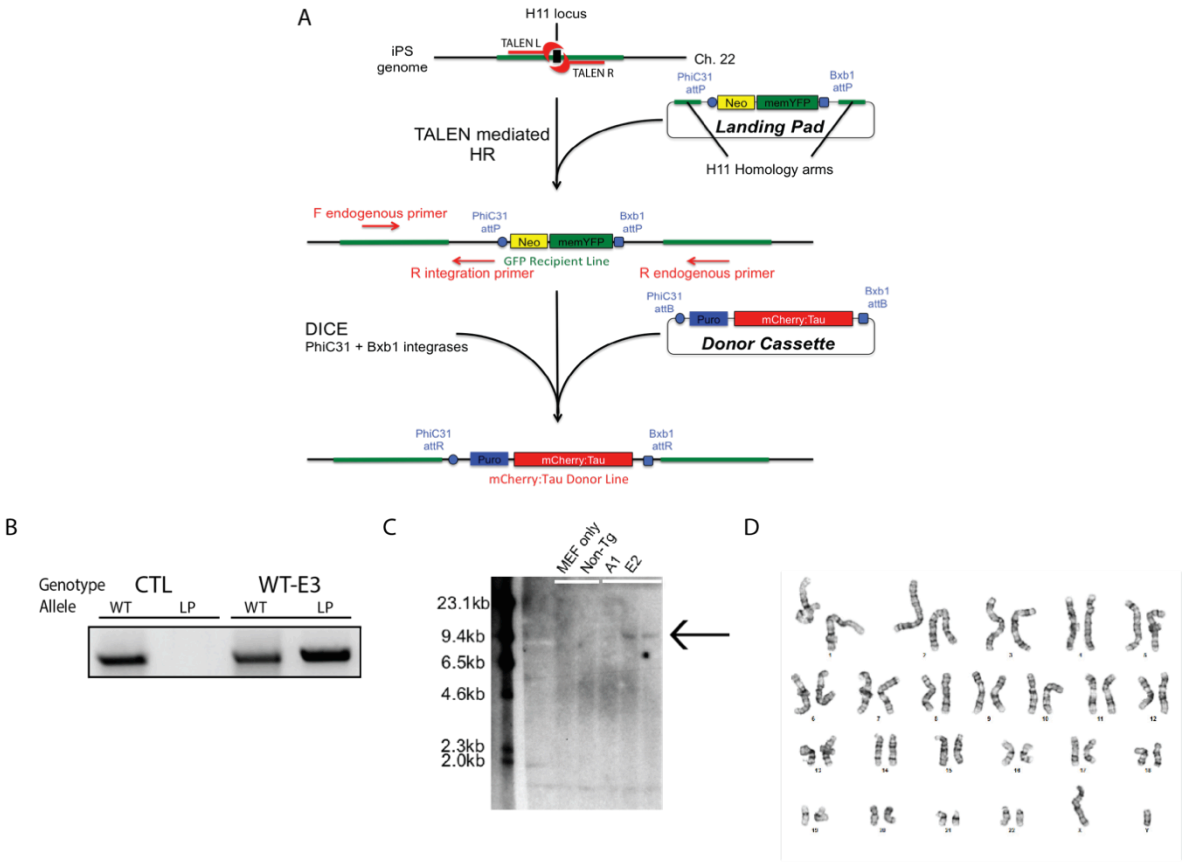
A
H11 locus
iPS genome
TALEN L
TALEN R
Ch. 22
PhiC31 attP
Bxb1 attP
Neo
memYFP
Landing Pad
TALEN mediated HR
H11 Homology arms
F endogenous primer
R integration primer
GFP Recipient Line
R endogenous primer
DICE
PhiC31 + Bxb1 integrases
PhiC31 attB
Bxb1 attB
Puro
mCherry:Tau
Donor Cassette
PhiC31 attR
Bxb1 attR
mCherry:Tau Donor Line
B
Genotype
Allele
CTL
WT-E3
WT
LP
C
MEF only
Non-Tg
A1
E2
23.1kb
9.4kb
6.5kb
4.6kb
2.3kb
2.0kb
D
E
Merge/DAPI
Oct4
memYFP
Tra-1-60
Merge/DAPI
SSEA4
memYFP
Nanog

Donor Cell Lines

For the generation of the donor cell lines harboring an inducible tagged tau transgene, we turned to a second genomic safe harbor, AAVS1, that had also been previously published (González et al., 2014; Hockemeyer et al., 2011; 2009). This system utilizes bi-allelic introduction of a doxycycline inducible system (Figure 2.2A). Briefly, a TALEN pair targeting the first intron of the *PPP1R12C* gene was introduced by electroporation into WT iPSCs along with two donor cassettes. The first of these cassettes contains a splice acceptor (SA) site, followed by a P2A ribosomal slip sequence and a puromycin resistance gene. On the opposite end of the cassette and inverted was the tetracycline response element (TRE), driving expression of mCherry tagged tau. Four separate cassettes expressing four different tau transgenes were cloned and introduced into iPSCs separately. In addition, we generated a control cell line that would express mCherry alone (**Table 2.1**). The four tau transgenic lines comprise two complementary pairs that would allow us to compare differences in the spreading or aggregation of wild-type tau vs tau containing a FTD-causing mutation (Dumanchin et al., 1998; Hutton et al., 1998). The first pair of transgenic lines express either the full length (FL) WT tau containing both N-terminal inserts (2N) and all four repeat domains (4R) or the FL 2N4R FAD mutant P301L tau, which has been shown to promote tau aggregation (Barghorn et al., 2000; Bergen et al., 2001; Fischer et al., 2007). The second pair of tau transgenic lines express only the repeat domains (RD) of tau, exons 9 through 12, in either the WT or P301L mutant form. These RDs form the microtubule binding

domains of tau, and are a major component of NFTs (Wischik et al., 1988). Prolonged overexpression of FL tau can be toxic in some cell models, but the RD form has been shown to be stable and propagate through numerous passages in a HEK293 model *in vitro* (Sanders et al., 2014).

The second cassette contains the same SA-P2A, but is followed by a neomycin resistance gene. Additionally, a tetracycline transactivator protein gene is constitutively expressed (**Figure 2.2A**). Upon addition of 5μg/mL of doxycycline, the transactivator binds to the TRE and initiates transcription of the mCherry tagged tau transgenes (**Figure 2.2B**).

All tau transgenic cell lines were generated in the background of a tau knock-out cell line that had been generated by Dominik Paquet, a post-doc in the Tessier-Lavigne Lab. The rationale of this approach was that it would overcome any confounding effects that endogenous expression of tau might have on our analysis of spreading of transgenic tau. After generating these donor cell lines, I differentiated two different inducible cell lines, the mCherry control and the RD-WT, and treated them with and without 5μg/mL of doxycycline for 7 days and examined the expression of the inducible transgenes by Western blot. Unfortunately, there was a troublesome observation. An antibody recognizing total tau (K9JA) revealed a faint, slightly truncated form of tau when compared to the WT (**Figure 2.2C, arrowhead**). To confirm the specificity of this band, I tested three other monoclonal antibodies against phosphorylated epitopes of tau, which recognized the same band, indicating that the knock-out line was not a true null (**Figure 2.2D**).

Figure 2.2. Inducible tau cell line characterization. A) Schematic for bi-allelic targeting of the AAVS1 locus for the generation of Tet-On inducible donor cell lines. B) Induction of expression of mCherry and mCherry:FL-WT tau in tau KO iPS cells after selection with neomycin and puromycin with 5µg/mL doxycycline for 16 hours. Shown is the live fluoresence of mCherry C) Western blot of WT and inducible donor cell lines (KO background) for total tau. Arrowheads indicate the truncated form of tau detected in the "KO." D) Western blot of WT and KO cell lines blotted with three monoclonal antibodies to separate epitopes of tau. E) WT of inducible donor cell lines with and without doxycycline induction for 7d at 5ug/mL. F) Representative pluripotency staining for Tra-1-60, Oct4, Nanog, and SSEA4 in mCherry tagged FL-WT tau iPSCs. G) Normal karyotype for mCherry tagged FL-WT tau iPSCs.

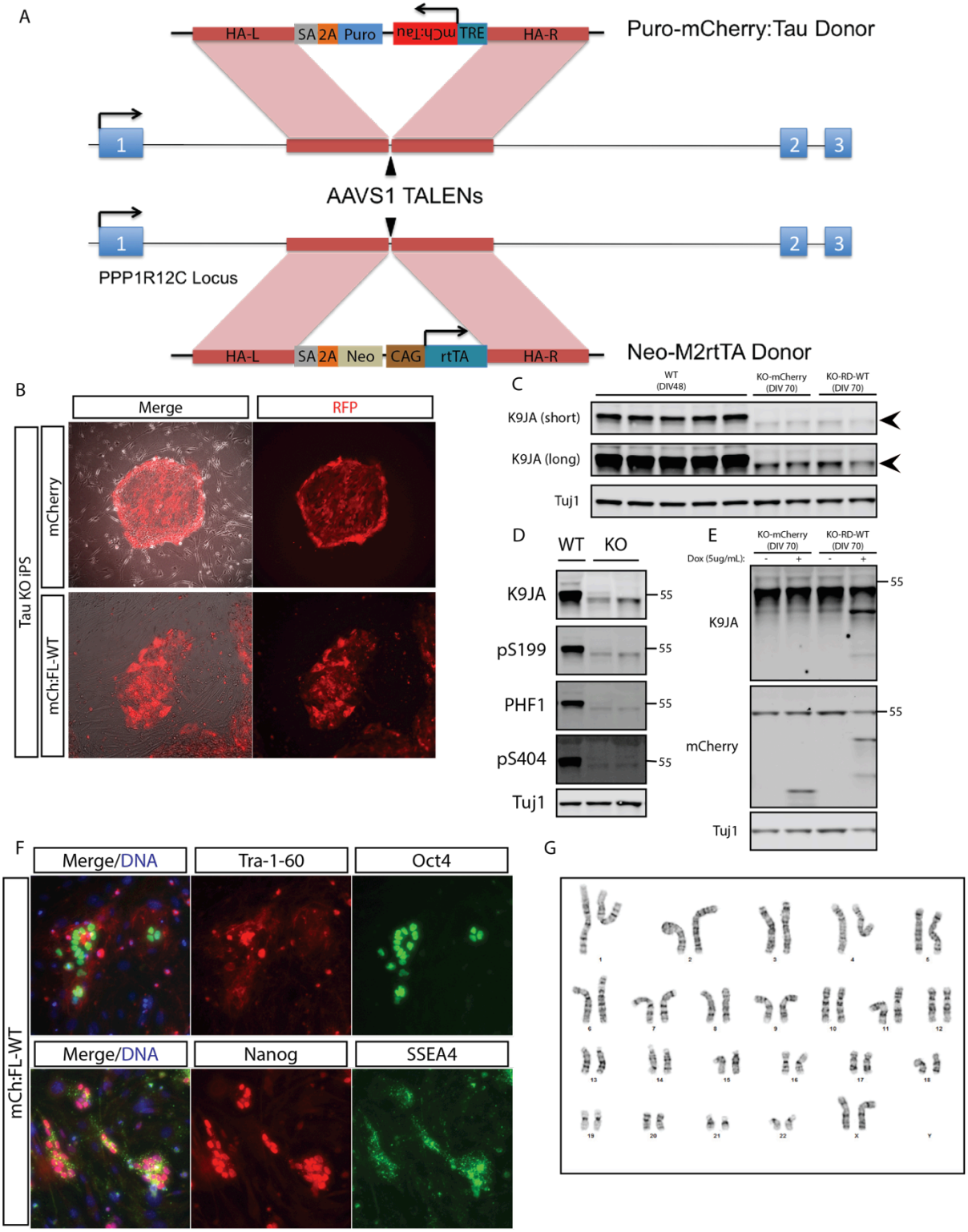
A
HA-L
SA
2A
Puro
mCh:Tau
TRE
HA-R
Puro-mCherry:Tau Donor
1
2
3
AAVS1 TALENs
PPP1R12C Locus
Neo
CAG
rtTA
Neo-M2rtTA Donor
B
Merge
RFP
Tau KO iPS
mCherry
mCh:FL-WT
C
WT (DIV48)
KO-mCherry (DIV 70)
KO-RD-WT (DIV 70)
K9JA (short)
K9JA (long)
Tuj1
D
WT
KO
K9JA
pS199
PHF1
pS404
Tuj1
55
E
Dox (5ug/mL):
K9JA
mCherry
Tuj1
F
Merge/DNA
Tra-1-60
Oct4
Nanog
SSEA4
G

While this was a troubling finding, the lines that I had generated in this background were still useful since they were still able to induce expression of the transgenic tau, without any leakiness of the promoter system (**Figure 2.2E**). Further quality control analysis revealed that these lines also maintained their pluripotency markers after genome editing and clonal expansion **(Figure 2.2F**), and also displayed a normal karyotype (**Figure 2.2G**). This concluded the TALEN genome editing for the generation of iPSC lines expressing inducible fluorescently tagged tau donor cell lines, and recipient cell lines with fluorescently labeled plasma membranes.

Generation of isogenic FAD *PSEN1* mutant iPSCs

Rationale

In this second iPSC model, we aimed to generate a series of *PSEN1* mutations across isogenic iPSC lines to better characterize the mechanism of Aβ production by PSEN1. Previous studies had used a variety of model systems, including transgenic mice, stable cell lines, and transient transfection and overexpression in stable cell lines in order to study the effects of *PSEN1* mutations on Aβ production. However, very few of these models utilize physiological levels of expression of both substrate, APP, and enzyme, PSEN1 or PSEN2 and the other functional components of γ-secretase, Aph1, PEN2 and NCT. Furthermore, these models have not studied these mechanisms in human cortical neurons, the disease

relevant cell type in AD. Therefore, we utilized WT human iPSCs to knock-in four FAD *PSEN1* mutations, *M146V, L166P, M233L*, and *A246E*, at the endogenous *PSEN1* locus using CRISPR/Cas9 mediated HDR. Because all these lines were generated from the same WT iPSC parental cell line, the mutant lines are isogenic, which allows for a cleaner interpretation of the results as genetic heterogeneity is ruled out. From these iPSC lines, human cortical neurons would be generated to characterize differences in Aβ production between WT and mutants, as well as any other changes in enzymatic activity that these mutants might have on substrates other than β-CTF.

CRISPR gRNA design and HDR templates

There are more than 200 mutations in *PSEN1* that cause FAD (alzforum.org). To design a manageable and representative study, we had to determine the number and identity of *PSEN1* mutations that would yield the most meaningful results. We initially selected 10 mutations to investigate, but due to limitations of the CRISPR/Cas9 system, we were only able to successfully target four of these loci. The limitations included the availability of NGG sequences that were in close proximity to the FAD mutations, low activity of gRNAs, and the sheer volume of cell culture work involved in generating a single mutant iPSC line. In the end, we introduced and studied four FAD *PSEN1* mutations: *M146V, L166P, M233L*, and *A246E* (**Table 2.2**).

Table 2.2. PSEN1 cell lines. List of WT and PSEN1 mutant isogenic iPSC cell lines.

Mutation	Line ID	Genotype	Karyotype
WT	A5	WT	Normal
L166P	L9	Homo	Normal
	L11	Het	Abnormal
M146V	M1	Homo	Normal
	M5	Homo	Normal
M233L	ML5	Het	Normal
A246E	A3	Het	Normal
	A4	Het/Ind	Normal

To introduce these mutations, we utilized a commonly used online tool to identify and generate gRNAs from the Zhang Lab (crispr.mit.edu). This tool analyzes the target sequence of interest for the presence of NGGs, and then generates a report for each gRNA, giving it a score based on the potential for a given gRNA to have off-target effects due to sequence similarity. gRNAs were selected based on their given score, as well as their proximity to the desired mutation. Our lab previously showed a monotonic relationship between the distance of the CRISPR cut site and mutation incorporation, with shorter cut-to-mutation distances being more favorable for mutation incorporation (Paquet et al., 2016). As such, we choose gRNAs cut-to-mutation distances of 10 base pairs (bp) or less. gRNAs used for each mutation are listed in **Table 2.3**.

Table 2.3. gRNAs targeting *PSEN1* mutant loci.

locus	gRNA	sequence*
M146V	6	GTTGTCATGACTATCCTCC**TGG**
L166P	10	GAGATGATATAATAAGCC**AGG**
M233L	18	GATTAGTGCCCTCATGGCCC**TGG**
A246E	17	**G**ATGGACTGCGTGGCTCATCT**TGG**

*** G** = added for use with pMLM3636,
green = NGG

For each mutation, an HDR template was designed with two important qualities in mind. First, each single stranded oligonucleotide (ssODN) template needed to have a silent PAM blocking mutation to abolish the NGG sequence, rendering that locus unrecognizable by Cas9 after successful HDR. To facilitate screening of clones, the PAM blocking mutations are designed to introduce, or abolish, an endonuclease recognition site to facilitate the rapid screening of hundreds of individual clones by restriction fragment length polymorphism (RFLP) assays. Secondly, the ssODNs must also incorporate the mutation of interest. Because we were interested in generating heterozygous clones in order to more accurately model FAD, additional factors needed to be taken into account because generating heterozygous clones is much more inefficient than generating homozygous clones (Paquet et al., 2016). To increase the odds of obtaining heterozygous clones, we created two separate ssODN templates, both harboring the PAM blocking silent mutation, and one template containing the pathogenic mutation, while the second template remained WT at the pathogenic mutation site. By mixing

these two ssODNs together (1:1 ratio of WT to mutant template), the rate of heterozygous clone generation increases as both templates could in theory be used for each allele (Paquet et al., 2016). A list of repair templates, with pathogenic and PAM blocking mutations, are annotated along with the RFLP enzyme used for clone screening in **Table 2.4**.

Table 2.4. HDR templates. HDR ssODN templates for each mutation, as well as each enzyme used for RFLP analysis.

* **guideRNA-binding site = 20-1, N = 0, G = -1, G = -2**

****bold** = cut site, **blue** = pathogenic mutation, **red** = CRISPR/Cas-blocking mutation, **black** = cut site, **green** = NGG

Locus	gRNA	strand (NGG and HDR oligo)	oligo #'s	codon mutation	position of CRISPR/Cas-blocking mutation; pathogenic mutation*	sequence**	Enzyme for RFLP
M146V	6	+	-			AATTCTGAATGCTGCCATCATGATCAGTGTCATTGTTGTCATGACTATC**CT**CC**TGG**TGGTTCTGTATAAATACAGGTGCTATAAGGTGAGCATGAGACAC	BssSI
			1	CTG>CT**A**	-1	AATTCTGAATGCTGCCATCATGATCAGTGTCATTGTTGTCATGACTATC**CT**CC**T**CGTGGTTCTGTATAAATACAGGTGCTATAAGGTGAGCATGAGACAC	
			2	CTG>CT**A**; ATG>GTG	-1; +13	AATTCTGAATGCTGCCATCATGATCAGTGTCATTGTTGTCGTGACTATC**CT**CC**T**CGTGGTTCTGTATAAATACAGGTGCTATAAGGTGAGCATGAGACAC	
L166P	10	-	-			CAAGTAAATGAATGAAAAAAAGAACAGCAACAATAGAGATGATATAATA**AG**CC**AGG**CATGGATGACCTAGAAAAGAAAGCATTTCAATATAATTAACAGG	NsiI
			1	GCC>GC**A**	-1	CAAGTAAATGAATGAAAAAAAGAACAGCAACAATAGAGATGATATAATA**AG**CC**A**TGCATGGATGACCTAGAAAAGAAAGCATTTCAATATAATTAACAGG	
			2	GCC>GC**A**; CTT>C**C**T	-1, +4	CAAGTAAATGAATGAAAAAAAGAACAGCAACAATAGAGATGATATAATA**GG**CC**A**TGCATGGATGACCTAGAAAAGAAAGCATTTCAATATAATTAACAGG	
M233L	18	+	-			TCCACTTCGACTCCAGCAGGCATATCTCATTATGATTAGTGCCCTC**A**TG**GC**C**T**GG**T**GTTTATCAAGTACCTCCCTGAATGGACTGCGTGGCTCATCTTG	ScrFI (loss of site)
			1	CTG>CT**A**	-1	TCCACTTCGACTCCAGCAGGCATATCTCATTATGATTAGTGCCCTC**A**TG**GC**C**T**AGTGTTTATCAAGTACCTCCCTGAATGGACTGCGTGGCTCATCTTG	
			2	CTG>CT**A**; ATG>CTG	-1; +7	TCCACTTCGACTCCAGCAGGCATATCTCATTATGATTAGTGCCCTC**T**G**GC**C**T**AGTGTTTATCAAGTACCTCCCTGAATGGACTGCGTGGCTCATCTTG	
A246E	17	+	-			CATGGCCCTGGTGTTTATCAAGTACCTCCCTGAATGGACTGCGTGGCTC**AT**CT**TGG**CTGTGATTTCAGTATATGGTAAAACCCAAGACTGATAATTTGTT	FokI
			1	TTG>CT**A**	-1, +1	CATGGCCCTGGTGTTTATCAAGTACCTCCCTGAATGGACTGCGTGGCTC**AT**CCT**AG**CTGTGATTTCAGTATATGGTAAAACCCAAGACTGATAATTTGTT	
			2	TTG>CT**A**; GCG>G**A**G	-1, +1; +9	CATGGCCCTGGTGTTTATCAAGTACCTCCCTGAATGGACTG**A**GTGGCTC**AT**CCT**AG**CTGTGATTTCAGTATATGGTAAAACCCAAGACTGATAATTTGTT	

Clone generation and quality control

Generation of single cell iPSC clones requires a series of steps. First, the WT parental iPSC line is grown without MEF feeders for 24-48 hours until roughly 60-70% confluent. These cells are then collected and electroporated with plasmids that express GFP and Cas9, and the gRNA. In addition, the WT and mutant ssODN repair templates are also mixed with the plasmids for electroporation. After electroporating 2 million iPSCs per reaction, with at least four to six reactions per electroporation totaling 8 to 12 million cells, the iPSCs are allowed to recover for two days to allow for GFP expression. GFP positive cells (GFP+) are then sorted by

fluorescence activated cell sorting (FACS) to select for GFP+ cells, which also express Cas9. The GFP positive cells are sorted into two groups, GFP^{hi} and GFP^{low}, based the level of expression of GFP (and therefore Cas9) (**Figure 2.3).**

Once sorted, iPSCs expressing Cas9 are then plated as single cells onto 10cm dishes with MEF feeders. The cells are then allowed to grow into individual colonies for 12-16 days, or until the colonies are large enough to be manually picked off the plate and placed into individual 96-well plates with MEFs. After allowing the isolated clones to grow until confluent, they are passaged and replicated once more into 96-well plates. The remaining cells are then harvested for analysis of mutation incorporation.

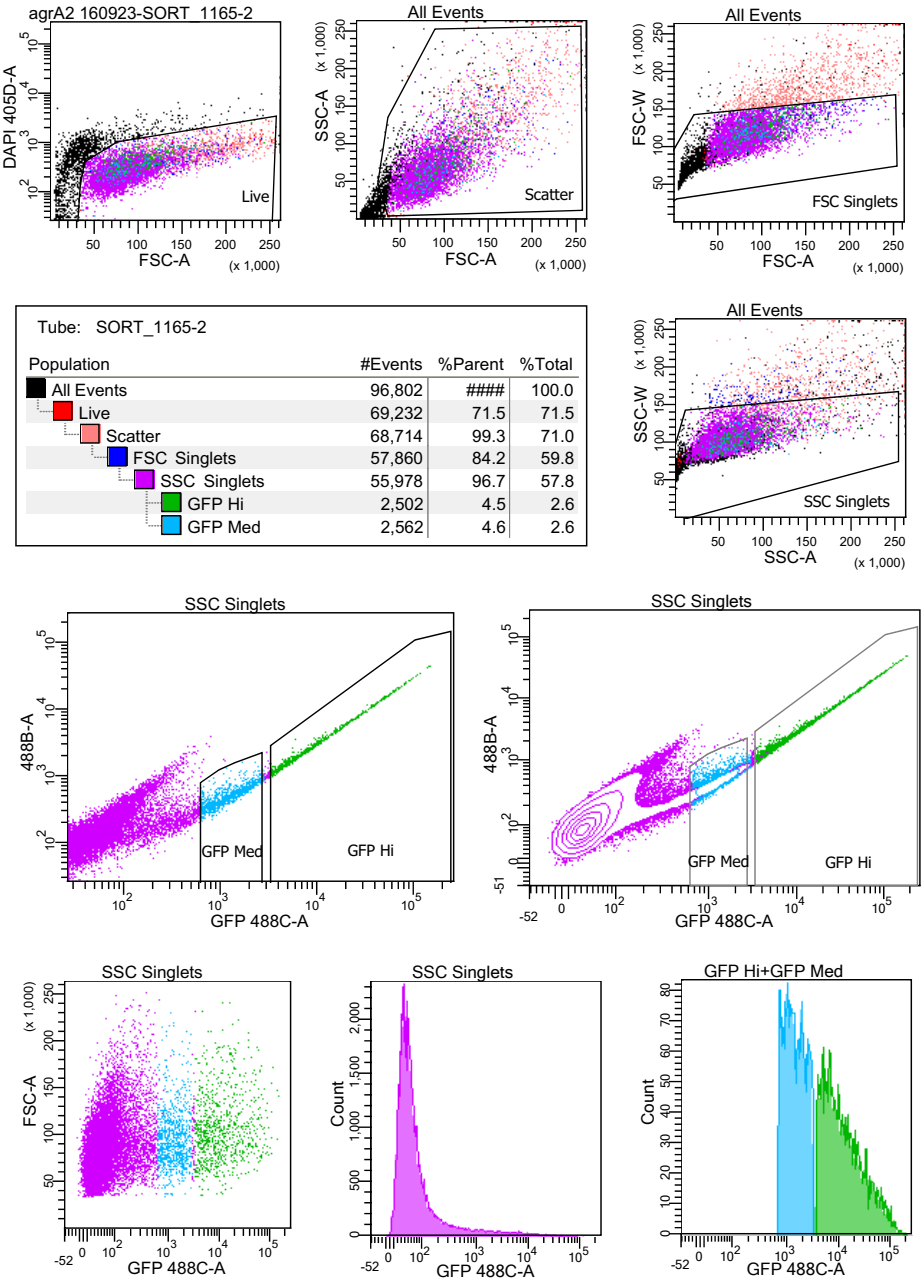

Figure 2.3. FACS of GFP+ iPSCs into GFP^{hi} and GFP^{low} subpopulations. Shown is a representative FACS sort for a given electroporation. iPSCs are sorted using DAPI dead cell exclusion, and subsequently gated for live single cells. Gates are then drawn to isolate two subpopulations of GFP+ cells, GFP^{hi} and GFP^{low}. These populations are sorted into individual tubes for subsequent plating as single cells.

The 96-well plates containing the leftover cell suspension are centrifuged to bring the cells to the bottom of the plate, at which point the cells are lysed for the isolation of genomic DNA (gDNA). Once the gDNA is purified, the targeted locus is amplified by PCR and the PCR products are digested with the restriction endonuclease to assess the presence or absence of the PAM-blocking mutation. Restriction fragment length polymorphisms (RFLP) fragments were then run on an agarose gel (**Figure 2.4**), and clones that were homozygous for the PAM blocking mutation were further analyzed by Sanger sequencing to look for the introduction of the pathogenic mutation. Cell lines that demonstrated the presence of homozygous PAM blocking silent mutations, without indels, and WT, heterozygous, or homozygous alleles at the pathogenic mutation site were subsequently expanded for further quality control.

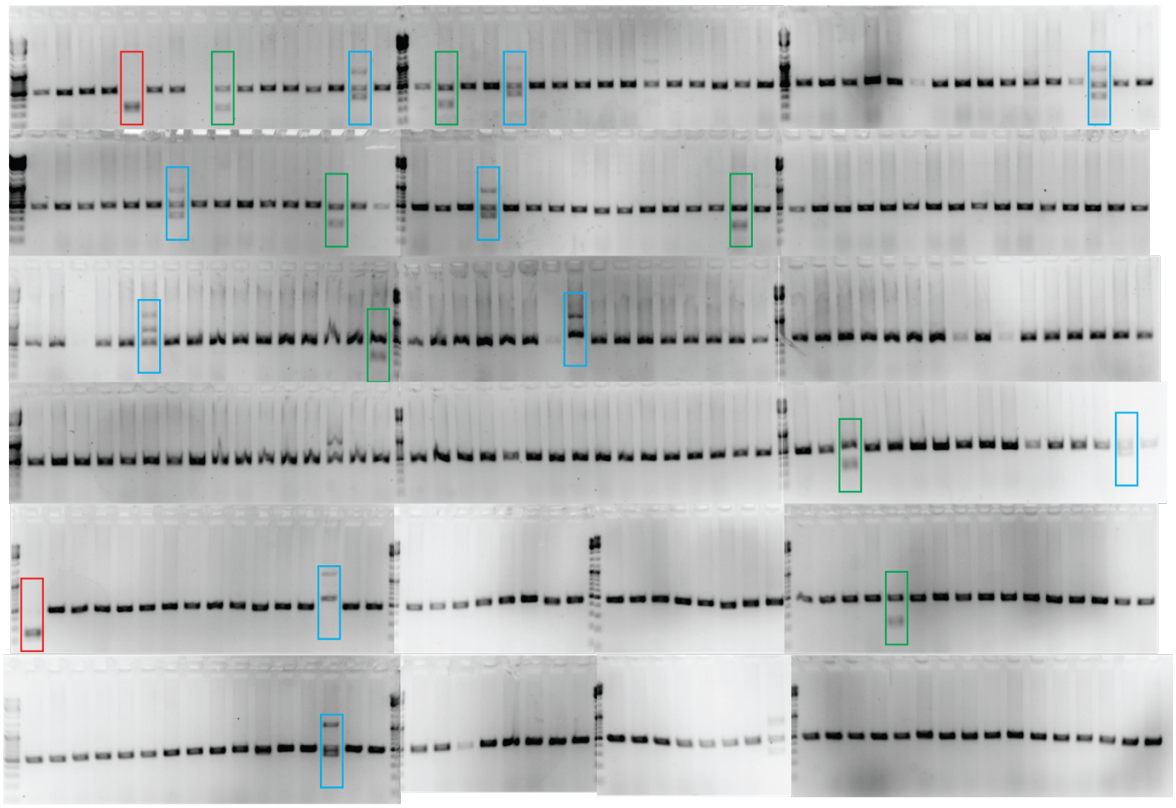

Figure 2.4. Representative RFLP screen from single experiment. Shown is a representative digest of roughly 300 individual clones from a single editing experiment. Red boxes show homozygous PAM blocking mutation integration, Green boxes show heterozygous PAM blocking integration, while Blue boxes demonstrate aberrant editing.

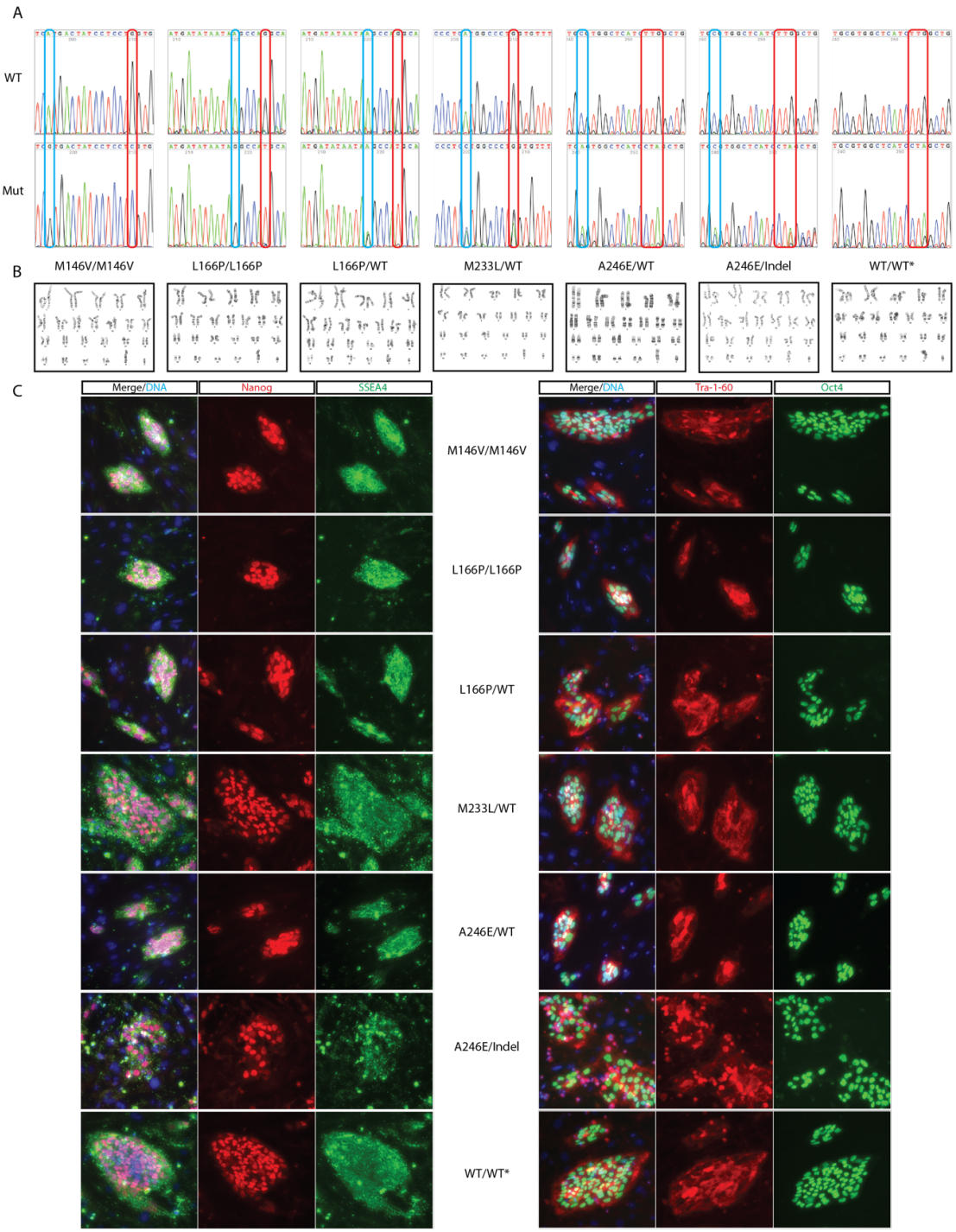

Figure 2.5. Edited iPSC lines quality control. A) Sanger sequencing traces, B) karyotype, and C) pluripotency staining for all edited lines. Red boxes highlight PAM blocking mutations, blue boxes highlight pathogenic mutations.

Each cell line that possessed an accurate editing event was then subject to a series of quality control measures, including a copy-number variant (CNV) assay to quickly determine the copy number of chromosome 20. Trisomy 20 is a common occurrence in iPSCs as it provides a growth advantage (Gaztelumendi and Nogués, 2014; Lefort et al., 2008), and is a phenomenon that our lab frequently observes with our WT iPSC line. Unfortunately, the genome editing events described here were not immune to aneuploidy, as numerous cell lines with accurate HDR exhibited trisomy 20. In addition, we occasionally lost cell lines to other aneuploidies, such as trisomy 1 or trisomy 12 upon karyotype testing. However, we were still able to generate several mutant and edited WT (harboring the PAM blocking silent mutation, but WT at the pathogenic mutation locus), that had normal karyotypes, and maintained pluripotency markers (**Figure 2.5**). Several cell lines unfortunately had accurate editing and normal karyotype, but did not differentiate well into neurons. Oftentimes these cells preferentially differentiated into glial-like cells instead of neurons, and were therefore eliminated from further analysis. Of note, one cell line with the L166P heterozygous mutation was trisomy 17, but happened to differentiate into neurons quite well. This cell line will be included in the analysis in Chapter 4, however this caveat should be considered when interpreting the data, and will be noted throughout the analysis.

CHAPTER III: Tau non-specifically transfers from donor to recipient neuron *in vitro* via macropinocytosis

Background and rationale

Tau pathology closely correlates with disease severity in AD patients (Arnold et al., 1991; Braak and Braak, 1991; Braak et al., 2011). As AD progresses, neurofibrillary inclusions, initially confined to a local region in the entorhinal cortex, spread to distant regions of the brain along anatomically connected pathways. This suggests that tau could propagate from neuron to neuron, effectively spreading the pathology to previously healthy regions of the brain and promoting disease progression.

As a result, there have been a series of studies aimed at showing that tau does in fact propagate. However, these studies have been restricted to non-human cell lines (Frost et al., 2009a; Holmes et al., 2013), human non-neuronal cell lines (Holmes et al., 2013; Kfoury et al., 2012; Michel et al., 2014; Sanders et al., 2014), and transgenic mice (Clavaguera et al., 2009; de Calignon et al., 2012; Dujardin et al., 2014b; Iba et al., 2013; Liu et al., 2012; Sanders et al., 2014; Yanamandra et al., 2013). Similar results have recently been published for other neurodegenerative proteinopathies, demonstrating that α-synuclein and huntingtin can spread from neuron to neuron in Parkinson's (Luk et al., 2012) and Huntington's (Pecho-Vrieseling et al., 2014) disease respectively. This supports the idea that pathologic

protein entities like α-synuclein, huntingtin, and tau can spread within the brain and contribute to disease progression. As such, these processes could provide a pharmacological target by therapeutically neutralizing the toxic species or the propagation pathways that spread these species to healthy brain regions. Indeed, a number of groups have attempted to elucidate the cellular mechanisms that underlie tau spreading (Chai et al., 2012; Dujardin et al., 2014b; 2014a; Holmes et al., 2013; Karch et al., 2012; Lee et al., 2012; Mohamed et al., 2014; Pooler et al., 2013; Saman et al., 2012; 2014). However, these studies have failed to agree on the pathway(s) that mediate the exit and entry of tau from the donor to the recipient cell in the context of disease. Mechanisms of tau secretion that have thus far been proposed include vesicle associated (exosomal) release (Kim et al., 2010a; 2010b; Lee et al., 2012; Saman et al., 2012; 2014), non-vesicular ("unconventional") release (Chai et al., 2012), and synapse mediated release (Pooler et al., 2013). Fewer studies have attempted to characterize tau uptake, but different mechanisms have been proposed including the involvement of an active endocytic process (Frost et al., 2009b; Guo and Lee, 2011; Wu et al., 2013), possibly mediated by heparan sulfate proteoglycan (HSPG) dependent macropinocytosis (Holmes et al., 2013). Nevertheless, these studies were all executed in model systems that significantly differ from disease relevant human cortical neurons. It is, therefore, still unclear whether these results translate well to humans.

We sought to provide better insights into the mechanism of tau spreading by generating a transgenic iPSC model system that will allow for the tracking of tau between iPSC-derived human cortical neurons. Our goal was to faithfully observe tau spreading using human cortical neurons, and to then elucidate the mechanism using pharmacological intervention to characterize the several cellular processes involved in the release and uptake of tau.

Preliminary studies in a human-mouse co-culture system highlight the need for non-physiologic conditions

During my rotation project, I developed a co-culture system utilizing WT human cortical neurons and mouse hippocampal neurons to study the transfer of tau between these neurons. The rationale behind this experiment was that human and mouse tau would be readily distinguishable from each other by taking advantage of human and murine specific tau antibodies (Kosik et al., 1989). Furthermore, transgenic mice expressing a ubiquitous GFP (Giel-Moloney et al., 2007) were readily available in the lab. After optimizing the conditions for co-culturing mouse hippocampal neurons and human cortical neurons, I analyzed three-week-old neurons by immunofluorescence, using a human specific tau antibody (HT7), specifically looking for the presence of human tau within GFP^+ mouse hippocampal neurons (Figure 3.1A and B). However, as these cells expressed cytosolic GFP, and did not label the plasma membrane, it proved difficult to distinguish intracellular and

extracellular compartments, preventing faithful determination of tau spreading. To circumvent this, we next utilized non-transgenic WT mice, and labeled mouse hippocampal neurons with an antibody to the murine specific neuronal cell surface marker L1 (N-CAM L1) (Lindner et al., 1983). Though I was able to distinguish the recipient cell border, I still failed to observe sufficient numbers of human tau entities within recipient mouse neurons, likely due to the low expression of tau in the donor cells (**Figure 3.1C and D**).

Lessons learned from these preliminary experiments using human-mouse co-cultures guided the direction of my research proposal, leading to the establishment of the donor/recipient co-culture system described in Chapter 2. This system uses a dox-inducible overexpression system to control the expression of fluorescently labeled tau transgenes. We turned to overexpression with the hope that increasing the protein levels of tau, so that we might increase the limit of detection of donor tau by immunofluorescence. Furthermore, it has been suggested that tau transfers trans-synaptically (Liu et al., 2012; Pooler et al., 2013), so we decided that an all human system would increase our chance of observing tau spread, as there was no evidence or guarantee that human and mouse neurons would form functional synapses between each other.

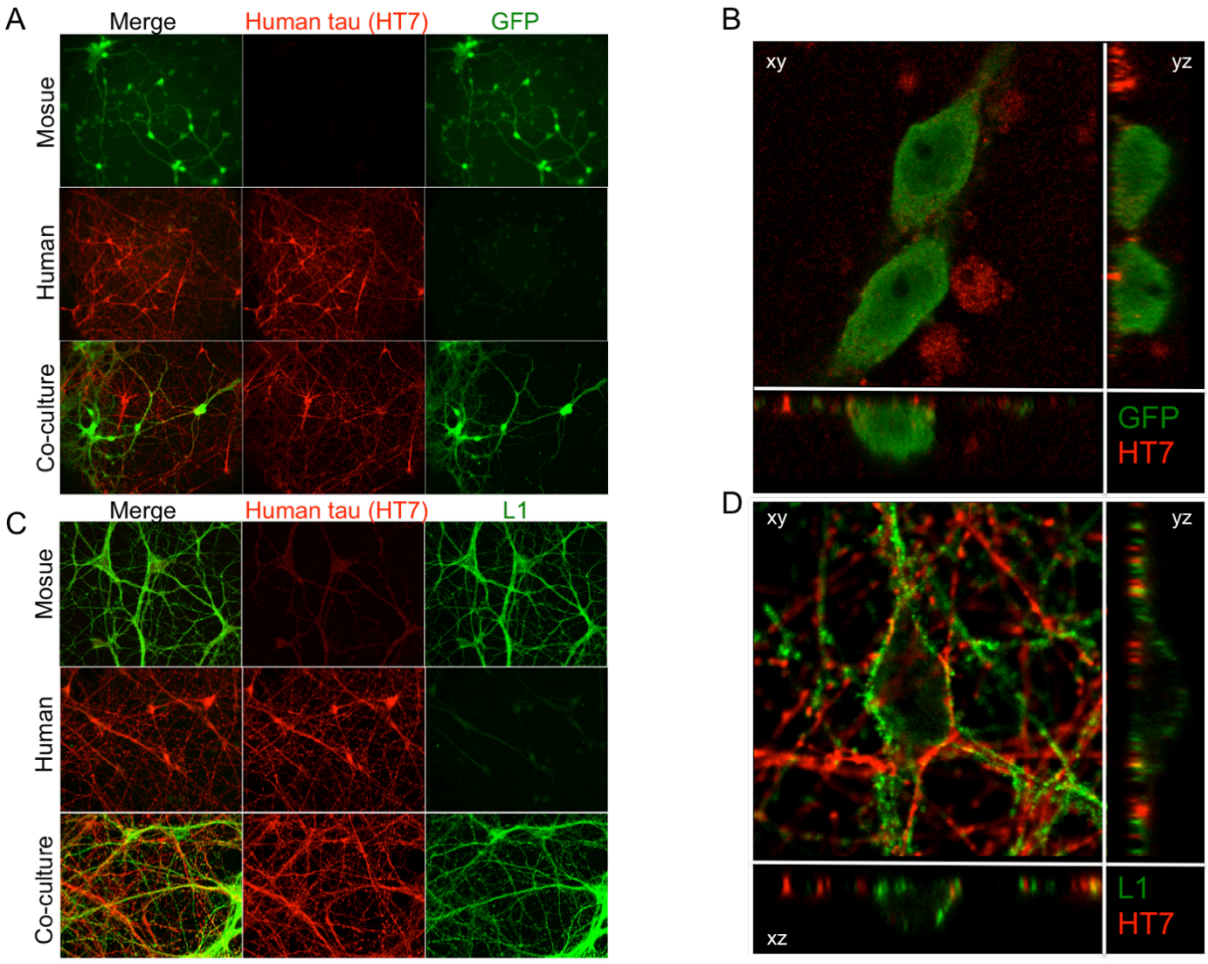

Figure 3.1: Human donor and mouse recipient co-culture model. Human iPSC-derived cortical neurons were co-cultured with mouse hippocampal neurons from either ROSA26-eGFP mice (**A, B**), or CD1 WT mice (**C, D**). **A** and **C** represent two-dimensional images of mouse, human and co-cultures **B** and **D** are representative orthogonal views of confocal images of co-cultures showing an optical plane on the level of mouse cell bodies. All cultures were stained with antibodies against human tau HT7, and either GFP (**A, B**) or L1 (**C, D**).

Alternative approaches to studying tau spreading

Concurrent with our genome editing efforts, we decided it would be prudent to consider alternative experimental paradigms to examine spreading. Because our lab has effectively used lentivirus delivery systems to overexpress transgenes as well as shRNAs in mouse DRGs to elucidate mechanisms of neurodegeneration, we decided to try using lentivirus to overexpress mCherry tagged tau transgenes into WT, human cortical neurons. For this purpose, a series of viruses that express GFP followed by a P2A sequence and the mCherry tagged tau transgenes were generated. The goal of these lentiviral experiments was to infect neurons at a low multiplicity of infection (MOI) such that only about half of the neurons are infected. The infected neurons would then be doubled labeled with GFP and mCherry, while the uninfected neurons would serve as unlabeled recipient cells. Should spreading of tau occur, it could be visualized as mCherry single positive neurons (**Figure 3.2A**).

Figure 3.2: Lentiviral over-expression of tau. A) Schematic of a neuron infected with a lentivirus expressing a GFP-P2A-mCherry:Tau (Yellow), with tau spreading to an uninfected, unlabeled neuron. B) Immunofluorescence images of cultures infected with lentivirus expressing GFP-P2A-mCherry, GFP-P2A-mCherry:FL-WT or GFP-P2A-mCherry:RD-WT at ~2MOI. 20x images showing mCherry single positive neurons. Stained with anti-RFP (Red) and anti-GFP (Green). C) Quantification of sorted neurons infected with the GFP-P2A-_ viruses indicated.

A

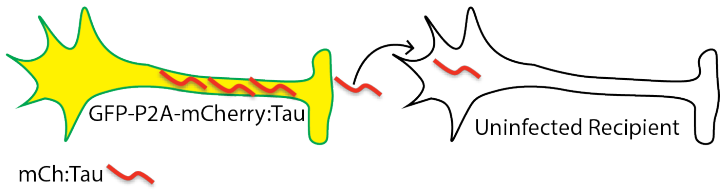
GFP-P2A-mCherry:Tau
Uninfected Recipient
mCh:Tau

B

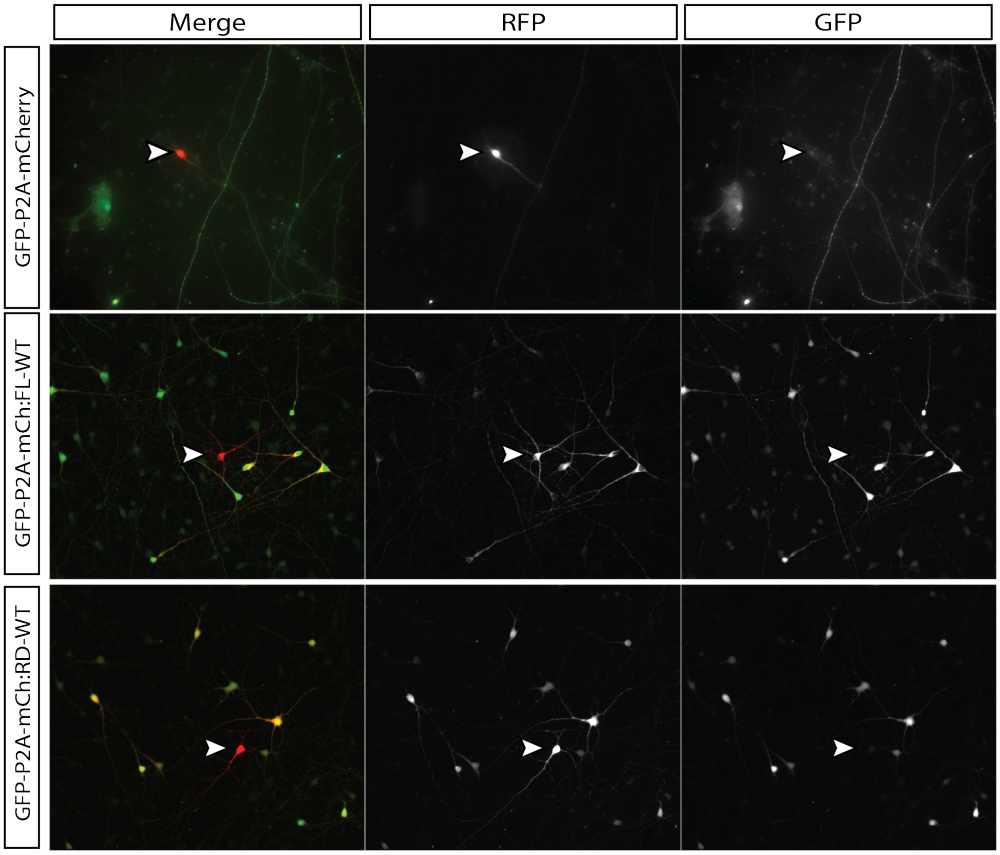
Merge
RFP
GFP
GFP-P2A-mCherry
GFP-P2A-mCh:FL-WT
GFP-P2A-mCh:RD-WT

C

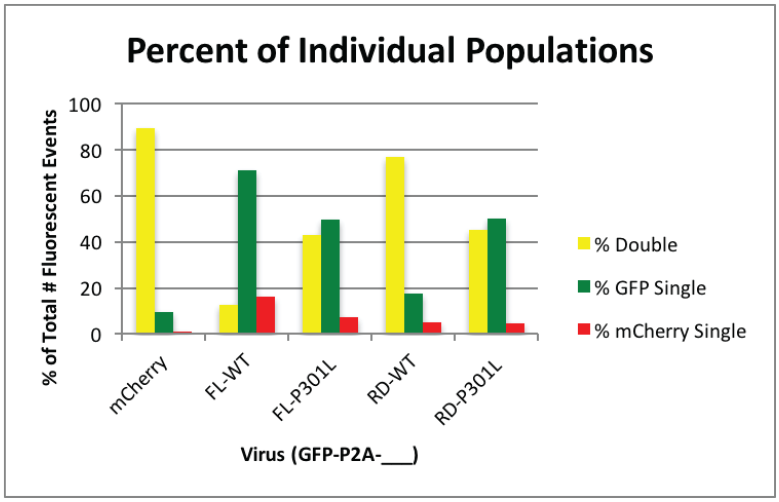
Percent of Individual Populations
% of Total # Fluorescent Events
100
80
60
40
20
0
mCherry
FL-WT
FL-P301L
RD-WT
RD-P301L
Virus (GFP-P2A-___)
% Double
% GFP Single
% mCherry Single

Initially, it was very surprising to see that the viruses expressing mCherry tagged tau showed a small percentage of cells that were only positive for mCherry, and not GFP, possibly indicating that tau was in fact spreading in this paradigm (**Figure 3.2B**). However, this first experiment was performed without the proper control, a GFP-P2A-mCherry virus without any tau. Upon repeating the experiment with the proper control, the mCherry only virus also showed some neurons that were singly positive for mCherry (**Figure 3.2B**). The challenge then became to rule out the presence of any viral transgene in these single positive cells, as it was possible that these mCherry single positive cells either had an incomplete incorporation of the virus, or the virus randomly mutated the transgenes, inactivating GFP. After discussing a number of ways to do this, we decided to FACS sort the cells to look at the percentage of single positive cells. Unfortunately, the sorting experiment demonstrated that this experimental paradigm was incredibly variable. Examining the percentage of cells of the three individual populations (GFP+, mCherry+, and GFP+/mCherry+) for each virus, it was clear that there was no consistent trend in the number of cells within each population in each infection (**Figure 3.2C**). While the experiment showed that there was in fact more mCherry:FL-WT-tau single positive cells compared to the mCherry only condition (16.13% vs 1.13%), it also showed that the percentage of GFP single positive cells was incredibly variable amongst all five transgenes tested (mCherry only, FL-WT, FL-P301L, RD-WT, RD-P301L; 9.57%, 71.1%, 49.4%, 17.77%, 50.16% respectively), highlighting that the lentivirus

is highly unpredictable, and may be randomly inactivating or mutating the transgenes (**Figure 3.2C**). As a result, we concluded that this paradigm was too variable to continue forward with it as a method to study tau spreading.

Tau spreads from donor to recipient neuron as efficiently as the control

Despite the background of the donor cell lines not being a full tau knockout as highlighted in Chapter 2, I continued to generate neurons from these lines with the intention of co-culturing donor and recipient cells to observe spreading. Donor and recipient iPSCs were induced alongside each other for 30-36 days, until they formed immature NPCs. At this point, donor and recipient NPCs were plated together at a donor to recipient ratio of 2:1. Initial experiments had demonstrated that as neurons mature (50-60 days), their ability to respond to doxycycline diminished based on the epifluorescence of mCherry (data not shown). As such, two days after plating NPCs, doxycycline was added to the culture media at 1 μg/mL, and was maintained by replacing half of the media every two to three days.

Previous work by Kim Olsen, Dominik Paquet, and Dylan Kwart in the lab demonstrated that neurons only begin to show the characteristics of mature neurons around DIV60-70, based on electrophysiological properties of the neurons (**data not shown**). As a result, all experiments were allowed to mature for at least 60 days, to ensure the formation of functional synapses.

After optimizing the cell culture conditions and doxycycline dosing, co-cultures were fixed and imaged using confocal microscopy to generate a three-dimensional image of cell bodies. I specifically focused on cell bodies because without super high-resolution imaging, I would not be able to differentiate donor tau within a recipient axon from two fasciculated donor and recipient axons or dendrites. Therefore, larger volume cell bodies were studied as the resolution of the confocal microscope would allow for the detection of mCherry puncta within the labeled membrane of the recipient cell.

In co-cultures with mCherry tagged FL-WT tau, I was in fact able to detect rare instances where there were mCherry+ puncta residing within a memYFP recipient cell bodies (**Figure 3.3A**). This event seemed to occur at a rate of roughly 10% of all counted recipient cells (**Figure 3.3A and C**). This was initially very encouraging evidence that tau spread between neurons. However, examination of the control cell line expressing the mCherry fluorophore alone showed that mCherry spread to recipient cells just as well as mCherry tagged tau (**Figure 3.3A and C**). In fact, it spread perhaps even better than tau (15% vs. 10%), and even resulted in some cells appearing to have space filling quantities of the mCherry fluorophore (**Figure 3.3B**). These results suggest that the spreading being observed in these co-cultures is not specific to tau, and may in fact be a generalized process such as bulk endocytosis. While this is not a far-fetched conclusion, to prove this was a non-specific process would have required the generation of several additional control

lines, including lines expressing tagged proteins of variable size, structure, phosphorylation state, charge, and subcellular localization. Another interpretation of these results is that the mCherry fluorophore is actually facilitating the transfer of tau, and the spreading observed is therefore unrelated to the potential disease mechanism. These interpretations, coupled with the fact that the inducible expression system only allowed for continuous expression of tau starting at the NPC stage of differentiation, led me to pursue a new method to model tau spreading in iPSC-derived neurons.

Figure 3.3. **Tau and mCherry CTL spread into recipient neurons**. A) Three representative images of memYFP WT recipient cells with mCherry+ staining within the recipient cell membrane (arrows) for FL-WT and mCherry CTL donor co-cultures. Immunolabeled with anti-GFP (green), anti-mCherry (red) and nuclei (blue), 63x orthogonal views in XZ and YZ planes. B) Representative image of mCherry CTL co-culture with memYFP WT recipient cell displaying space filling mCherry staining. C) Quantification of the rate of spreading in the mCherry CTL and FL-WT co-cultures. N=32 recipient cells counted for mCherry CTL, and n=78 recipient cells counted for FL-WT in two experiments. Error bars represent the standard error of the mean (SEM).

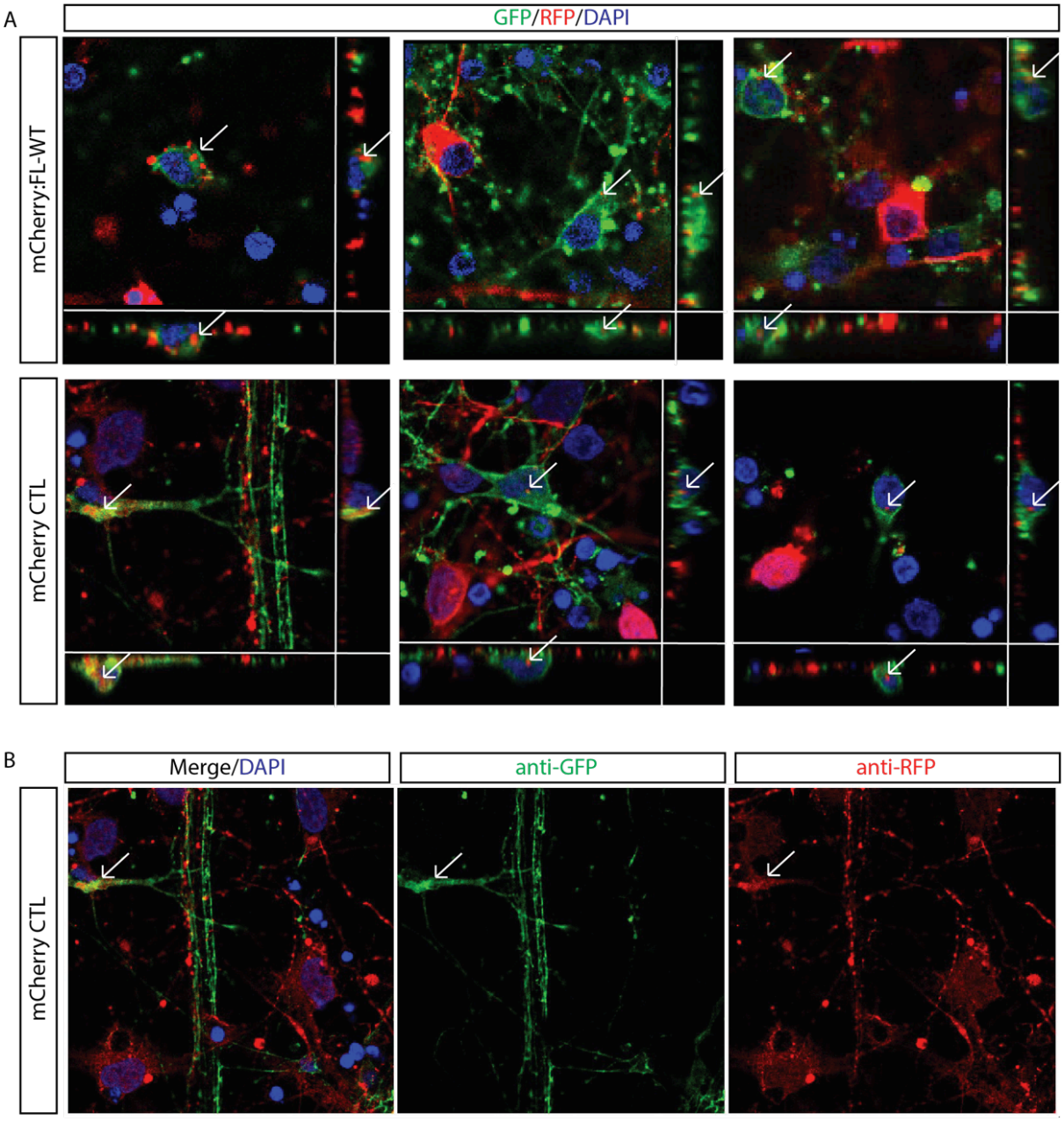
A
GFP/RFP/DAPI
mCherry:FL-WT
mCherry CTL
B
Merge/DAPI
anti-GFP
anti-RFP
mCherry CTL
C
Percent Spreading
% memYFP+ cells with RFP+ cytosolic puncta
25
20
15
10
5
0
mCherry
FL-WT

Recombinant tau aggregates are macropinocytosed in HEK293 cells

Because the donor and recipient co-culture method for studying the spread of tau posed a number challenges that would be difficult to overcome, I turned to using recombinant tau aggregates to investigate the mechanism of tau uptake in human neurons. The ability to generate purified recombinant tau has been described and utilized for over a decade now (Barghorn et al., 2005). Fortunately, numerous protocols have been established to induce recombinant tau preparations to aggregate *in vitro*. The most common method requires a simple incubation with a poly-anionic molecule, such as heparin. Thankfully, my committee member and rotation advisor, Dr. David Eliezer, offered to share recombinant tau protein that I generated in his laboratory to use in the subsequent experiments.

Table 3.1 Pharmacological inhibitors of cellular uptake mechanisms.

Target Pathway	Compound
Clathrin Endocytosis	Pitstop 1/2
Macropinocytosis	Cytochalasin-D
	Latrunculin
	Heparin
	Sodium Chlorate
	EIPA
Proteasomal Degradation	Lactacystin

The goal of these experiments was to use pharmacological inhibitors of various cellular uptake mechanisms to prevent, or enhance recombinant tau uptake, in order to pinpoint how tau aggregates enter neurons. These pathways included clathrin mediated endocytosis, and macropinocytosis (**Table 3.1**). Furthermore, I also wanted to test whether tau aggregates would get degraded by the proteasomal degradation pathway after uptake, by treating cells with lactacystin (**Table 3.1**).

Following the methods of a recently published protocol (Holmes et al., 2013), I used Western blotting to confirm the successful aggregation of FL-WT tau preparations by heparin incubation (**Figure 3.4A**). After blotting for total tau (K9JA) under reducing and non-reducing conditions, a streak of tau appears in the aggregate preparation, indicating the successful aggregation of tau into dimers, trimers, and larger oligomers and fibrils (**Figure 3.4A**). Furthermore, these aggregates return to monomeric form after exposure to reducing agent (BME), suggesting that these aggregates form disulfide bridges (**Figure 3.4A**)

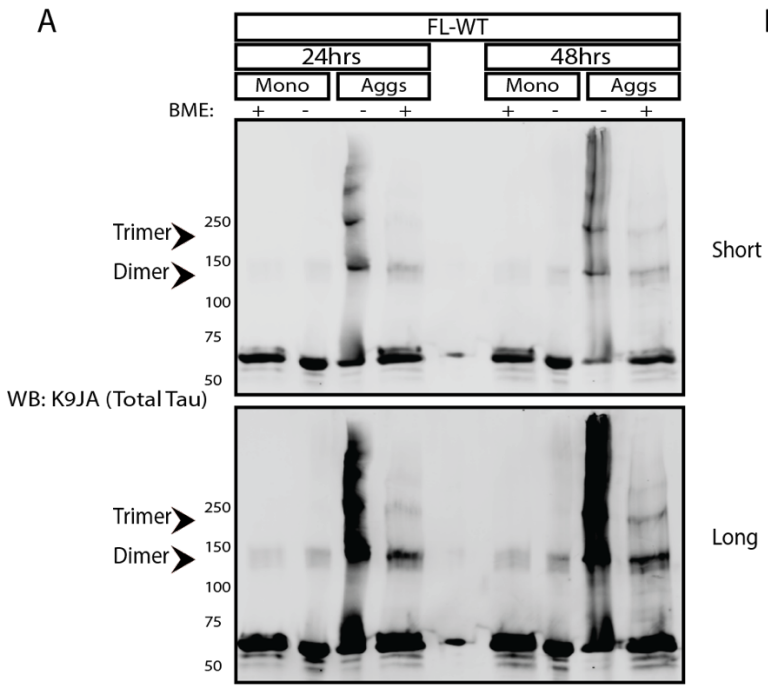

Figure 3.4. Characterization of recombinant tau aggregates. A) Western blot for total tau (K9JA) of recombinant FL-WT tau. Recombinant protein was incubated in the presence or absence of heparin to generate aggregates (Aggs) and monomers (Mono) respectively. Preparations were incubated with heparin for either 24 or 48hrs, under reducing and non-reducing conditions (+/- BME).

Prior to testing these aggregates and their mechanism of uptake in neurons, I first wanted to confirm that these aggregates were in fact capable of seeding and inducing aggregation of soluble, monomeric tau *in vitro*. Recent studies have demonstrated that tau aggregates induce monomeric tau to misfold and aggregate, much like prion protein (PrP) in CJD and Scrapie (Sanders et al., 2014). Importantly, the injection of brain homogenates containing tau aggregates from affected transgenic mice are capable of transmitting its pathological conformation to

unaffected WT animals, confirming tau aggregates possess bona fide prion-like properties (Sanders et al., 2014). Recently, an *in vitro* human embryonic kidney 293 (HEK293) cell culture tool was generated that acts as a biological sensor for tau aggregation potential (Holmes et al., 2014). These cells express a CFP:YFP FRET pair tagged to a P301S mutant tau RD in the cytosol. Upon introduction of tau seeds, the RDs aggregate and the CFP:YFP FRET pairs are brought into close proximity, allowing for the detection of a FRET signal. The RD aggregates are readily visible under a fluorescent microscope.

I took advantage of the tau biosensor cells to test whether our aggregates were capable of seeding soluble tau. Importantly, I was only able to detect aggregation of CFP:YFP tagged RD when aggregates were pre-incubated with liposomes (**Figure 3.5A**), demonstrating that the aggregates required liposomes, or at least some sort of lipophilic interaction, to access the cytosol. In addition, aggregates consisting of only a RD was much more efficient at inducing aggregation that the FL-WT aggregates, suggesting a possible seeding barrier between FL tau aggregates and the soluble RD sensor (**Figure 3.5B**).

Having demonstrated that these aggregates can enter these biosensor cell lines, I performed a small scale pharmacological screen to assess the potential uptake mechanism using the inhibitors listed in **Table 3.1**. Interestingly, pretreatment of the biosensor cells with heparin or 5-N-ethyl-N-isopropyl-amiloride (EIPA), inhibitors of macropinocytosis, completely blocked intracellular aggregation of tau in

cells treated with the liposomal RD aggregate preparations (**Figure 3.6C**). In addition, cytochalasin-D and latrunculin, which partially inhibit micropinocytosis via inhibition of actin polymerization, reduced, but did not completely inhibit aggregate formation. These data support and confirm previously reported findings that macropinocytosis, and specifically heparan sulfate proteoglycans, HSPGs, mediate the entry of tau fibrils into HEK293 cells (Holmes et al., 2013).

Figure 3.5. Tau aggregates require liposomes and bulk endocytosis for seeding. A) HEK293 Tau-Biosensor cell line treated with recombinant tau preparations for 24 hrs at 50nM, with and without liposomal pre-treatment of tau preps. B) Enlarged image of tau FL and RD aggregates with liposomes demonstrating seeding. C) Pretreatment with inhibitors of cellular uptake and proteasomal degradation for 24 hrs prior to RD aggregate treatment with liposomes. All images shown are CFP and YFP epifluorescence, 20x. FRET signal not reported.

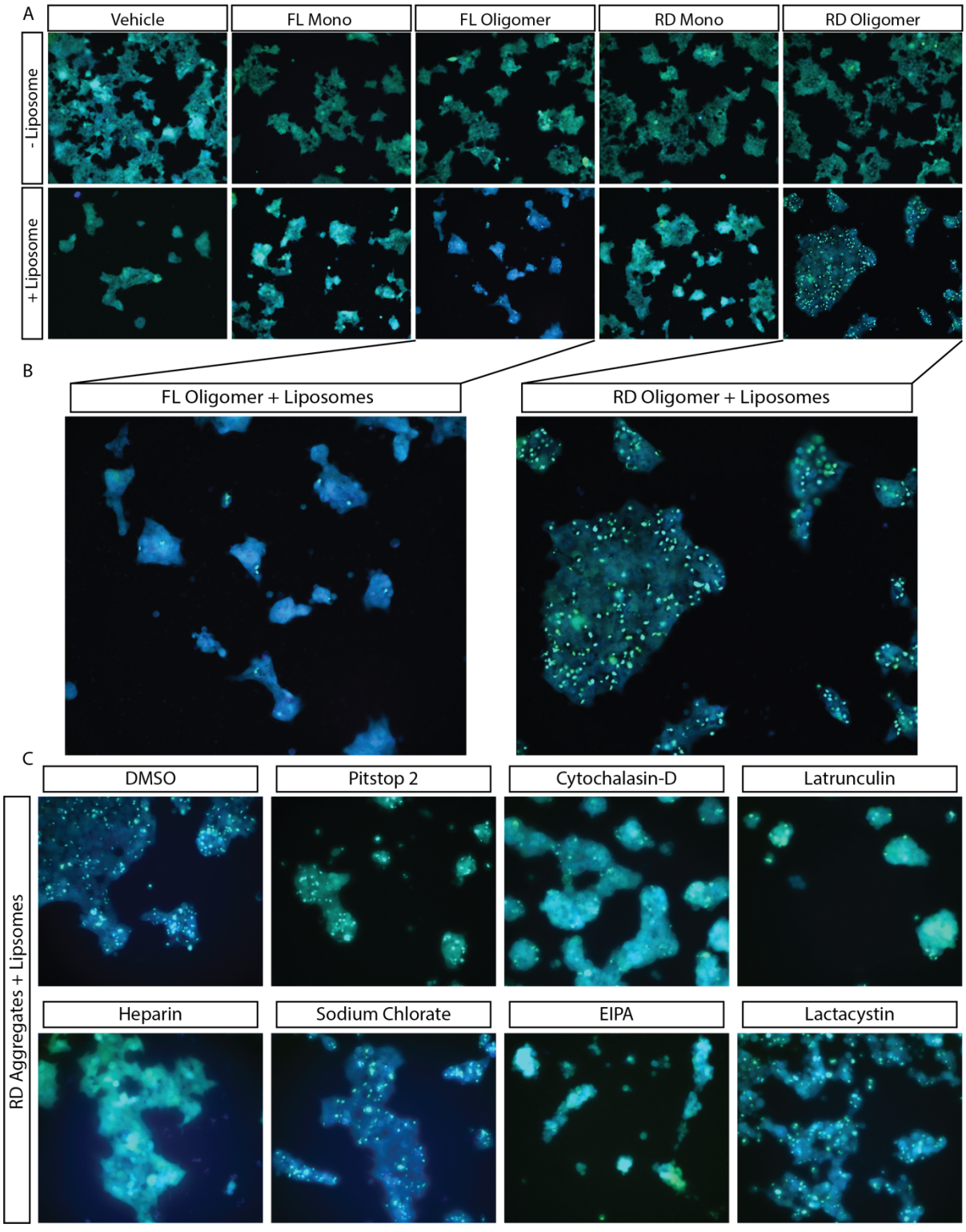
A
Vehicle
FL Mono
FL Oligomer
RD Mono
RD Oligomer
- Liposome
+ Liposome
B
FL Oligomer + Liposomes
RD Oligomer + Liposomes
C
RD Aggregates + Lipsomes
DMSO
Pitstop 2
Cytochalasin-D
Latrunculin
Heparin
Sodium Chlorate
EIPA
Lactacystin

I next wanted to determine whether this approach could also be applied in iPSC-derived neurons. Specifically, I set out to test if exogenous aggregates would be taken up by neurons and, if so, whether they would induce a conformational change in endogenous tau. Such a system would allow me to test and confirm whether macropinocytosis also mediated uptake of tau aggregates in human cortical neurons. However, this required a method to detect aggregated cellular tau, and discriminate aggregated cellular tau from the recombinant tau used for seeding. For this purpose, I took advantage of an antibody that specifically recognizes misfolded or aggregated tau (MC1) (Jicha et al., 1997). Because the MC1 antibody recognizes two epitopes on the tau protein when they come into close proximity, one in the N-terminus, and one more C-terminal in the third RD (**Figure 3.6A**), it should not cross-react with recombinant tau aggregates as they are composed of only the RD. I confirmed this specificity by Western blot, demonstrating that the MC1 antibody only recognizes FL tau (**Figure 3.6B**). Unfortunately, the MC1 antibody only stained neuronal cultures incubated with FL aggregates, and not RD aggregates (**Figure 3.6C**). Because the RD aggregates were more efficient than the FL aggregates at aggregating endogenous tau in 293 cells, it is probable that the signal in neurons incubated with FL aggregates is caused by recognition of the recombinant protein by the MC1 antibody. If these aggregates were capable of seeding endogenous tau produced by the neurons and inducing conformational change, then I would expect that cultures seeded with RD aggregates would have also been stained with the

MC1 antibody. Because this was not the case, I suspect that these aggregates are not capable of entering neurons to induce a conformational change in endogenous tau. Therefore, these neurons are not fit to study the mechanism of tau uptake and seeding using the aggregates I produced.

Conclusions

In this chapter I explored tau spreading, a potential AD disease mechanism. My initial goal was to establish a model that reproducibly exhibits tau spreading in human iPSC-derived cortical neurons. Once established, this model would then be used to determine the mechanism of tau spreading using pharmacological inhibitors of various cellular release and uptake mechanisms.

Preliminary studies with human and mouse co-cultures demonstrated the need for appropriately labeled donor and recipient cell lines in order to track tau as it moves from neuron to neuron. Furthermore, these studies highlighted the need for inducible overexpression of tau in order to increase the probability of observing tau spreading, and temporally control the expression of tau so that I may reliably determine the mechanism of spreading. An alternative approach to studying tau spreading using lentiviral overexpression of labeled tau yielded results that demonstrated the highly unpredictable nature of lentiviral infection, as neurons infected with a virus expressing GFP followed by a P2A sequence and mCherry tagged tau not only showed GFP+/mCherry+ cells, but also a significant proportion

of GFP+ and RFP singly positive neurons. As such, I proceeded forward with the donor and recipient co-culture method I originally proposed.

Once optimized, these co-cultures demonstrated a low baseline of tau spreading from donor to recipient neurons, about 10%. However, the fluorophore control cell line also spread at a roughly equal rate as tau, indicating that the spreading observed was not specific to tau, and therefore likely a generalizable mechanism of uptake of random extracellular contents. Furthermore, the inducible system I designed unfortunately did not allow for the temporal expression of the fluorescently labeled tau, therefore making the model system unsuitable for direct modulation of tau spreading and determination of the spreading mechanism via pharmacological inhibition.

Figure 3.6. Recombinant tau aggregates cannot induce conformational change in endogenous tau. A) Schematic of tau protein with MC1 antibody epitopes. B) Western blot of FL and RD recombinant monomers and aggregates. Blotted for total tau (K9JA) and MC1. C) Immunostaining of memYFP WT neurons, DIV70, treated for 96hrs with 50nM vehicle, monomer and aggregates of both FL and RD, for MC1 (red) and GFP (green). Nuclei stained with Hoechst (Blue).

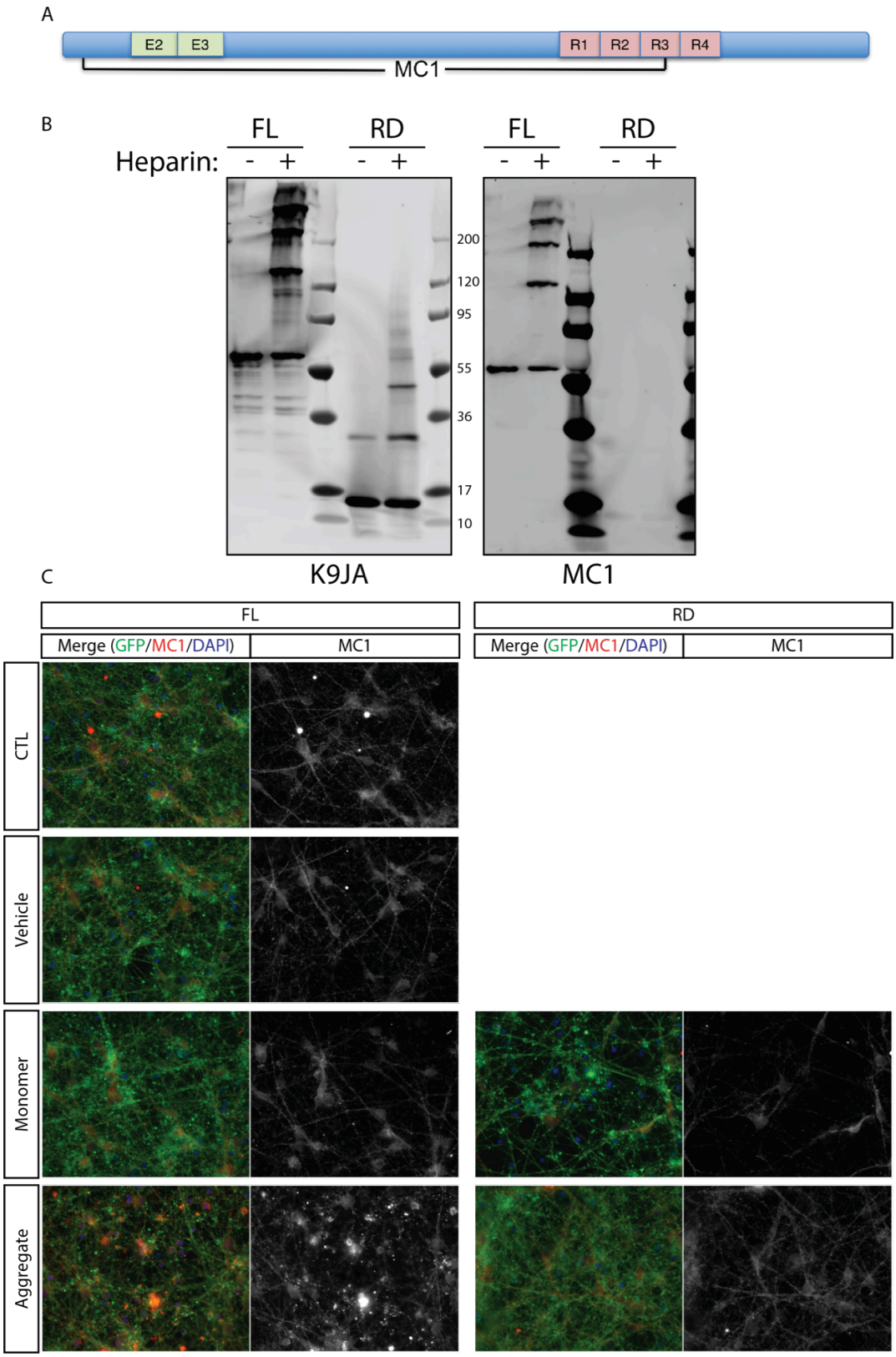
A
E2
E3
R1
R2
R3
R4
MC1
B
FL
RD
FL
RD
Heparin:
- + - + - + - +
200
120
95
55
36
17
10
K9JA
MC1
C
FL
RD
Merge (GFP/MC1/DAPI)
MC1
Merge (GFP/MC1/DAPI)
MC1
CTL
Vehicle
Monomer
Aggregate

I therefore turned to using recombinant tau preparations in order to hopefully study the uptake of tau aggregates *in vitro*. Initially, I characterized tau uptake in a recently generated HEK293-biosensor cell line to measure the ability of tau aggregates to induce seeding and conformational change of soluble tau. Aggregates prepared with liposomes were able to induce aggregation of the tau RD expressed in these biosensor cells, indicating that they were readily accessing the cytosol and inducing conformational change of previously normal tau. Upon pharmacological inhibition of macropinocytosis, aggregates were incapable of seeding in these biosensor cell lines, confirming previous studies and supporting the hypothesis generated from the donor and recipient cell line data, that tau and other cellular products are being taken up by a non-specific bulk endocytic mechanism.

I then attempted to translate these findings to human iPSC-derived neurons. Unfortunately, in my hands tau aggregates were not able to seed endogenously expressed tau, therefore limiting my ability to determine the mechanism of entry into neurons as I did not have a functional assay. This does not preclude the possibility that these aggregates are gaining access to the intracellular compartment. However, it is clear that these aggregates were incapable of causing templated misfolding of endogenous tau in this experimental paradigm, which could reflect that the aggregates simply are not getting into the neurons, or are getting degraded in subcellular compartments upon entry, such as in the endosomal/lysosomal system.

Chapter IV: *PSEN1* FAD mutations impair γ-secretase function

Background and Rationale

The amyloid cascade hypothesis has been a widely accepted theory that describes the molecular pathogenesis of AD (Hardy and Higgins, 1992). Central to this hypothesis is the idea that Aβ, the major protein entity in amyloid plaques, is not only necessary for the development of AD, but also the initiator and key mediator of the downstream effects that follow Aβ deposition. For the last 25 years, this hypothesis has been widely supported, but has yet to be completely confirmed.

From a genetic viewpoint, it makes sense that Aβ would be central to the disease, as mutations in *APP* as well as *PSEN1* and *PSEN2*, which function in Aβ production, are all causal of FAD. Furthermore, mutations in *APP* generally cluster around the sites of APP processing by either BACE or γ-secretase, or promote aggregation of Aβ peptides (**Figure 4.1**) (Grant et al., 2007; Lazo et al., 2005; Van Dam and De Deyn, 2006; Weggen and Beher, 2012). On the flip-side, a missense mutation in the Aβ region of APP that protects against AD has now been described (Jonsson et al., 2012; Kero et al., 2013), supporting how critical Aβ is to the development of AD.

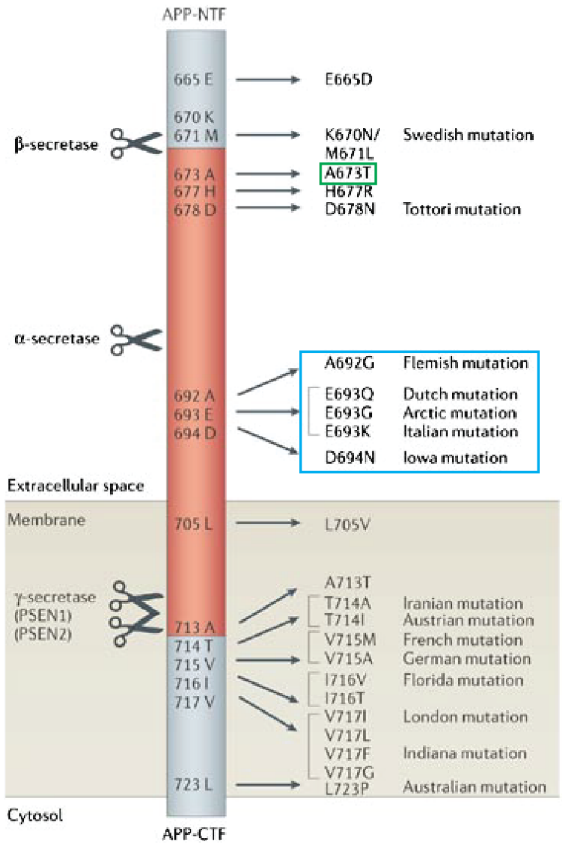

Figure 4.1. FAD mutations in APP. Schematic of mutations in APP that cause FAD cluster around the BACE and γ-secretase processing sites. Mutations within the Aβ fragment themselves do not alter processing of Aβ, but rather enhance aggregation (blue box). One mutation, A673T, is protective against AD (green box). (Figure reprinted with permission from (Van Dam and De Deyn, 2006)).

Interestingly, more than two-thirds of all FAD mutations are found in *PSEN1,* 228 in total, highlighting the importance of the production and processing of Aβ. PSEN1 is a multipass transmembrane aspartyl-protease of 467-amino acids, 121 of which are mutated in FAD (alzforum.org). PSEN1 is the catalytic component of the multiprotein γ-secretase complex. This multiprotein complex has numerous biological

functions in addition to the production of Aβ, including the cleavage of Notch1 to release the Notch intracellular domain (NICD) (De Strooper et al., 1999; Hartmann et al., 1999), and the cleavage of N-Cadherin (Marambaud et al., 2003) (Haapasalo and Kovacs, 2011). Importantly, PSEN1/γ-secretase performs its protease activity within the plasma membrane, designating it as an intramembrane cleaving protease (I-CLiP), and explaining its ability to process Aβ, which resides within the membrane, from β-CTF (Weihofen and Martoglio, 2003).

Initial insight into how PSEN1 and γ-secretase function in AD came from the demonstration that the enzyme complex acts to increase the amount of Aβ42 relative to Aβ40, or in other words increase the ratio of Aβ 42:40, in the diseased state (Borchelt et al., 1996; Citron et al., 1996; 1997; Duff et al., 1996; Klafki et al., 1996; Scheuner et al., 1996). These initial findings concluded that *PSEN1* mutations in FAD lead to the preferential generation of Aβ42, the longer and more aggregation prone Aβ species. Unfortunately, many interpreted these data to mean that *PSEN1* mutations were gain-of-function due to elevated production of longer Aβ species. However, these experiments were performed prior to a complete understanding of the mechanism of PSEN1/γ-secretase cleavage of β-CTF, and therefore a true designation of gain-, or loss-of-function could not be given. Shortly after these initial experiments, researchers began to collect data that suggested the opposite, that *PSEN1* mutations may result in a partial loss of function (Lewis et al., 2000; Song et al., 1999). One such study showed that FAD *PSEN1* mutations reduce Notch

processing (Song et al., 1999), while another showed that a known loss of function mutation in *PSEN1* that does not occur in humans, also increases the amount of Aβ42 relative to Aβ40 similar to FAD *PSEN1* mutations (Lewis et al., 2000), suggesting that the rise in Aβ42 is perhaps a consequence of decreased PSEN1 function.

In fact, as cellular models of FAD PSEN1 began to emerge, more evidence supported that these mutations may actually result in a partial loss of function because many mutations demonstrated that the increase in Aβ 42:40 could also be caused by decreases in Aβ40 (Bentahir et al., 2006; De Strooper, 2007). Furthermore, an FAD mutation was discovered in intron 8 at the splice acceptor site, along with a point mutation at the splice junction site between exons 8 and 10, resulting in the skipping of exon 9 (ΔE9) (Dumanchin et al., 2006; Perez-tur et al., 1995). Importantly, exon 9 is the site of autocatalytic cleavage of PSEN1 into its NTF and CTF, which is required for catalytic activity of PSEN1, and therefore supports the idea that loss of PSEN1 function may be critical to the development of FAD (Bentahir et al., 2006; Dumanchin et al., 2006; Perez-tur et al., 1995; Thinakaran et al., 1996). Interestingly, *PSEN1* knockout mice die shortly after birth due to severe skeletal and circulatory defects, which can be attributed to defects in Notch signaling (De Strooper et al., 1999; Hartmann et al., 1999; Shen et al., 1997). These results imply that *PSEN1* FAD mutations are not complete loss of function, but rather partial loss of PSEN1 function.

Nevertheless, the debate over *PSEN1* FAD mutation function has raged on. Fortunately, new insights reveal how PSEN1 processes APP (Takami et al., 2009). The study shows that PSEN1 initially performs an endopeptidase cleavage between either residue 50/49 or 49/48 of β-CTF, generating the AICD and Aβ49 or Aβ48. PSEN1 then goes on to create successive tri- or tetra-peptide carboxy-peptidase cleavages of Aβ49 and Aβ48 to ultimately create Aβ40 or Aβ38 respectively. Importantly, Aβ38 is created from a tetra-peptide cleavage of Aβ42, and Aβ40 is generated from a tri-peptide cleavage of Aβ43 (**Figure 1.2**). Both of these events occur during the fourth cleavage of Aβ by PSEN1. With this in mind, it becomes apparent that the cause for the increase in the ratio of Aβ 42:40 may be due to impaired function of PSEN1 during the fourth cleavage of β-CTF, resulting in increased Aβ42, and perhaps even larger species of Aβ like Aβ43, as well as decreased Aβ40 or Aβ38. In fact, the increase in Aβ42 initially observed in human serum and CSF (Scheuner et al., 1996), and transgenic mice (Citron et al., 1996; 1997; Duff et al., 1996), may all be explained by a partial loss of function in the processing of APP by PSEN1. Recently, an elegant biochemical analysis examined the processing of Aβ by several FAD *PSEN1* mutations, showing consistent impairment of the fourth enzymatic cleavage of β-CTF by these FAD mutations (Chávez-Gutiérrez et al., 2012). While the study showed a consistent lowering of Aβ38 and Aβ40, the levels of longer Aβ42 and Aβ43 varied. Furthermore, these experiments were performed in the background of a *PSEN1/PSEN2* double

knockout MEFs rescued with overexpressed WT or FAD mutant PSEN1, along with overexpression of β-CTF, highlighting the extreme artificial nature of the experimental system.

With these studies in mind, I decided to investigate the function of PSEN1 in iPSC-derived human cortical neurons. This approach allows us to study the mechanism of Aβ production in human neurons expressing physiologically relevant levels of γ-secretase and its substrates. As discussed in Chapter 2, I utilized recent advances in CRISPR/Cas9 genome editing to accurately introduce several FADS causing *PSEN1* mutations (*M146V, L166P, M233L* and *A246E*) into WT iPSCs. All of these mutations are reported to increase the ratio of Aβ 42:40. In addition, members of our lab demonstrated that the *M146V* mutation increased the Aβ 42:40 ratio in the parental iPSCs line I would use for introducing the other FAD *PSEN1* mutations (**Figure 4.2**) (Paquet et al., 2016). However, I intended to elaborate on their findings, and specifically describe how each mutation alters the production of each Aβ species (Aβ38, Aβ40, and Aβ42). This information, along with the total amount of Aβ produced, and the effects on other PSEN1 substrates such as Notch1 and N-Cadherin, would be informative in determining how FAD mutations in *PSEN1* affect its function.

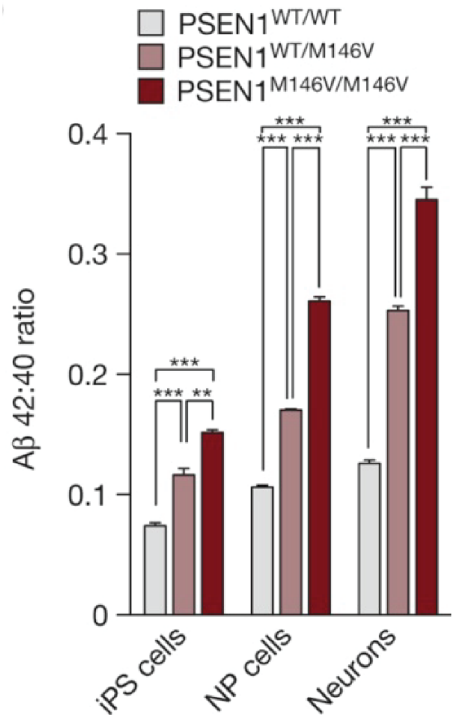

Figure 4.2. The *M146V* mutation causes a genotype dependent increase in the Aβ 42:40 ratio. Isogenic *PSEN1 M146V* mutant iPSCs demonstrate a mutation-load dependent increase in the ratio of Aβ 42:40 in iPSCs (DIV0), neural precursors (NPs, DIV34), and neurons (DIV72). Values represent mean (n=3 biological replicates) ± s.e.m. $^{**}P < 0.05$ and $^{***}P < 0.001$, one-way ANOVA (Reprinted with permission from (Paquet et al., 2016)).

PSEN1 mutations cause increases in Aβ42 and decreases in Aβ40 and Aβ38

Following generation of the isogenic iPSC mutant lines, I differentiated them into cortical neurons. Neurons from each mutation were grown alongside WT neurons in each experiment, in order to better quantify and compare the changes in Aβ production from experiment to experiment. Further, cell lines were divided into

three biological replicates on each plate. Neurons were differentiated for roughly three weeks after NPC plating, at which point media was completely changed, and allowed to condition for seven days. In each experiment, neurons were analyzed around day 60 (DIV 58-68). Each replicate was then harvested, collecting both supernatant and cellular lysates. Each supernatant was analyzed by an electrochemiluminescent (ECL) assay for Aβ38, Aβ40, and Aβ42, as well as sAPPα and sAPPβ. The total sAPP measurements were used to normalize samples for comparing Aβ levels across samples as well as experiments. The rationale for using total sAPP is that it is a measure of a soluble secreted protein.

Each of the FAD *PSEN1* mutations demonstrated significant increases in the Aβ 42:40 ratio (**Figure 4.3A**), and the Aβ 42:38 ratio (**Figure 4.3B**). Importantly, the edited WT (WT/WT*) showed no change in these ratios when compared to the WT control, demonstrating that the silent PAM blocking mutation and manipulations of gene editing had no effect on these measurements (**Figures 4.3A and B**). Strikingly, the L166P homozygous mutant demonstrated dramatic increase in the Aβ 42:40 and Aβ 42:38 ratios, increasing ~13- and ~47-fold compared to WT respectively. This homozygous mutation also significantly reduced the total amount of Aβ produced by almost two thirds (of note, total Aβ refers to simply the sum of Aβ38, Aβ40 and Aβ42) (**Figure 4.3C**). Though less dramatic, the heterozygous L166P mutant also demonstrated a significant reduction in total secreted Aβ (**Figure 4.3C**). In addition,

the M146V homozygote, M233L heterozygote, and A246E homozygote also demonstrated significant reductions in total Aβ (**Figure 4.3C**).

When the individual components of these measurements are examined, an interesting pattern emerges. All mutants, except the A246E heterozygote and A246E hemizygote, demonstrated significant reductions in the amount of secreted Aβ38 (**Figure 4.3D**). The A246E mutation also produced less Aβ38 than WT, but this difference was not statistically significant. In addition, Aβ40 levels were also significantly reduced in all mutants, except for the A246E heterozygote (**Figure 4.3E**). Aβ 42 levels, on the other hand, were significantly increased in all mutant neurons (**Figure 4.3F**). These data support the hypothesis that mutations in *PSEN1* impair the final carboxypeptidase cleavage, causing reduced production of Aβ40 and Aβ38, and elevated levels of Aβ42. Interestingly, not all mutations behaved identically, with some mutations demonstrating more severe changes in Aβ production than others.

Figure 4.3. *PSEN1* mutants increase the Aβ 42:40 and 42:38 ratio by lowering Aβ40 and Aβ38, and increasing Aβ42. A) Secreted Aβ 42:40 ratio. Aβ 42 and Aβ40 measurements were normalized to secreted total sAPP. B) Secreted Aβ 42:38 ratio. Aβ42 and Aβ38 measurements were normalized to secreted total sAPP. C) Total secreted Aβ as determined by the sum of Aβ42, Aβ40 and Aβ38 when normalized to total secreted sAPP. D) Secreted Aβ38. E) Secreted Aβ40. Secreted Aβ42. Bars represent measurements from at least three individual experiments (inductions). Error bars represent S.E.M. $^{*}P < 0.05$, $^{**}P < 0.01$, $^{***}P < 0.001$, $^{****}P < 0.0001$, one-way ANOVA with Dunnett's multiple comparisons post-test.

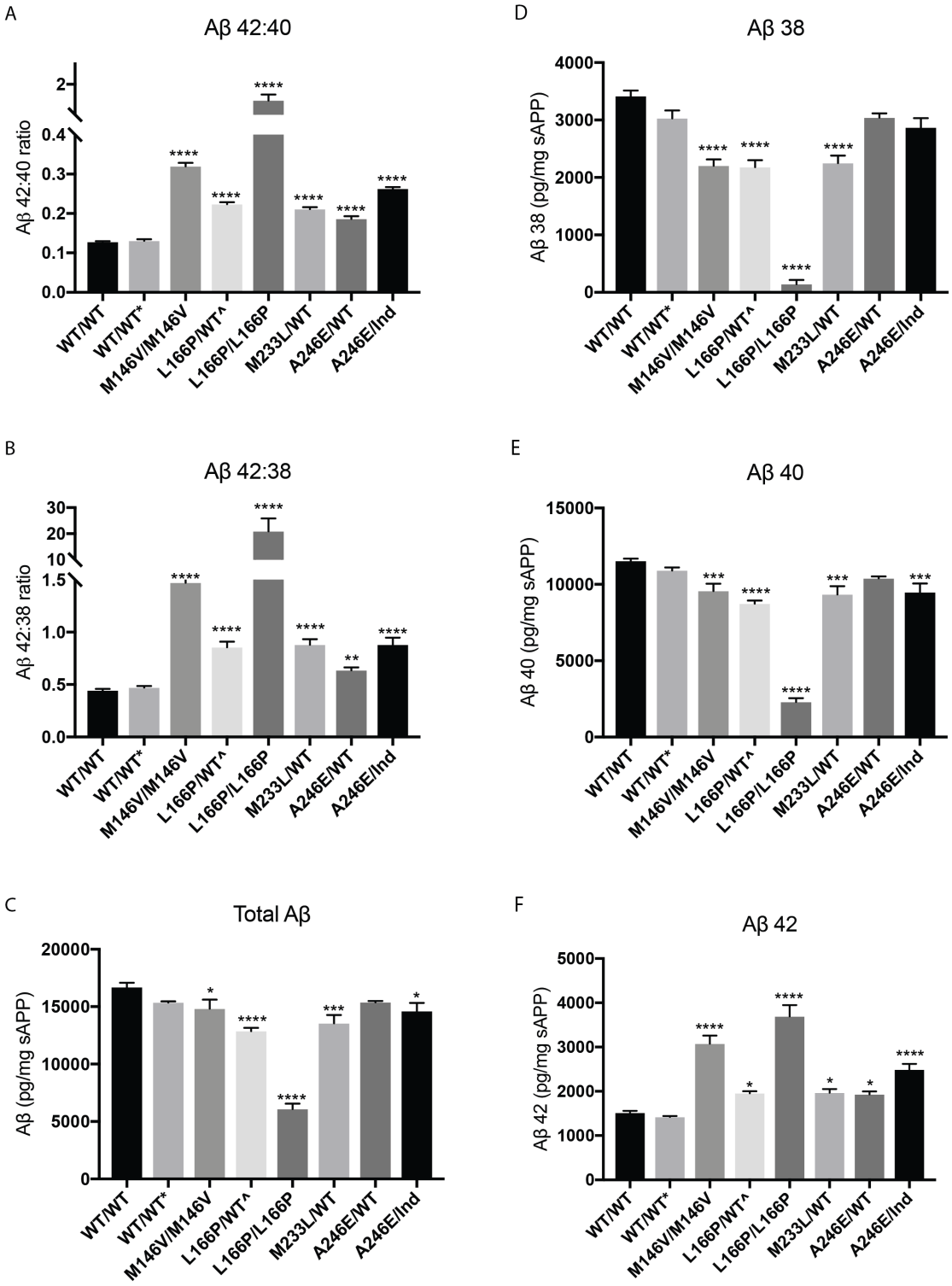
A
Aβ 42:40
Aβ 42:40 ratio
2
0.4
0.3
0.2
0.1
0.0
****
WT/WT
WT/WT*
M146V/M146V
L166P/WT^
L166P/L166P
M233L/WT
A246E/WT
A246E/Ind
D
Aβ 38
Aβ 38 (pg/mg sAPP)
4000
3000
2000
1000
0
B
Aβ 42:38
Aβ 42:38 ratio
30
20
10
1.5
1.0
0.5
0.0
**
E
Aβ 40
Aβ 40 (pg/mg sAPP)
15000
10000
5000
0
***
C
Total Aβ
Aβ (pg/mg sAPP)
20000
15000
10000
5000
0
*
F
Aβ 42
Aβ 42 (pg/mg sAPP)
5000
4000
3000
2000
1000
0

With this in mind, I examined whether any of these measurements correlated with, or could predict, disease onset. For this analysis, I plotted the Aβ 42:40 ratio, Aβ 42:38 ratio, total Aβ, Aβ38, Aβ40, and Aβ42 values for each heterozygous mutant cell line against the mean age of onset for each mutation as determined from clinical data, as the heterozygotes represent the actual patient genotype (Moehlmann et al., 2002; Ryman et al., 2014). Remarkably, the Aβ 42:40 ratio, and Aβ40 levels showed a significant linear correlation with the age of onset, with correlation coefficients (R^2) of 0.9996 and 1 respectively (**Figure 4.4A and E**). As expected, the Aβ 42:40 ratio showed a negative correlation with disease onset, with higher ratios corresponding to lower age of onset. Aβ40, on the other hand, exhibits a positive correlation, with lower Aβ40 values corresponding to a lower age of onset. In addition, while the Aβ 42:38 ratio, total Aβ, and Aβ38 did not show linear correlations, these values did demonstrate monotonic relationships. (**Figure 4.4B, C, and D**). Interestingly, the Aβ42 levels were relatively similar between the mutants, demonstrating the importance of the WT allele in processing Aβ42 to Aβ38 (**Figure 4.4F).**

Interestingly, when the values for the homozygous mutants are similarly plotted against the mean age of onset, a different correlation emerges. Namely, the only value with a linear correlation to age of onset in homozygotes is Aβ42 levels, with an R^2 value of 0.9949 (**Figure 4.5F**). Importantly, all other values plotted demonstrate monotonic relationships with age of onset (**Figure 4.5A, B, C, D, and E).**

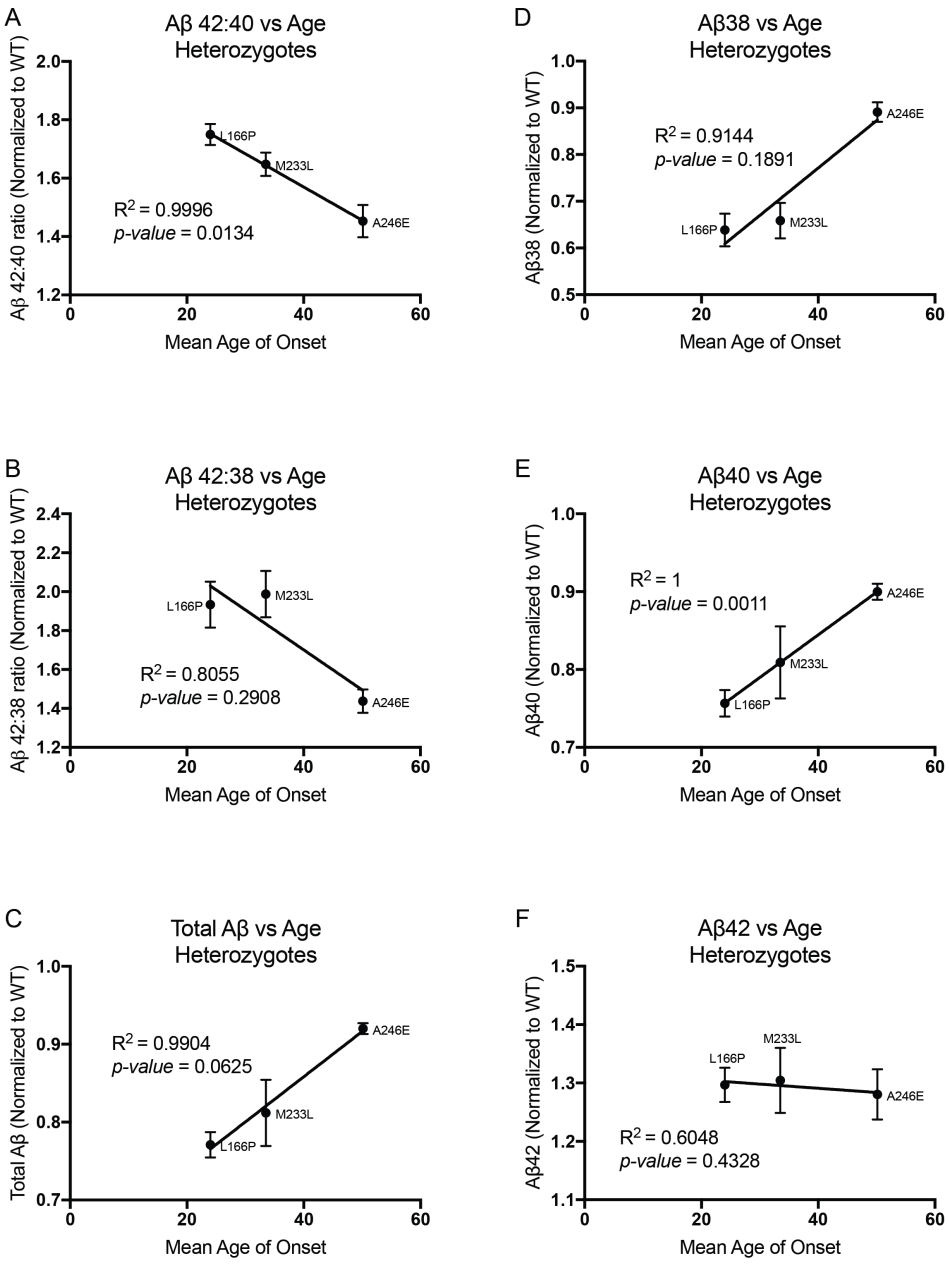

Figure 4.4. Aβ 42:40 ratio and Aβ40 correlate with disease onset in heterozygotes. Mean age of onset plotted against heterozygous mutant measurements for A) Aβ 42:40, B) Aβ 42:38, C) Aβ Total, D) Aβ38, E) Aβ40 and F) Aβ42. Error bars represent S.E.M, with a best fit linear regression line. Pearson correlation coefficient (R^2) and *P* value reported.

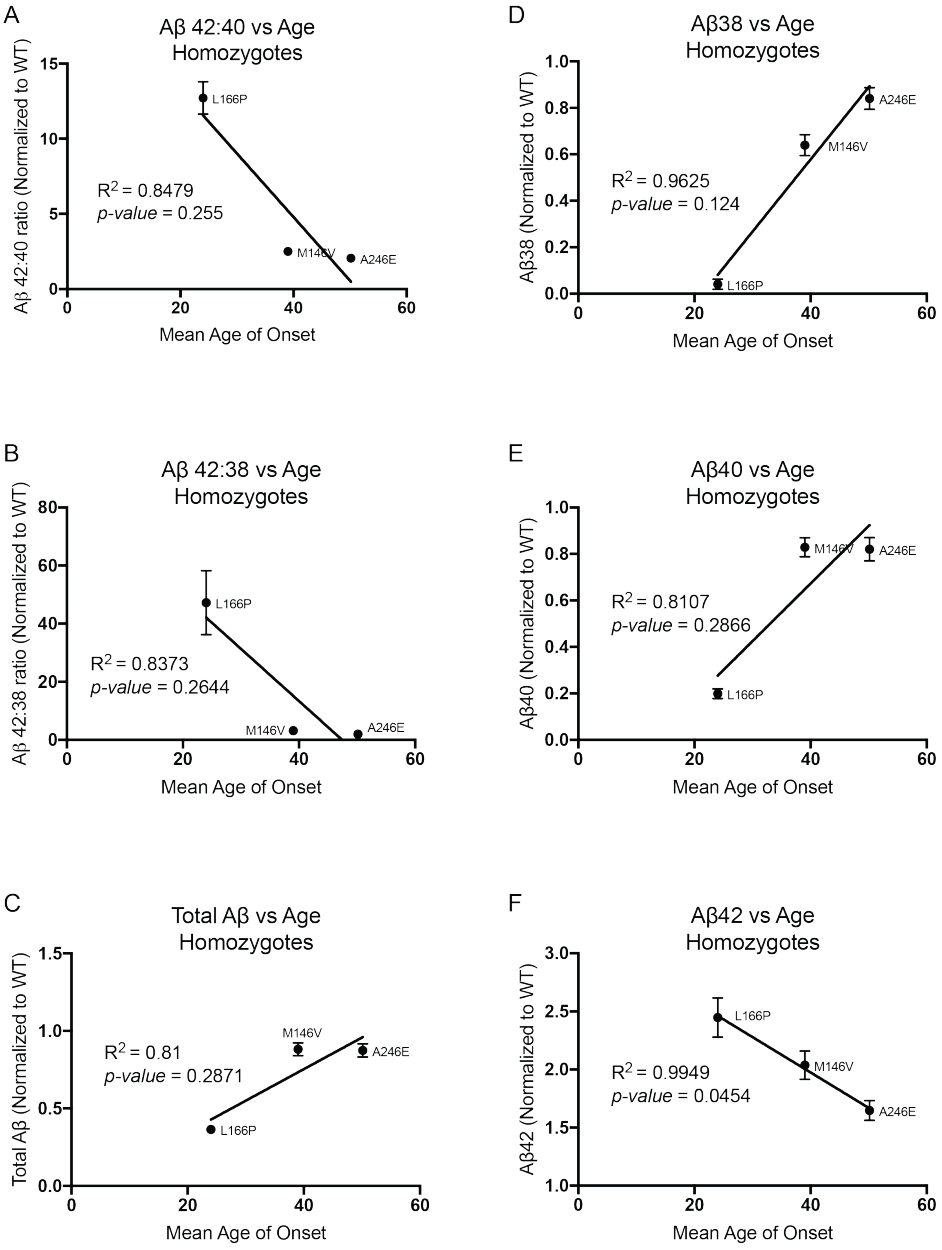

Figure 4.5. Aβ42 correlates with disease onset in homozygotes. Mean age of onset plotted against homozygous mutant measurements for A) Aβ 42:40, B) Aβ 42:38, C) Aβ Total, D) Aβ38, E) Aβ40 and F) Aβ42. Error bars represent S.E.M, with a best fit linear regression line. Pearson correlation coefficient (R^2) and *P* value reported.

PSEN1 mutations impair γ-secretase-dependent functions

γ-secretase cleaves over 90 different substrates, some of which carry out critical cellular functions such as Notch1 signaling (Haapasalo and Kovacs, 2011). To further examine the partial loss of function phenotype observed in Aβ production, I also measured the processing of APP CTFs, Notch1 CTF and N-Cadherin CTF by Western blot. If these mutations impair γ-secretase processing, then these CTFs would be expected to accumulate. Unfortunately, Notch1 CTF levels were not detectable in these samples, and thus could not be assessed. Interestingly, heterozygous mutants showed slight increases in the CTFs assessed (**Figure 4.6B**). However, the homozygous mutants M146V, L166P and A246E showed large increases in APP α- and β-CTFs compared to WT (**Figure 4.6B**). In contrast, only the L166P homozygous mutant demonstrated an increase in the N-Cadherin CTF (**Figure 4.6B**). Importantly, none of the mutations had an effect on the ability to form functional γ-secretase products, as no drastic changes in the abundance of the key components of γ-secretase, PSEN1 N-terminal fragment (NTF), PSEN2, NCT, and PEN2 were observed (**Figure 4.6A**).

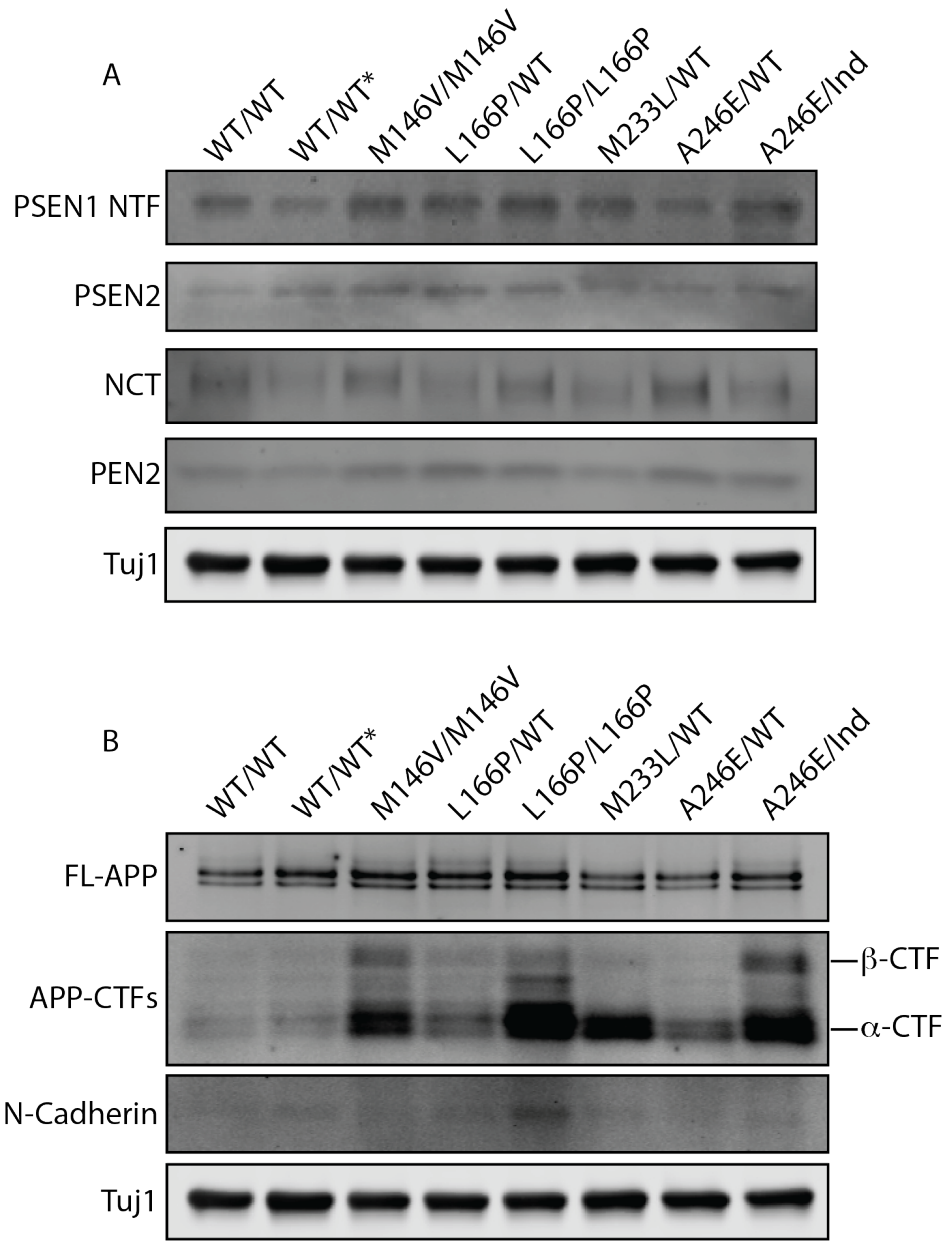

Figure 4.6. Mutant neurons do not demonstrate significant changes in γ-secretase expression, and impaired cleavage of β-CTF and N-Cadherin. A) Western Blot of WT and mutant neurons showed similar expression profiles of γ-secretase components, PSEN1, PSEN2, NCT, and PEN2. B) Western Blot of APP (FL and CTFs) and N-Cadherin show impaired γ-secretase cleavage of APP α- and β-CTFs, as well as N-Cadherin CTF in the L166P homozygote.

Conclusions

In this chapter I explored the specific contributions of several FAD PSEN1 mutations to Aβ production, and γ-secretase function in general. I found that these mutations, *M146V, L166P, M233L* and *A246E*, all increase the ratios of Aβ 42:40 and Aβ 42:38, which are attributed to by both decreases in Aβ40 and Aβ38, and increases in Aβ42. From this I can conclude that the last carboxy-peptidase cleavage of APP is impaired, demonstrating that these FAD mutants cause a partial loss of PSEN1 function. Furthermore, Aβ 42:40 and Aβ40 show significant correlation to the mean age of onset for these mutations in heterozygotes, suggesting that these measurements may have clinical predictive value. In addition, homozygotes show a correlation in the levels of Aβ42 with the mean age of onset, indicating not only that Aβ42 levels are important, but also that the WT allele in heterozygotes plays an important role in limiting the accumulation of Aβ42. Lastly, I show that only homozygous mutations cause an elevation in APP CTFs, and the L166P homozygous mutation causes an increase in the N-Cadherin CTF. This supports the conclusion that these mutations are partial loss of function, but also demonstrates that in the presence of a WT allele, γ-secretase exhibits some normal function, as heterozygous mutants showed reduced effects on APP or N-Cadherin CTF processing compared to the homozygotes. Taken together, these isogenic cell lines demonstrate the ability to replicate APP processing phenotypes in a physiologically relevant manner.

Chapter V: Discussion and Future Directions

Despite decades of advances, there is still much to learn about the pathogenesis of AD. While it is clear that all AD patients exhibit amyloid plaques and NFTs, we still don't fully understand how, or even if, these protein deposits cause neurodegeneration and subsequent cognitive decline. Therefore, it is critical to thoroughly investigate the molecular and cellular events that lead to the formation of amyloid plaques, NFTs, and the downstream consequences of all of their resulting byproducts. Understanding all of these mechanisms will dictate which therapeutic targets could be most effective. Perhaps the lack of a clear understanding of pathogenic mechanisms in AD can be attributed to the inability of *in vivo* or *in vitro* models to adequately recapitulate AD phenotypes. Even the models that come close to replicating most histopathological and behavioral phenotypes still require non-physiologic overexpression of several transgenes. Here, I attempt to address the lack of appropriate AD models by generating two models in human iPSCs with the intention of improving our understanding of two specific disease mechanisms. The first model attempts to recapitulate tau spreading in order to examine the mechanism by which tau propagates. Unfortunately, I show that this model was not only cumbersome and non-physiologic, but also that the control mCherry protein spreads just as efficiently as tau. The second model utilized CRISPR/Cas9 genome editing to introduce several FAD *PSEN1* point mutations at endogenous loci into WT

iPSCs. This method preserves endogenous levels of expression of γ-secretase and APP, allowing for the characterization of Aβ production in a physiologically relevant system. I show that *PSEN1* mutations cause a partial loss of function in γ-secretase processing of APP, which not only replicate AD phenotypes, but also correlate with disease onset. By demonstrating these disease phenotypes with endogenous expression levels, we believe that this model system is an improvement upon the existing cell culture models, and should be used in future studies to further our understanding of AD mechanisms, and screen for potential therapeutics.

Spreading may not be a property inherent to tau

In Chapter 3, I established a co-culture system comprised of tau donor and recipient cell lines with the hopes of confirming that tau spreads from neuron to neuron. I reasoned that this system, if successful, would be a significant advance for the field, as it would allow for the direct observation and manipulation of tau spreading in human neurons. The current view in the field is that an uncharacterized pathologic tau species spreads trans-synaptically along anatomically connected paths in the brain, facilitating the misfolding and aggregation of previously healthy tau protein in a prion-like manner, and thus potentiating the disease. However, the mechanism by which this species is released and taken up is still debated. Therefore, understanding this mechanism would identify potential therapeutic

targets. Importantly, understanding this process in human neurons *in vitro* may increase the probability of translating these findings to human patients.

Indeed, I observed that mCherry tagged tau does in fact spread from donor to recipient neurons in this transgenic inducible system (**Figure 3.3A and C**). However, I was disappointed to find that the control, mCherry alone, also spreads just as efficiently as tau (**Figure 3.3B and C**). This complicates the interpretation of the results, as there are two possible interpretations of these data: 1) tau and mCherry are randomly internalized by recipient neurons by a non-specific process such as bulk endocytosis or 2) the mCherry tag is actually facilitating tau spreading. Future studies required to distinguish these possibilities are outlined in the section below, and would have required a substantial time commitment, several more years, that the lab and I unfortunately could not afford. As such, my effort to study the mechanism of tau release and uptake in human neurons was stalled.

Because of these difficulties, I turned to studying one particular aspect of tau spreading in isolation, namely, cellular uptake of tau oligomers. Recently, a cell culture tool was established that could sense the aggregation potential of tau aggregates (Holmes et al., 2014). These HEK293 cells express the tau RD tagged to a CFY or YFP FRET pair. Upon introduction of exogenous recombinant aggregates, lysates from transgenic mouse brains harboring NFTs, or even human AD brain lysates, the RD FRET pairs aggregate which is visible with fluorescence microscopy. Using recombinant tau preparations from Dr. David Eliezer's laboratory, I

demonstrated that exogenous tau aggregates, but not monomers, were capable of seeding aggregation in these biosensor cells (**Figure 3.5A and B**).

Importantly, these aggregates required the assistance of liposomes in order to seed aggregation (**Figure 3.5A**). This could have important biological implications, as it suggests that for tau to enter cells and access the cytosolic compartment where endogenous tau is expressed, a lipophilic carrier, such as an exosome, may be necessary. In fact, exosomal delivery of tau seeds has gained significant support as a possible mechanism for tau spreading, as several groups have reported detecting tau within exosomes, and have demonstrated their potential role in tau spreading *in vivo* (Asai et al., 2015; Saman et al., 2012; 2014; Santa-Maria et al., 2012). Our data support, but do not directly test, a role for exosomal transport of tau from donor to recipient, and should be investigated in an appropriate iPSC model.

I next attempted to elucidate the mechanism by which liposomal tau aggregates gain entry into the biosensor cell line. Using pharmacological manipulation of cellular uptake mechanisms, I observed that inhibition of macropinocytosis, a form of non-specific endocytosis, reduced or completely inhibited aggregation in the biosensor cell line. These inhibitors included heparin, EIPA, latrunculin, and cytochalasin-D, which suggests that extracellular HSPGs are involved in mediating recognition of liposomal tau, and actin polymerization precipitates its physical engulfment. These data support previous studies, but elaborate upon them by demonstrating that these mechanisms are in fact required

for seeding and aggregation of tau expressed in the biosensor cell line (Holmes et al., 2013; Karch et al., 2012; Wu et al., 2013). Once inside the macropinosome, the liposomal tau somehow escapes the macropinosome to facilitate seeding and aggregation of the biosensor, however the escape mechanism remains uninvestigated.

Nevertheless, with this mechanism in HEK293 cells confirmed, I then attempted to translate it to human neurons. Liposomal tau was added to WT neurons, anticipating that the endogenous tau would aggregate in a similar manner to the biosensor tau. To measure this, I used an antibody that recognizes only misfolded and aggregated tau, MC1. Initially I observed robust MC1 staining in neurons treated with FL-WT aggregates (**Figure 3.7C**). However, this experiment did not exclude the possibility that the MC1 antibody was recognizing and staining the exogenous aggregates, rather than endogenous seeded tau. To overcome this, I repeated the experiment with tau RD aggregates, which lack one of the epitopes required for recognition by MC1. If endogenous tau was in fact being seeded by these aggregates, then the MC1 antibody would still recognize and stain these cultures. Unfortunately, treatment with RD aggregates showed no staining with MC1, indicating that the liposomal tau preparations were not capable of replicating the results from the biosensor cell line in human neurons (**Figure 3.7C**).

While these data were collectively disappointing, there are still some important takeaways. First, tau was able to transfer from one cell to another in a co-

culture system. Though we could not conclude that the spreading observed was either a non-specific macropinocytosis, or the mCherry tag facilitating the transfer, both of these potential conclusions warrant follow up studies. Currently the field firmly believes that tau spread trans-synaptically by some mechanism that is inherent to tau. However, our data suggest the opposite, that tau spreads either via tau-independent bulk endocytosis, or with help from other protein interactions. These are important hypotheses that need to be fully investigated prior to developing therapies that target tau spreading, as blocking a generalized spreading mechanism may have unintended consequences if other proteins use similar pathways, or even use tau, to move from cell to cell under normal conditions.

Second, I demonstrate that recombinant liposomal tau aggregates are capable of seeding aggregation in a HEK293 biosensor cell line via macropinocytosis. This observation fits with the hypothesis that tau spreads via non-specific bulk endocytosis. Although I could not confirm the findings in neurons, I cannot exclude that this process is unique only to the biosensor cell line. I relied on the recombinant aggregates being able to seed endogenously expressed tau, which assumes that 1) the neurons take up tau, 2) the engulfed tau is not degraded and can access the cytosol, and 3) the recombinant tau can seed endogenous tau. These are several steps that can be addressed more systematically in future experiments, which should ensure that the aggregates are in fact taken up in

neurons, are not degraded upon engulfment, and subsequently access the cytosol to promote seeding.

Future directions for tau spreading

Future studies should begin with a focus on elucidating the mechanism by which recombinant tau preparations enter a neuron, and if they can induce aggregation. This property is at the center of the tau spreading hypothesis, that oligomeric tau can cause conformational changes in tau in a previously healthy neuron. I have already established that tau can enter and seed tau in the biosensor cell line. The next experiment should attempt to replicate the seeding phenotype in biosensor cells, however with the aggregates labeled with a fluorophore, such as an Alexa Fluor (Panchuk-Voloshina et al., 1999). If these labeled aggregates are still capable of seeding the biosensor cell line, then these could be used to track cellular uptake in neurons and ensure that the aggregates are being endocytosed. Subsequent experiments can then track where these aggregates are shuttled, either into the lysosomal system, or if they escape into the cytosol.

Interestingly, in an experiment performed in collaboration with Dylan Kwart, whose work in the lab is focused on endosomal trafficking of APP and β-CTF, we observed that liposome-free tau aggregates accumulated in the endosomes of HeLa cells that were transiently transfected with a constitutively active Rab5A, which halts endocytic sorting at the early endosome stage, leading to enlarged endosomes that

do not mature into lysosomes (data not shown) (Calafate et al., 2016). While this experiment was not performed with the intent of studying tau uptake, it is highly suggestive that tau aggregates are potentially taken up and sorted through the endosomal-lysosomal system for degradation. An interesting follow-up experiment would be to transfect constitutively active Rab5 into the biosensor cell line, and then attempt to seed these cell with liposome-free aggregates. If liposome-free aggregates are capable of seeding the biosensor cell line, this would provide evidence that endosome-lysosome disruption (one of the earliest known pre-clinical changes seen in AD patient brains (Cataldo et al., 2000; 2001)) is responsible for allowing tau aggregates to escape and access the cytosol and may in fact be necessary for tau spreading and seeding in neurons.

Once the recombinant aggregate experiments are completed and demonstrate an ability to enter neurons, and a mechanism by which they enter neurons is confirmed, the results should be subsequently confirmed in a co-culture system similar to what I originally proposed. This is important because recombinant aggregates, while useful, do not represent what occurs in an AD patient. In patients, spreading tau is produced by cells and post-translationally modified accordingly, whereas recombinant tau has no such alterations. Therefore, a donor and recipient co-culture method would more closely resemble what occurs *in vivo.*

In order to rule out the potential effect that a protein tag could have on tau spreading, several more iPSC lines will need to be generated. First, I would attempt

tagging tau with smaller polypeptide tags such as FLAG or His. I would also attempt tagging proteins that have similar properties to tau, but show no evidence of spreading so far, such as microtubule associated protein 2 (MAP2) and MAP4. If all of these cell lines, including the tag-only controls, spread in a similar manner, then this would be highly suggestive of a tau-independent mechanism of protein spreading. Alternatively, and more ideally, future studies should avoid tagging tau altogether. To achieve this, the recipient iPSC cell line must be a true knockout of tau that does not exhibit any background immunofluorescence staining. This would allow for the faithful detection of donor tau within the knockout recipient without the use of fluorescent or short polypeptide tags. If tau is still observed to spread, pharmacological modulation of cellular release and uptake mechanisms could be used to elucidate a spreading mechanism, focusing on mechanisms elucidated in the recombinant tau experiments. In theory, this experiment could also be carried out in the absence of overexpression, allowing for the observation and manipulation of tau spreading at endogenous levels of expression.

Is tau spreading a reasonable target for AD therapies?

If these experiments are capable of defining a mechanism by which tau can spread from one cell to another, it doesn't necessarily mean that this pathway is a therapeutic candidate. As I have so far demonstrated, tau spreading may not be inherent to tau itself, and instead could be a more generalizable mechanism that

many proteins and cells utilize for critical biological functions. Targeting the pathway, therefore, may have unintended consequences in the clinic. However, since tau pathology closely correlates with disease severity, targeting tau is still a reasonable approach. In fact, several clinical trials have been initiated that either aim to break up and solubilize existing tau aggregates (Crowe et al., 2013; Wischik et al., 1996), or immunize patients against aggregated tau (Kontsekova et al., 2014). While we eagerly anticipate the results of these trials, it is still too early, and frankly unsafe, to presume that tau spreading is also a viable therapeutic target, as there is still much to understand.

PSEN1 FAD mutants alter the processing of APP by γ-secretase

In chapter 4 I explored whether *PSEN1* FAD mutations result in gain- or loss-of-function of γ-secretase. Critical to making this determination is understanding what constitutes the normal function of γ-secretase. It was initially assumed that γ-secretase preferentially made Aβ40, the smaller Aβ peptide that does not aggregate as readily as Aβ42, and was therefore presumed to be less toxic. When it was discovered that *PSEN1* mutations preferentially increased the amount of Aβ42 relative to Aβ40, this was attributed to a toxic gain-of-function. Unfortunately, these experiments and conclusions were performed prior to a detailed understanding of how exactly PSEN1 cleaves β-CTF to produce Aβ. Shortly after these seminal studies, researchers began to question whether these *PSEN1* mutations were due to a gain of function to overproduce Aβ42. Unfortunately, this has led to a sometimes-

heated debate over *PSEN1* FAD mutation function, and perhaps unfairly placed the blame for perceived misdirection on the investigators in these early studies.

Fortunately, a detailed explanation of how PSEN1 cleaves Aβ has been provided (Takami et al., 2009), which demonstrated that the β-CTF undergoes successive tri- and tetra-peptide cleavages which produce Aβ of varying lengths (**Figure 1.2**). This work demonstrated that a rise in Aβ42 could actually be caused by a reduction in PSEN1 activity, specifically during the last carboxy-peptidase cleavage of β-CTF.

With this in mind, I set out to determine whether *PSEN1* FAD mutations could alter Aβ production in iPSC-derived isogenic neurons. This system would provide a significant advance in the field, as most model systems that have been used to date have relied on massive overexpression of PSEN1, APP, and/or β-CTF, yielding results that have been variable from model to model, and could be difficult to translate to human patients. Only a handful of studies have used iPSC-derived neurons to study FAD *PSEN1* mutations, however these either used non-isogenic controls (Liu et al., 2014; Nieweg et al., 2015; Sproul et al., 2014; Yagi et al., 2011), or overexpression of *PSEN1* transgenes (Honda et al., 2016; Koch et al., 2012). Only one study has reported results from isogenic *PSEN1* FAD iPSC lines, however only one mutation, ΔE9, was studied (Woodruff et al., 2013). The results presented here investigate four different isogenic iPSC lines, demonstrating the utility and

power of the recently establish CRISPR/Cas9 genome editing protocols in generating isogenic iPSCs for studying disease phenotypes.

Analysis of the quantities of Aβ peptides Aβ42, Aβ40 and Aβ38 produced in isogenic mutant iPSC-derived neurons demonstrate a partial loss of function phenotype in γ-secretase. In all mutant cell lines, Aβ42 was increased (**Figure 4.3F**), while Aβ38 and Aβ40 were significantly decreased in all cell lines except for in the A246E heterozygote (Aβ38 and Aβ40), and the A246E homozygote (Aβ38) (**Figure 4.3D and E**). The L166P mutant cell lines demonstrated the most severe alterations in Aβ production, particularly in a drastic reduction in Aβ40 and Aβ38 (**Figure 4.3D and E**). As a result of these alterations in Aβ production, the Aβ 42:40 and Aβ 42:38 ratios were accordingly increased in all mutants (**Figure 4.3A and B**). These data clearly demonstrate that γ-secretase is impaired in *PSEN1* FAD mutants, specifically during the last carboxy-peptidase cleavage of β-CTF, supporting the hypothesis that *PSEN1* mutations are in fact partial loss of function.

Because each mutation behaved differently with respect to altered Aβ production, I reasoned that these measurements might correlate with disease severity in FAD patients of a given mutation. To explore this, I attempted to correlate the age of onset for a given mutation to the various Aβ measurements in heterozygous mutants, as these cell lines represent the FAD genotype. Fascinatingly, there were significant correlations between the Aβ 42:40 ratio and the Aβ40 levels (**Figure 4.4A and D**). While it is relatively easy to generate a line

between three points, it was still remarkable that there was a significant correlation between these values. In addition, because there was a significant correlation between age of onset and Aβ40, not Aβ42, we can infer that the significance in the Aβ 42:40 ratio is due to Aβ40. While it has been shown that lower Aβ42 in cerebrospinal fluid (CSF) is somewhat predictive of AD due to Aβ42 incorporation into plaques, these data here could have implications in clinical practice and management of FAD and AD patients, as Aβ40 measurements may be a more valuable diagnostic tool. Extrapolating further, these data may provide a hint that Aβ40 may in fact have protective qualities, and that loss of Aβ40 may precipitate Aβ42 deposition.

Further support for PSEN1 partial loss of function in FAD was observed when I examined other products of γ-secretase cleavage. APP CTFs accumulated in the M146V and L166P homozygotes. Furthermore, the L166P homozygote also demonstrated an accumulation of the N-Cadherin CTF. These data suggest that these mutations impair γ-secretase's ability to cleave not only APP, but also other substrates. Interestingly, the presence of a single WT allele in heterozygotes is capable of maintaining the level of APP and N-Cadherin CTFs at or near WT levels. Because AD and FAD take decades to present with cognitive impairment, it is reasonable to assume that these CTFs may accumulate over time in AD and FAD brains, possibly contributing to cognitive impairment along with Aβ.

In sum, these experiments demonstrate that *PSEN1* mutations result in partial loss of γ-secretase functions, as APP processing is significantly altered in a manner that points to an impaired carboxy-peptidase cleavage. Importantly, these data demonstrate the utility of the iPSC model system, as all of these experiments were carried out at endogenous levels of expression, therefore closely mimicking what occurs in human FAD patients. In addition, these studies highlight the importance of comparing iPSC mutant cell lines to isogenic controls, as all mutant iPSC lines had an identical genetic background, ruling out potential confounding genetic differences. We also demonstrate that recent advances in CRISPR/Cas9 techniques increase the feasibility of generating a large number of isogenic cell lines in a short amount of time, as this project was initiated only one year ago.

Is Aβ the source of disease in AD?

While our results presented here establish a functional role for PSEN1 in AD and FAD, we provide no evidence that Aβ peptides are in fact the source of disease in AD. Future studies should, therefore, attempt to understand if, and if so, how, Aβ ultimately leads to synapse loss and neurodegeneration, as this is the ultimate phenotype that leads to the manifestations of the disease in patients. Many studies have demonstrated that fibrillar Aβ species are in fact synaptotoxic (Koffie et al., 2009; Mucke et al., 2000; Nieweg et al., 2015; Walsh et al., 2002), which may in fact be a true mechanism by which Aβ precipitates AD. However, this does not

necessarily fit with the observations that Aβ plaque burden does not correlate with disease severity (Braak and Braak, 1991), that many aged humans have abundant plaques without any evidence of disease, or that all clinical trials aimed at directly reducing amyloid burden have so far failed (Selkoe and Hardy, 2016).

Interestingly, other byproducts of APP processing, such as the AICD, α- and β-CTFs, and longer intermediate forms of Aβ such as Aβ46, Aβ45 and Aβ43, remain understudied. Recently, work by Dylan Kwart in our lab identified alterations in the endosomal sorting pathway of neurons with isogenic FAD mutations. Namely, he noticed that homozygous FAD mutations result in increased levels of APP CTFs, which I confirmed in my homozygous mutants as well. Importantly, he observed these changes in *PSEN1* mutants, *and APP* mutants, potentially identifying APP CTFs and endosomal-lysosomal sorting, not Aβ, as a potential common perturbation underlying AD pathogenesis. Future studies are therefore aimed at identifying whether this is a common occurrence in all FAD genes (*PSEN1, PSEN2, and APP*), and whether these CTFs and impaired endosomal trafficking are responsible for neurodegeneration in FAD.

Our data, together with the last several decades of studies, unequivocally demonstrates that alterations in APP processing leads to AD. Exactly how, and which byproduct of APP processing leads to AD remains elusive. However, I remain hopeful that cellular systems like the one presented here will be a useful tool in identifying targets for future therapies, and even screening for compounds that alter

disease related phenotypes. Whether that phenotype is increased Aβ42, decreased Aβ40, accumulation of APP CTFs, or tau spreading, I cannot definitely say. However, I am confident that the answers will soon become apparent.

Chapter VI: Materials and Methods

iPSC lines. iPSCs were reprogrammed from human skin fibroblasts (Coriell Institute, Catalog ID: AG07889) of an 18-year old male individual using the Cytotune-iPS Sendai Reprogramming Kit (Life Technologies) according to the manufacturer's instructions (Paquet et al., 2016). Fibroblasts were confirmed to be wildtype for all studied loci by genotyping. Multiple clones were selected based on characteristic morphology. Clone 7889SA possessed a normal karyotype (Cell Line Genetics) and was characterized for typical iPSC properties.

Expression of pluripotent genes was analyzed by NanoString nCounter gene expression system using a pre-designed codeset (Kahler et al., 2013). Data was normalized to the geometric mean of three housekeeping genes (ACTB, POLR2A, ALAS1) using the nSolver Analysis Software v1.0 (NanoString). 100 ng of total RNA from line 7889SA was compared to RNA extracted from the human ESC lines HUES9 (Cowan et al., 2004). Gene expression for 7 pluripotency markers and the 4 Yamanaka factors introduced as Sendai transgenes (s-t) was compared. Note that the s-tSox2 probe detects some expression of endogenous Sox2, leading to larger values for both lines.

Expression of pluripotency markers Oct4, Tra160, SSEA4 and Nanog was confirmed by immunofluorescence. *In vivo* pluripotency was confirmed by teratoma analysis. Undifferentiated iPSCs were embedded into Matrigel and subcutaneously

injected into the dorsal flank of immune-compromised mice (Jackson Laboratory). Paraffin sections of the teratomas were subjected to hematoxylin and eosin (H&E) staining and structures characteristic for the three germ layers (ectoderm, mesoderm and endoderm) were identified by microscopy.

iPS Cell culture. iPSCs were maintained on irradiated MEFs (Globalstem) plated on cell culture plates coated with 0.1% gelatin and grown in HUESM (Knock-out Dulbecco's modified Eagle's Medium (KO-DMEM), 20% knock-out serum, 0.1 mM non-essential amino acids, 2 mM Glutamax, 100 U/mL-0.1 mg/mL penicillin-streptomycin (all Life Technologies), 0.1 mM 2-Mercaptoethanol (Sigma-Aldrich), 10 ng/mL FGF2 (Stemgent), at 37 ºC with 5% CO_2. Prior to transfection, iPSCs were transferred to Geltrex-coated (Life Technologies) cell culture plates and grown in MEF-conditioned HUESM containing 10 μM ROCK inhibitor (Stemgent).

TALEN gene editing. iPSCs were transfected with TALEN pairs targeting the H11 locus (a gift from Michele Carlos, Addgene plasmid #51554 and 51555 (Zhu et al., 2013)) and AAVS1 locus (a gift from Danwei Huangfu, Addgene plasmid #59025 and 59026 (González et al., 2014)), by electroporation in order to generate recipient and donor cell lines respectively. Along with the TALEN pairs, repair templates were also electroporated with homology arms to H11 (a gift from Michele Carlos, Addgene plasmid #51546 (Zhu et al., 2013)) and AAVS1 (a gift from Rudolph Jaenisch,

Addgene #60843 and 22077 (Hockemeyer et al., 2009)). 2 million cells were resuspended in 100 μL cold BTXpress electroporation buffer (Harvard Apparatus) with 4 μg of each TALEN, and a total of 32 μg of donor repair template(s). Cells were electroporated at 70 mV for 20 ms in a 1 mm cuvette (Harvard Apparatus). After electroporation, cells were transferred to Geltrex-coated cell culture plates and grown in MEF-conditioned HUSEM containing ROCK inhibitor for 2 days. 100,000 cells were then plated on 10 cm plates lined with MEFs. Cells were allowed to grow for 2 days before selection with either 250 μg/mL neomycin (G418, Life Technologies), or 250 μg/mL neomycin and 0.5 μg/mL Puromycin (Life Technologies). After selection for 7 days, colonies were allowed to grow until large enough to be manually picked into individual wells of a flat-bottom 96-well plate lined with MEFs in 100 μL of HUSEM with ROCK inhibitor. Incorporation of the mutant transgenes was analyzed by PCR (**Table 6.1**).

Table 6.1. PCR primers for TALEN genome editing.

Locus	PCR Product	Primer Name	Primer Sequence
AAVS1	Endogenous Locus	AAVS1 WT F1	TTTCTGTCTGCAGCTTGTGG
		AAVS1 WT R1	CAGCTCAGGTTCTGGGAGAG
	Integration (Puro Donor)	AAVS1 WT F1	TTTCTGTCTGCAGCTTGTGG
		AAVS1 Puro Integration R1	GTGGGCTTGTACTCGGTCAT
	Integration (Neo Donor)	AAVS1 WT F1	TTTCTGTCTGCAGCTTGTGG
		AAVS1 Neo Integration R1	TGTCTGTTGTGCCCAGTCAT
H11	Endogenous Locus	H11 F1	GCAGGACTGAAAAACCTCCA
		H11 R1	GGGAGGCTGAGACAGAAGAA
	Integration (Landing Pad)	H11 F1	GCAGGACTGAAAAACCTCCA
		H11 Landing Pad R1	CACAACCCCTTGTGTCATGT

Southern blot. Southern blot was performed as previously described (Southern, 2006). Probe was generated by PCR amplification of the memYFP transgene.

Lentiviral production. Lentiviral constructs and the associated packaging plasmids psPAX2 and pMD2G were transfected into 293FT cells using calcium phosphate. After 16-hours the media was switched to serum free viral production media: Ultraculture (Lonza), with 1% (v/v) penicillin-streptomycin/L-glutamine (Gibco), 1% (v/v) 100 mM sodium pyruvate (Lonza), 1% (v/v) 7.5% sodium bicarbonate (Lonza), and 5 mM sodium butyrate. 293FT supernatants were collected at 46-hours after transfection, neutralized with 1M Tris-HCl, pH 7.5 to 50 mM final concentration, and filtered through a 0.45 μm polyethersulfone syringe filter. Supernatants were then concentrated using Lenti-X concentrator (Clontech) and re-suspended in Neurobasal/B27. Lentiviral titer was determined using an ELISA-based quantification of p24 viral coat protein according to the manufacturer's instructions (Clontech). Lentivirus was added to iPSC-derived neuron cultures 1-2 days after splitting of NPCs at the MOIs indicated.

gRNA design and construction. gRNAs were designed using the Zhang lab CRISPR design tool (crispr.mit.edu). gRNA sequences targeting *PSEN1* (**Table 2.3**) were cloned into plasmid MLM3636 (a gift from Keith Joung, Addgene # 43860) as previously described (Fu et al., 2013). Briefly, DNA oligonucleotides were annealed

to generate double-stranded fragments that were ligated into BsmBI-digested plasmid.

Design of ssODN repair templates. 100-nt ssODN repair templates (PAGE-purified, IDT) were designed with homologous genomic flanking sequence centered around the predicted CRISPR cut site and containing pathogenic and/or CRISPR-blocking mutations (**Table 2.4**). CRISPR-blocking silent mutations were selected based on codon-usage of the edited gene by changing the codon to another codon already used in the same mRNA for the respective amino acid.

CRISPR/Cas9 gene editing. iPSCs were transfected with Cas9- and gRNA-expressing plasmids, and ssODNs by electroporation. 2 million cells were resuspended in 100 μL cold BTXpress electroporation buffer (Harvard Apparatus) with 20 μg pCas9_GFP (a gift from Kiran Musunuru, Addgene plasmid # 44719), 5 μg gRNA plasmid, and a total of 30 μg ssODN (oligo mixing of WT and mutant ssODNs was used to obtain heterozygous clones; a 1:1 ratio of WT:MUT ssODN was used in all experiments (Paquet et al., 2016)). Cells were electroporated at 70 mV for 20 ms in a 1 mm cuvette (Harvard Apparatus). After electroporation cells were transferred to Geltrex-coated cell culture plates and grown in MEF-conditioned HUESM containing ROCK inhibitor for 2 days. In all transfections, 7889SA-derived iPSCs wildtype at genome-edited loci were used.

Recombinant tau preparation and aggregation. Recombinant tau was produced in Dr. David Eliezer's lab by transfecting *E. coli* BL21/DE3 cells (Novagen, San Diego, CA) with plasmids encoding FL-WT tau (2N4R) or 4RD tau. These cells were lysed via sonication, and cellular debris was pelleted by ultracentrifugation at 150,000 x g. Tau was further purified by cation-exchange chromatography, followed by reverse-phase high-performance liquid chromatography (HPLC). Purified tau protein was lyophilized and stored at -20°C.

Following a protocol generated by Dr. Marc Diamond, lyophilized tau protein was weighed first resuspended in 10mM DTT to a final concentration of 800 μM and incubated at room temperature for 1 hour. This preparation was further incubated in 10mM HEPES, 100 mM NaCl, with or without 8 μM heparin to generate aggregates or monomers respectively, with a final concentration of 8_μM tau. This preparation was allowed to incubate at 37°C for 24 hours. Aggregates, monomers and vehicle were subsequently snap-frozen in liquid nitrogen in single use aliquots, and stored at -80°C.

HEK293 Biosensor Cell Culture. Human embryonic kidney (HEK) 293 cells that expressed a tau P301S RD fused to a CFP/YFP FRET pair was gifted from Marc Diamond (ATCC). Biosensor HEK293 cells were maintained in DMEM with 10% FBS, 2 mM Glutamax and 100 U/mL-0.1 mg/mL penicillin-streptomycin (all Life

Technologies) at 37 ºC with 5% CO_2. HEK293 cells were seeded on 96-well plates at 50,000 cells/mL. Cells were treated with DMSO control or inhibitors at the following concentrations: Pitstop 2 20 μM (Sigma), Cytochalasin-D 1 μM (Sigma), Latrunculin 1 μM (Sigma), Heparin 20 μg/mL (Sigma), Sodium Chlorate 25 mM (Sigma), 5-N-ethyl-N-isopropyl-amiloride (EIPA) 1 mM (Sigma), Lactacystin 10 μM (Sigma).

Immunocytochemistry and microscopy. Cells were fixed in 4% paraformaldehyde, permeabilized in PBS/0.1% TritonX-100 and stained with primary and secondary antibodies (see below). Stained cells were imaged on a Nikon Eclipse Ti inverted microscope and acquired using NIS Elements imaging software (Nikon). Fiji (www.Fiji.sc / National Institutes of Health) and Adobe Photoshop were used to pseudo-color images, adjust contrast, and add scale bars.

Fluorescence activated cell sorting. GFP^{hi} and GFP^{low} cells were collected in the Rockefeller University Flow Cytometry Resource Center using a FACSAria II flow cytometer (BD Biosciences). 48h following transfection, cells were resuspended in PBS with 0.5% BSA fraction V solution, 10 mM HEPES, 100 U/mL-0.1 mg/mL penicillin-streptomycin (all from Life Technologies), 0.5 M EDTA, 20 mM glucose, 10 ng/L DAPI in the presence of ROCK inhibitor for iPSC sorts. For single-cell derived

iPSC clone derivation, 30,000 – 70,000 GFP+ cells were immediately plated on a 10-cm plate of MEFs in HUESM and ROCK inhibitor following cell sorting.

Sanger sequencing for genotyping single cell clones. To assess zygosity of genome edited single cell-derived iPSC clones, colonies on MEF-containing 10 cm plates (in HUESM + ROCK inhibitor) were manually picked into a single well of a Flat-bottom 96-well tissue culture plate in 100 μL HUESM + ROCK inhibitor. Cells were pelleted by centrifugation, and plates were immediately frozen in liquid N_2 and stored at -80 ºC.

Genomic DNA was extracted as previously described (González et al., 2014). Briefly, cells were resuspended in 25 μL lysis buffer (10 mM Tris-HCl (pH 7.6), 10 mM EDTA, 20% SDS, 10 mM NaCl, 1 mg/mL Proteinase K (Ambion)), and incubated at 55 ºC for overnight. Proteinase K was inactivated by incubating plates at 96 ºC for 10 min. The genomic region surrounding the *PSEN1* loci was amplified by Taq polymerase (Roche) according to the manufacturer's directions and genome-edited clones were identified by RFLP analysis (**Table 2.4**). Clones with HR-mediated incorporation of the CRISPR-blocking silent mutation (determined by RFLP analysis) were selected and zygosity was determined by Sanger sequencing (Genewiz).

Table 6.2. Primers for PCR amplification, RFLP analysis, and sanger sequencing for CRISPR/Cas9 genome editing of *PSEN1*.

Name	purpose	sequence
M146V-F1	PCR/RFLP/Sanger-Seq.	GGTGAGTTGGGGAAAAGTGA
M146V-R1	PCR/RFLP	CTGGCATTACACATGCACCT
L166P-F1	PCR/RFLP	CGTGGTTCCACCTACTCAGG
L166P-R2	PCR/RFLP/Sanger-Seq.	AAGCAAGGAGCAACAGAAGAA
Exon7-F3 (M233L/A246E)	PCR/RFLP/Sanger-Seq.	ATGTTTGGGAGCCATCACA
Exon7-R2 (M233L/A246E)	PCR/RFLP	CAGCCTCCCAAAGTGCTAAG
Exon11-F1 (G384A/D385A)	PCR/RFLP/Sanger-Seq.	GCAGCATCTACAGTTAAGACTCCA
Exon11-R1 (G384A/D385A)	PCR/RFLP	AATGTGTGGCCAGGGTAGAG

Cortical neuron differentiation. iPSC-derived cortical neurons were generated as previously described (Shi et al., 2012b) with modifications. Specifically, to generate neural precursor cells (NPCs), iPSCs were plated on 12-well tissue culture plates coated with Geltrex (Life Technologies) in MEF-conditioned HUESM with ROCK inhibitor. When cells were 100% confluent, medium was replaced with neural induction (NI) medium (day in vitro 0 (DIV0)) and maintained for 8 days. On DIV8 day cells were dissociated using Accutase (Life Technologies) and resuspended in NI medium at 30 million cells/mL. Cells were plated on dried poly-L-ornithine (Sigma-Aldrich) and laminin-coated (Life Technologies) 6-well plates in 200 μL spots. Cells were left to adhere for ~45 min and NI medium was added. On DIV10 NI was replaced with neural maintenance (NM) medium. Upon the appearance of neural rosettes, 20 ng/mL FGF2 was added for 2 days. When neurons started to form (~DIV21), rosettes were isolated manually after treatment with STEMdiff Neural Rosette Selection Reagent (STEMCELL Technologies) for 1 h. Rosettes were washed and plated on poly-L-ornithine/laminin-coated 6-well plates. 7 days after

rosettes were plated, the NPCs were expanded, again with STEMdiff Neuroal Rosette Selection Reagent (STEMCELL Technologies) for 1.5hr. NPCs were washed and plated on poly-L-ornithine/laminin coated 6-well plates. Between DIV35 and DIV 38 NPCs were frozen in NM supplemented with 10% DMSO and 20 ng/mL FGF2.

For cortical neuron maturation, ~600,000-1,000,000 NPCs were plated on 12-well poly-L-ornithine/laminin-coated plates and maintained in Neurobasal medium supplemented with B-27 serum-free supplement, 2 mM Glutamax and 100 U/mL-0.1 mg/mL penicillin-streptomycin (all Life Technologies). During the first 7 days after plating, cells were treated with 10 μM DAPT (Sigma-Aldrich) to augment neuronal maturation.

Western Blotting. Neurons were harvested and RNA and protein were purified using the NucleoSpin RNA/Protein kit (Macherey Nagel) according to the manufacturer's instructions. Lysates were run on Criterion™ TGX™ 4-20% precast gels for SDS-PAGE at 100V, or Criterion™Tris-Tricine 10-20% precast gels for SDS-PAGE of APP β-CTFs at 100V (Bio-Rad). Gels were then blotted using standard techniques onto an Odyssey nitrocellulose membrane (LI-COR). Membranes were blocked in 5% non-fat dairy milk in TBS-T, and were probed with primary antibodies listed above. IRDye conjugated secondary antibodies (LI-COR) were used at 1:10,000. Proteins were detected using the Odyssey CLx Imaging System (LI-COR).

Antibodies. The following antibodies were used: Oct4 (1:500, Stemgent S090023), Tra160 (1:500, Millipore MAB4360), SSEA4 (1:500, Abcam ab16287), Nanog (1:500, Cell Signaling 4903), MAP2 (1:2000, Abcam 5392), Tuj1 (mouse 1:1000, Covance MMS-435P / rabbit 1:1000, Covance MRB-435P), Presenilin-1 NTF (1:500 Milipore MAB1563), Presenilin 1 CTF (1:500, Milipore MAB5232), Nicastrin (1:5000, Milipore MAB5556), PEN2 (1:1000, Abcam ab18189), Aph1 (1:1000, Milipore ABC1696), APP C-term (1:10000, Abcam Y188 ab32136), Presenilin-2 (1:1000, Cell Signaling 9979), K9JA (1:10000 (WB), 1:500 IF, Dako), HT7 (1:1000, Thermo-Fisher), MC1 (1:1000; gift from Peter Davies)(anti-mouse/rabbit/rat/chicken Alexa Fluor 488/568/647 (Invitrogen 1:500).

Amyloid-β measurements. Aβ was measured in cell supernatant conditioned for 1 day (DIV8 NPCs), or 7 days (~DIV60 cortical neurons) after full media washout. Experiments were performed in 3 biological replicates. Supernatants from experiments collected at different time points were frozen at -80 ˚C. Secreted Aβ1-38, Aβ1-40 and Aβ1-42 was measured with MSD Human (6E10) Aβ V-PLEX kits (Meso Scale Discovery) according to the manufacturer's directions. Secreted sAPPα and sAPPβ were also measured simultaneously, and from matching supernatants, with MSD sAPPα/sAPPβ kit (Meso Scale Discovery) according to the

manufacturer's directions. NPC and neuronal total Aβ levels were normalized to total sAPPβ levels (Meso Scale Discovery).

Mice. Animals were bred according to IACUC protocols at the Rockefeller University. Newborn mice (P0) were collected from either ROSA26-EGFP (Giel-Moloney et al., 2007), or CD1 WT mice (Jackson Laboratories).

Statistical Analysis. Experimental data was analyzed for significance using Graphpad Prism 7. $P<0.05$ was considered statistically significant. All experiments were analyzed by one-way ANOVA followed by post testing with Dunnett's method, as alterations were compared to controls.

Appendix 1: Rights and permissions

Figure 1.3

Reprinted by permission from Macmillan Publishers Ltd: Nature Reviews Neuroscience. Götz, J., and Ittner, L.M. Animal models of Alzheimer's disease and frontotemporal dementia. *9*, 532–544., copyright (2008).

Figure 4.1

Reprinted by permission from Macmillan Publishers Ltd: Nature Reviews Drug Discovery. Van Dam, D., and De Deyn, P.P. Drug discovery in dementia: the role of rodent models. *5*, 956–970., copyright (2006).

Figure 4.2

Reprinted by permission from Macmillan Publishers Ltd: Nature. Götz, J., and Ittner, L.M. Paquet, D., Kwart, D., Chen, A., Sproul, A., Jacob, S., Teo, S., Olsen, K.M., Gregg, A., Noggle, S., and Tessier-Lavigne, M. Efficient introduction of specific homozygous and heterozygous mutations using CRISPR/Cas9. *533*, 125–129., copyright (2016)

References

Alonso, A.D., Grundke-Iqbal, I., Barra, H.S., and Iqbal, K. (1997). Abnormal phosphorylation of tau and the mechanism of Alzheimer neurofibrillary degeneration: sequestration of microtubule-associated proteins 1 and 2 and the disassembly of microtubules by the abnormal tau. Proc Natl Acad Sci U S A *94*, 298–303.

alzforum.org Alzforum Mutation Database.

Alzheimer's Association (2017). 2017 Alzheimer's disease facts and figures. Alzheimer's & Dementia *13*, 325–373.

Alzheimer, A. (1907). Uber eine eigenartige Erkrankung der Hirnrinde. Allgemeine Zeitschrife Psychiatrie *64*, 146–148.

American Psychiatric Association (2013). Diagnostic and Statistical Manual of Mental Disorders (DSM-5®) (American Psychiatric Pub).

Arnold, S.E., Hyman, B.T., Flory, J., Damasio, A.R., and Van Hoesen, G.W. (1991). The topographical and neuroanatomical distribution of neurofibrillary tangles and neuritic plaques in the cerebral cortex of patients with Alzheimer's disease. Cereb. Cortex *1*, 103–116.

Asai, H., Ikezu, S., Tsunoda, S., Medalla, M., Luebke, J., Haydar, T., Wolozin, B., Butovsky, O., Kügler, S., and Ikezu, T. (2015). Depletion of microglia and inhibition of exosome synthesis halt tau propagation. Nature Publishing Group *18*, 1584–1593.

Barghorn, S., Zheng-Fischhofer, Q., Ackmann, M., Biernat, J., Bergen, von, M., Mandelkow, E.M., and Mandelkow, E. (2000). Structure, microtubule interactions, and paired helical filament aggregation by tau mutants of frontotemporal dementias. Biochemistry *39*, 11714–11721.

Barghorn, S., Biernat, J., and Mandelkow, E. (2005). Purification of recombinant tau protein and preparation of Alzheimer-paired helical filaments in vitro. Methods Mol. Biol. *299*, 35–51.

Bentahir, M., Nyabi, O., Verhamme, J., Tolia, A., Horre, K., Wiltfang, J., Esselmann, H., and Strooper, B. (2006). Presenilin clinical mutations can affect gamma-secretase activity by different mechanisms. J Neurochem *96*, 732–742.

Bergen, von, M., Barghorn, S., Li, L., Marx, A., Biernat, J., Mandelkow, E.M., and Mandelkow, E. (2001). Mutations of tau protein in frontotemporal dementia promote aggregation of paired helical filaments by enhancing local beta-structure. J Biol Chem *276*, 48165–48174.

Boch, J., Scholze, H., Schornack, S., Landgraf, A., Hahn, S., Kay, S., Lahaye, T., Nickstadt, A., and Bonas, U. (2009). Breaking the Code of DNA Binding Specificity of TAL-Type III Effectors. Science *326*, 1509–1512.

Borchelt, D.R., Thinakaran, G., Eckman, C.B., Lee, M.K., Davenport, F., Ratovitsky, T., Prada, C.M., Kim, G., Seekins, S., Yager, D., et al. (1996). Familial Alzheimer's disease-linked presenilin 1 variants elevate A beta 1-42/1-40 ratio in vitro and in vivo. Neuron *17*, 1005–1013.

Braak, H., and Braak, E. (1991). Neuropathological stageing of Alzheimer-related changes. Acta Neuropathol *82*, 239–259.

Braak, H., Thal, D.R., Ghebremedhin, E., and Del Tredici, K. (2011). Stages of the Pathologic Process in Alzheimer Disease: Age Categories From 1 to 100 Years. J. Neuropathol. Exp. Neurol. *70*, 960–969.

Calafate, S., Flavin, W., Verstreken, P., and Moechars, D. (2016). Loss of Bin1 Promotes the Propagation of Tau Pathology. CellReports *17*, 931–940.

Canver, M.C., Bauer, D.E., Dass, A., Yien, Y.Y., Chung, J., Masuda, T., Maeda, T., Paw, B.H., and Orkin, S.H. (2014). Characterization of genomic deletion efficiency mediated by clustered regularly interspaced palindromic repeats (CRISPR)/Cas9 nuclease system in mammalian cells. J Biol Chem *289*, 21312–21324.

Castellano, J.M., Kim, J., Stewart, F.R., Jiang, H., DeMattos, R.B., Patterson, B.W., Fagan, A.M., Morris, J.C., Mawuenyega, K.G., Cruchaga, C., et al. (2011). Human apoE isoforms differentially regulate brain amyloid-β peptide clearance. Science Translational Medicine *3*, 89ra57–89ra57.

Cataldo, A., Peterhoff, C.M., Troncoso, J.C., Gómez-Isla, T., Hyman, B.T., and Nixon, R.A. (2000). Endocytic Pathway Abnormalities Precede Amyloid ? Deposition in Sporadic Alzheimer?s Disease and Down Syndrome. Am. J. Pathol. *157*, 277–286.

Cataldo, A., Rebeck, G.W., Ghetti, B., and Hulette, C. (2001). Endocytic disturbances distinguish among subtypes of Alzheimer's disease and related disorders. Annals of ….

Chai, X., Dage, J.L., and Citron, M. (2012). Constitutive secretion of tau protein by an unconventional mechanism. Neurobiol Dis *48*, 356–366.

Chambers, S.M., Fasano, C.A., Papapetrou, E.P., Tomishima, M., Sadelain, M., and Studer, L. (2009). Highly efficient neural conversion of human ES and iPS cells by dual inhibition of SMAD signaling. Nat Biotechnol *27*, 275–280.

Chávez-Gutiérrez, L., Bammens, L., Benilova, I., Vandersteen, A., Benurwar, M., Borgers, M., Lismont, S., Zhou, L., Van Cleynenbreugel, S., Esselmann, H., et al. (2012). The mechanism of γ-Secretase dysfunction in familial Alzheimer disease. Embo J. *31*, 2261–2274.

Citron, M., Diehl, T.S., Gordon, G., Biere, A.L., Seubert, P., and Selkoe, D.J. (1996). Evidence that the 42- and 40-amino acid forms of amyloid beta protein are generated from the beta-amyloid precursor protein by different protease activities. Proc Natl Acad Sci U S A *93*, 13170–13175.

Citron, M., Westaway, D., Xia, W., Carlson, G., and Diehl, T. (1997). Mutant presenilins of Alzheimer's disease increase production of 42-residue amyloid β-protein in both transfected cells and transgenic mice. Nature Medicine *3*, 67–72.

Clark, R.F., Hutton, M., Fulder, R.A., Froelich, S., Karran, E., Talbot, C., Crook, R., Lendon, C., PRIHAR, G., HE, C., et al. (1995). The Structure of the Presenilin-1 (S182) Gene and Identification of 6 Novel Mutations in Early-Onset Ad Families. Nat Genet *11*, 219–222.

Clavaguera, F., Bolmont, T., Crowther, R.A., Abramowski, D., Frank, S., Probst, A., Fraser, G., Stalder, A.K., Beibel, M., Staufenbiel, M., et al. (2009). Transmission and spreading of tauopathy in transgenic mouse brain. Nat Cell Biol *11*, 909–U325.

Cong, L., Ran, F.A., Cox, D., Lin, S., Barretto, R., Habib, N., Hsu, P.D., Wu, X., Jiang, W., Marraffini, L.A., et al. (2013). Multiplex genome engineering using CRISPR/Cas systems. Science *339*, 819–823.

Corder, E.H., Saunders, A.M., Risch, N.J., Strittmatter, W.J., Schmechel, D.E., Gaskell, P.C., Rimmler, J.B., Locke, P.A., Conneally, P.M., and Schmader, K.E. (1994). Protective effect of apolipoprotein E type 2 allele for late onset Alzheimer disease. Nat Genet *7*, 180–184.

Corder, E.H., Saunders, A.M., Strittmatter, W.J., Schmechel, D.E., Gaskell, P.C., Small, G.W., Roses, A.D., Haines, J.L., and Pericak-Vance, M.A. (1993). Gene dose of apolipoprotein E type 4 allele and the risk of Alzheimer's disease in late onset families. Science *261*, 921–923.

Cowan, C.A., Klimanskaya, I., McMahon, J., Atienza, J., Witmyer, J., Zucker, J.P., Wang, S., Morton, C.C., McMahon, A.P., Powers, D., et al. (2004). Derivation of embryonic stem-cell lines from human blastocysts. N. Engl. J. Med. *350*, 1353–1356.

Crowe, A., James, M.J., Lee, V.M.-Y., Smith, A.B., Trojanowski, J.Q., Ballatore, C., and Brunden, K.R. (2013). Aminothienopyridazines and methylene blue affect Tau

fibrillization via cysteine oxidation. J Biol Chem *288*, 11024–11037.

Davis, D.G., Schmitt, F.A., and Wekstein, D.R. (1999). Alzheimer neuropathologic alterations in aged cognitively normal subjects. Journal of ….

de Calignon, A., Polydoro, M., Suárez-Calvet, M., William, C., Adamowicz, D.H., Kopeikina, K.J., Pitstick, R., Sahara, N., Ashe, K.H., Carlson, G.A., et al. (2012). Propagation of Tau Pathology in a Model of Early Alzheimer's Disease. Neuron *73*, 685–697.

De Strooper, B., Annaert, W., Cupers, P., and Saftig, P. (1999). A presenilin-1-dependent γ-secretase-like protease mediates release of Notch intracellular domain. Nature *398*, 518–522.

De Strooper, B., Beullens, M., and Contreras, B. (1997). Phosphorylation, subcellular localization, and membrane orientation of the Alzheimer's disease-associated presenilins. J Biol Chem *272*, 3590–3598.

De Strooper, B., Saftig, P., Craessaerts, K., Vanderstichele, H., Guhde, G., Annaert, W., Figura, Von, K., and Van Leuven, F. (1998). Deficiency of presenilin-1 inhibits the normal cleavage of amyloid precursor protein. Nature *391*, 387–390.

De Strooper, B. (2007). Loss-of-function presenilin mutations in Alzheimer disease. Talking Point on the role of presenilin mutations in Alzheimer disease. *8*, 141–146.

DeFrancesco, L. (2011). Move over ZFNs. Nat Biotechnol *29*, 681–684.

Dow, L.E., Fisher, J., O'Rourke, K.P., Muley, A., Kastenhuber, E.R., Livshits, G., Tschaharganeh, D.F., Socci, N.D., and Lowe, S.W. (2015). Inducible in vivo genome editing with CRISPR-Cas9. Nat Biotechnol *33*, 390–394.

Duff, K., Eckman, C., Zehr, C., Yu, X., Prada, C.M., Perez-tur, J., Hutton, M., Buee, L., Harigaya, Y., Yager, D., et al. (1996). Increased amyloid-beta42(43) in brains of mice expressing mutant presenilin 1. Nature *383*, 710–713.

Dujardin, S., Bégard, S., Caillierez, R., Lachaud, C., Delattre, L., Carrier, S., Loyens, A., Galas, M.-C., Bousset, L., Melki, R., et al. (2014a). Ectosomes: a new mechanism for non-exosomal secretion of tau protein. PLoS ONE *9*, e100760.

Dujardin, S., Lécolle, K., Caillierez, R., Bégard, S., Zommer, N., Lachaud, C., Carrier, S., Dufour, N., Aurégan, G., Winderickx, J., et al. (2014b). Neuron-to-neuron wild-type Tau protein transfer through a trans-synaptic mechanism: relevance to sporadic tauopathies. Acta Neuropathol Commun *2*, 14.

Dumanchin, C., Camuzat, A., Campion, D., Verpillat, P., Hannequin, D., Dubois, B., Saugier-Veber, P., Martin, C., Penet, C., Charbonnier, F., et al. (1998). Segregation of a missense mutation in the microtubule-associated protein tau gene with familial frontotemporal dementia and parkinsonism. Human Molecular Genetics *7*, 1825–1829.

Dumanchin, C., Tournier, I., Martin, C., Didic, M., Belliard, S., Carlander, B., Rouhart, F., Duyckaerts, C., Pellissier, J.F., Latouche, J.B., et al. (2006). Biological effects of four PSEN1 gene mutations causing Alzheimer disease with spastic paraparesis and cotton wool plaques. Human Mutation *27*, 1063–1063.

Ebneth, A., Godemann, R., Stamer, K., Illenberger, S., Trinczek, B., and Mandelkow, E. (1998). Overexpression of tau protein inhibits kinesin-dependent trafficking of vesicles, mitochondria, and endoplasmic reticulum: implications for Alzheimer's disease. J. Cell Biol. *143*, 777–794.

Fischer, D., Mukrasch, M.D., Bergen, von, M., Klos-Witkowska, A., Biernat, J., Griesinger, C., Mandelkow, E., and Zweckstetter, M. (2007). Structural and microtubule binding properties of tau mutants of frontotemporal dementias. Biochemistry *46*, 2574–2582.

Frost, B., Jacks, R.L., and Diamond, M.I. (2009a). Propagation of tau misfolding from the outside to the inside of a cell. J Biol Chem *284*, 12845–12852.

Frost, B., Ollesch, J., Wille, H., and Diamond, M.I. (2009b). Conformational diversity of wild-type Tau fibrils specified by templated conformation change. J Biol Chem *284*, 3546–3551.

Fu, Y., Foden, J.A., Khayter, C., Maeder, M.L., Reyon, D., Joung, J.K., and Sander, J.D. (2013). High-frequency off-target mutagenesis induced by CRISPR-Cas nucleases in human cells. Nat Biotechnol *31*, 822–826.

Gaztelumendi, N., and Nogués, C. (2014). Chromosome instability in mouse embryonic stem cells. Sci Rep.

George-Hyslop, P.S., Haines, J., Rogaev, E., Mortilla, M., Vaula, G., Pericak-Vance, M., Foncin, J.F., Montesi, M., Bruni, A., Sorbi, S., et al. (1992). Genetic evidence for a novel familial Alzheimer's disease locus on chromosome 14. Nat Genet *2*, 330–334.

Giel-Moloney, M., Krause, D.S., Chen, G., Van Etten, R.A., and Leiter, A.B. (2007). Ubiquitous and uniform in vivo fluorescence in ROSA26-EGFP BAC transgenic mice. Genesis *45*, 83–89.

Goate, A., CHARTIERHARLIN, M.C., Mullan, M., BROWN, J., Crawford, F., FIDANI, L., GIUFFRA, L., HAYNES, A., IRVING, N., JAMES, L., et al. (1991). Segregation of a Missense Mutation in the Amyloid Precursor Protein Gene with Familial Alzheimers-Disease. Nature *349*, 704–706.

Goldgaber, D., Lerman, M.I., McBride, O.W., and Saffiotti, U. (1987). Characterization and chromosomal localization of a cDNA encoding brain amyloid of Alzheimer's disease. Science.

González, F., Zhu, Z., Shi, Z.-D., Lelli, K., Verma, N., Li, Q.V., and Huangfu, D. (2014). An iCRISPR Platform for Rapid, Multiplexable, and Inducible Genome Editing in Human Pluripotent Stem Cells. Stem Cell *15*, 215–226.

Gossen, M., and Bujard, H. (1992). Tight control of gene expression in mammalian cells by tetracycline-responsive promoters. Proc Natl Acad Sci U S A *89*, 5547–5551.

Götz, J., and Ittner, L.M. (2008). Animal models of Alzheimer's disease and frontotemporal dementia. Nat Rev Neurosci *9*, 532–544.

Grant, M.A., Lazo, N.D., Lomakin, A., Condron, M.M., Arai, H., Yamin, G., Rigby, A.C., and Teplow, D.B. (2007). Familial Alzheimer's disease mutations alter the stability of the amyloid beta-protein monomer folding nucleus. Proc Natl Acad Sci U S A *104*, 16522–16527.

Grundke-Iqbal, I., Iqbal, K., Quinlan, M., Tung, Y.C., Zaidi, M.S., and Wisniewski, H.M. (1986). Microtubule-associated protein tau. A component of Alzheimer paired helical filaments. J Biol Chem *261*, 6084–6089.

Guerreiro, R., and Hardy, J. (2014). Genetics of Alzheimer's disease. Neurotherapeutics *11*, 732–737.

Guerreiro, R., Brás, J., and Hardy, J. (2013). SnapShot: genetics of Alzheimer's disease. Cell *155*, 968–968.e1.

Guo, J.L., and Lee, V.M.-Y. (2011). Seeding of normal Tau by pathological Tau conformers drives pathogenesis of Alzheimer-like tangles. J Biol Chem *286*, 15317–15331.

Haapasalo, A., and Kovacs, D.M. (2011). The Many Substrates of Presenilin/γ-Secretase. J Alzheimers Dis *25*, 3–28.

Hall, A.M., and Roberson, E.D. (2012). Mouse models of Alzheimer's disease. Brain Research Bulletin *88*, 3–12.

Hardy, J.A., and Higgins, G.A. (1992). Alzheimers-Disease - the Amyloid Cascade Hypothesis. Science *256*, 184–185.

Hartmann, D., De Strooper, B., and Saftig, P. (1999). Presenilin-1 deficiency leads to loss of Cajal-Retzius neurons and cortical dysplasia similar to human type 2 lissencephaly. Current Biology *9*, 719–727.

Hendriks, L., van Duijn, C.M., Cras, P., Cruts, M., Van Hul, W., van Harskamp, F., Warren, A., McInnis, M.G., Antonarakis, S.E., Martin, J.-J., et al. (1992). Presenile dementia and cerebral haemorrhage linked to a mutation at codon 692 of the l[beta]ll[ndash]lamyloid precursor protein gene. Nat Genet *1*, 218–221.

Hockemeyer, D., Soldner, F., Beard, C., Gao, Q., Mitalipova, M., DeKelver, R.C., Katibah, G.E., Amora, R., Boydston, E.A., Zeitler, B., et al. (2009). Efficient targeting of expressed and silent genes in human ESCs and iPSCs using zinc-finger nucleases. Nat Biotechnol *27*, 851–857.

Hockemeyer, D., Wang, H., Kiani, S., Lai, C.S., Gao, Q., Cassady, J.P., Cost, G.J., Zhang, L., Santiago, Y., Miller, J.C., et al. (2011). Genetic engineering of human pluripotent cells using TALE nucleases. Nat Biotechnol *29*, 731–734.

Holcomb, L.A., Gordon, M.N., Jantzen, P., Hsiao, K., Duff, K., and Morgan, D. (1999). Behavioral Changes in Transgenic Mice Expressing Both Amyloid Precursor Protein and Presenilin-1 Mutations: Lack of Association with Amyloid Deposits. Behav Genet *29*, 177–185.

Holmes, B.B., Furman, J.L., Mahan, T.E., Yamasaki, T.R., Mirbaha, H., Eades, W.C., Belaygorod, L., Cairns, N.J., Holtzman, D.M., and Diamond, M.I. (2014). Proteopathic tau seeding predicts tauopathy in vivo. Proceedings of the National Academy of Sciences *111*, E4376–E4385.

Holmes, B.B., DeVos, S.L., Kfoury, N., Li, M., Jacks, R., Yanamandra, K., Ouidja, M.O., Brodsky, F.M., Marasa, J., Bagchi, D.P., et al. (2013). Heparan sulfate proteoglycans mediate internalization and propagation of specific proteopathic seeds. Proc Natl Acad Sci U S A *110*, E3138–E3147.

Honda, M., Minami, I., Tooi, N., Morone, N., Nishioka, H., Uemura, K., Kinoshita, A., Heuser, J.E., Nakatsuji, N., and Aiba, K. (2016). The modeling of Alzheimer's disease by the overexpression of mutant Presenilin 1 in human embryonic stem cells. Biochemical and Biophysical Research Communications *469*, 587–592.

Hong, M., Zhukareva, V., Vogelsberg-Ragaglia, V., Wszolek, Z., Reed, L., Miller, B.I., Geschwind, D.H., Bird, T.D., McKeel, D., Goate, A., et al. (1998). Mutation-specific functional impairments in distinct tau isoforms of hereditary FTDP-17.

Science *282*, 1914–1917.

Horvath, P., and Barrangou, R. (2010). CRISPR/Cas, the Immune System of Bacteria and Archaea. Science *327*, 167.

Hsiao, K., Chapman, P., Nilsen, S., and Eckman, C. (1996). Correlative memory deficits, A beta elevation, and amyloid plaques in transgenic mice. Science.

Hsu, P.D., Lander, E.S., and Zhang, F. (2014). Development and Applications of CRISPR-Cas9 for Genome Engineering. Cell *157*, 1262–1278.

Hutton, M., Lendon, C.L., Rizzu, P., Baker, M., Froelich, S., Houlden, H., Pickering-Brown, S., Chakraverty, S., Isaacs, A., Grover, A., et al. (1998). Association of missense and 5'-splice-site mutations in tau with the inherited dementia FTDP-17. Nature *393*, 702–705.

Iba, M., Guo, J.L., McBride, J.D., Zhang, B., Trojanowski, J.Q., and Lee, V.M.-Y. (2013). Synthetic tau fibrils mediate transmission of neurofibrillary tangles in a transgenic mouse model of Alzheimer's-like tauopathy. J. Neurosci. *33*, 1024–1037.

Iqbal, K., Liu, F., and Gong, C.-X. (2015). Tau and neurodegenerative disease: the story so far. Nature Publishing Group *12*, 15–27.

Iwatsubo, T., Mann, D.M., Odaka, A., Suzuki, N., and Ihara, Y. (1995). Amyloid beta protein (A beta) deposition: A beta 42(43) precedes A beta 40 in Down syndrome. Annals of Neurology *37*, 294–299.

Janssen, J.C., Beck, J.A., Campbell, T.A., Dickinson, A., Fox, N.C., Harvey, R.J., Houlden, H., Rossor, M.N., and Collinge, J. (2003). Early onset familial Alzheimer's disease: Mutation frequency in 31 families. Neurology *60*, 235–239.

Jarrett, J.T., Berger, E.P., and Lansbury, P.T. (1993). The carboxy terminus of the beta amyloid protein is critical for the seeding of amyloid formation: implications for the pathogenesis of Alzheimer's disease. Biochemistry *32*, 4693–4697.

Jicha, G.A., Bowser, R., Kazam, I.G., and Davies, P. (1997). Alz-50 and MC-1, a new monoclonal antibody raised to paired helical filaments, recognize conformational epitopes on recombinant tau. J Neurosci Res *48*, 128–132.

Jin, M., Shepardson, N., Yang, T., Chen, G., Walsh, D., and Selkoe, D.J. (2011). Soluble amyloid beta-protein dimers isolated from Alzheimer cortex directly induce Tau hyperphosphorylation and neuritic degeneration. Proceedings of the National Academy of Sciences *108*, 5819–5824.

Jinek, M., Chylinski, K., Fonfara, I., Hauer, M., Doudna, J.A., and Charpentier, E. (2012). A programmable dual-RNA-guided DNA endonuclease in adaptive bacterial immunity. Science *337*, 816–821.

Jonsson, T., Atwal, J.K., Steinberg, S., Snaedal, J., Jonsson, P.V., Bjornsson, S., Stefansson, H., Sulem, P., Gudbjartsson, D., Maloney, J., et al. (2012). A mutation in APP protects against Alzheimer's disease and age-related cognitive decline. Nature *488*, 96–99.

Kahler, D.J., Ahmad, F.S., Ritz, A., Hua, H., Moroziewicz, D.N., Sproul, A.A., Dusenberry, C.R., Shang, L., Paull, D., Zimmer, M., et al. (2013). Improved Methods for Reprogramming Human Dermal Fibroblasts Using Fluorescence Activated Cell Sorting. PLoS ONE *8*, e59867–12.

Kang, J., Lemaire, H.G., Unterbeck, A., Salcaum, J.M., Masters, C.L., Grzeschik, K.H., Multhaup, G., Beyreuther, K., and Mullerhill, B. (1987). The Precursor of Alzheimers-Disease Amyloid-A4 Protein Resembles a Cell-Surface Receptor. Nature *325*, 733–736.

Karch, C.M., Jeng, A.T., and Goate, A.M. (2012). Extracellular Tau levels are influenced by variability in Tau that is associated with tauopathies. J Biol Chem *287*, 42751–42762.

Kero, M., Paetau, A., Polvikoski, T., Tanskanen, M., Sulkava, R., Jansson, L., Myllykangas, L., and Tienari, P.J. (2013). Amyloid precursor protein (APP) A673T mutation in the elderly Finnish population. Neurobiol. Aging *34*, 1518.e1–1518.e3.

Kfoury, N., Holmes, B.B., Jiang, H., Holtzman, D.M., and Diamond, M.I. (2012). Trans-cellular Propagation of Tau Aggregation by Fibrillar Species. J Biol Chem *287*, 19440–19451.

Kim, W., Lee, S., and Hall, G.F. (2010a). Secretion of human tau fragments resembling CSF-tau in Alzheimer's disease is modulated by the presence of the exon 2 insert. FEBS Lett. *584*, 3085–3088.

Kim, W., Lee, S., Jung, C., Ahmed, A., Lee, G., and Hall, G.F. (2010b). Interneuronal transfer of human tau between Lamprey central neurons in situ. J Alzheimers Dis *19*, 647–664.

Klafki, H., Abramowski, D., Swoboda, R., Paganetti, P.A., and Staufenbiel, M. (1996). The carboxyl termini of beta-amyloid peptides 1-40 and 1-42 are generated by distinct gamma-secretase activities. J Biol Chem *271*, 28655–28659.

Koch, P., Tamboli, I.Y., Mertens, J., Wunderlich, P., Ladewig, J., Stüber, K.,

Esselmann, H., Wiltfang, J., Brüstle, O., and Walter, J. (2012). Presenilin-1 L166P mutant human pluripotent stem cell-derived neurons exhibit partial loss of γ-secretase activity in endogenous amyloid-β generation. Am. J. Pathol. *180*, 2404–2416.

Koffie, R.M., Meyer-Luehmann, M., Hashimoto, T., Adams, K.W., Mielke, M.L., Garcia-Alloza, M., Micheva, K.D., Smith, S.J., Kim, M.L., Lee, V.M., et al. (2009). Oligomeric amyloid beta associates with postsynaptic densities and correlates with excitatory synapse loss near senile plaques. Proceedings of the National Academy of Sciences *106*, 4012–4017.

Kondo, T., Asai, M., Tsukita, K., Kutoku, Y., Ohsawa, Y., Sunada, Y., Imamura, K., Egawa, N., Yahata, N., Okita, K., et al. (2013). Modeling Alzheimer's disease with iPSCs reveals stress phenotypes associated with intracellular Aβ and differential drug responsiveness. Cell Stem Cell *12*, 487–496.

Kontsekova, E., Zilka, N., Kovacech, B., Novak, P., and Novak, M. (2014). First-in-man tau vaccine targeting structural determinants essential for pathological tau–tau interaction reduces tau oligomerisation and neurofibrillary degeneration in an Alzheimer's disease model. Alzheimers Res Ther *6*, 44.

Kosik, K.S., Orecchio, L.D., Bakalis, S., and Neve, R.L. (1989). Developmentally regulated expression of specific tau sequences. Neuron *2*, 1389–1397.

Kwart, D., Paquet, D., Teo, S., and Tessier-Lavigne, M. (2017). Precise and efficient scarless genome editing in stem cells using CORRECT. Nat Protoc *12*, 329–354.

Lazo, N.D., Grant, M.A., Condron, M.C., Rigby, A.C., and Teplow, D.B. (2005). On the nucleation of amyloid β-protein monomer folding. Protein Science *14*, 1581–1596.

Lee, S., Kim, W., Li, Z., and Hall, G.F. (2012). Accumulation of vesicle-associated human tau in distal dendrites drives degeneration and tau secretion in an in situ cellular tauopathy model. Int J Alzheimers Dis *2012*, 172837.

Lefort, N., Feyeux, M., Bas, C., and Féraud, O. (2008). Human embryonic stem cells reveal recurrent genomic instability at 20q11. 21. Nature.

Levitan, D., Doyle, T.G., Brousseau, D., Lee, M.K., Thinakaran, G., Slunt, H.H., Sisodia, S.S., and Greenwald, I. (1996). Assessment of normal and mutant human presenilin function in Caenorhabditis elegans. Proc Natl Acad Sci U S A *93*, 14940–14944.

Levy-Lahad, E., Wasco, W., Poorkaj, P., Romano, D.M., Oshima, J., Pettingell,

W.H., Yu, C.E., Jondro, P.D., Schmidt, S.D., Wang, K., et al. (1995). Candidate Gene for the Chromosome-1 Familial Alzheimers-Disease Locus. Science *269*, 973–977.

Lewis, P.A., Perez-tur, J., Golde, T.E., and Hardy, J. (2000). The Presenilin 1 C92S Mutation Increases Aβ 42 Production. Biochemical and Biophysical Research Communications *277*, 261–263.

Li, X., and Greenwald, I. (1996). Membrane topology of the C. elegans SEL-12 presenilin. Neuron *17*, 1015–1021.

Lindner, J., Rathjen, F.G., and Schachner, M. (1983). L1 mono- and polyclonal antibodies modify cell migration in early postnatal mouse cerebellum. Nature *305*, 427–430.

Liu, L., Drouet, V., Wu, J.W., Witter, M.P., Small, S.A., Clelland, C., and Duff, K. (2012). Trans-synaptic spread of tau pathology in vivo. PLoS ONE *7*, e31302–e31302.

Liu, Q., Waltz, S., Woodruff, G., Ouyang, J., Israel, M.A., Herrera, C., Sarsoza, F., Tanzi, R.E., Koo, E.H., Ringman, J.M., et al. (2014). Effect of Potent γ-Secretase Modulator in Human Neurons Derived From Multiple Presenilin 1–Induced Pluripotent Stem Cell Mutant Carriers. JAMA Neurol *71*, 1481–1489.

Luk, K.C., Kehm, V., Carroll, J., Zhang, B., O'Brien, P., Trojanowski, J.Q., and Lee, V.M.-Y. (2012). Pathological α-synuclein transmission initiates Parkinson-like neurodegeneration in nontransgenic mice. Science *338*, 949–953.

Mali, P., Yang, L., Esvelt, K.M., Aach, J., Guell, M., DiCarlo, J.E., Norville, J.E., and Church, G.M. (2013). RNA-guided human genome engineering via Cas9. Science *339*, 823–826.

Marambaud, P., Wen, P.H., Dutt, A., Shioi, J., Takashima, A., Siman, R., and Robakis, N.K. (2003). A CBP Binding Transcriptional Repressor Produced by the PS1/?-Cleavage of N-Cadherin Is Inhibited by PS1 FAD Mutations. Cell *114*, 635–645.

Masters, C.L., Simms, G., Weinman, N.A., Multhaup, G., McDonald, B.L., and Beyreuther, K. (1985). Amyloid Plaque Core Protein in Alzheimer-Disease and Down Syndrome. Proc Natl Acad Sci U S A *82*, 4245–4249.

Mawuenyega, K.G., Sigurdson, W., Ovod, V., Munsell, L., Kasten, T., Morris, J.C., Yarasheski, K.E., and Bateman, R.J. (2010). Decreased clearance of CNS beta-amyloid in Alzheimer's disease. Science *330*, 1774–1774.

Michel, C.H., Kumar, S., Pinotsi, D., Tunnacliffe, A., St George-Hyslop, P., Mandelkow, E., Mandelkow, E.M., Kaminski, C.F., and Kaminski Schierle, G.S. (2014). Extracellular Monomeric Tau Protein Is Sufficient to Initiate the Spread of Tau Protein Pathology. J Biol Chem *289*, 956–967.

Millecamps, S., and Julien, J.-P. (2013). Axonal transport deficits and neurodegenerative diseases. Nat Rev Neurosci *14*, 161–176.

Moehlmann, T., Winkler, E., Xia, X.F., Edbauer, D., Murrelll, J., Capell, A., Kaether, C., Zheng, H., Ghetti, B., Haass, C., et al. (2002). Presenilin-1 mutations of leucine 166 equally affect the generation of the Notch and APP intracellular domains independent of their effect on A beta(42) production. Proc Natl Acad Sci U S A *99*, 8025–8030.

Mohamed, N.-V., Plouffe, V., Rémillard-Labrosse, G., Planel, E., and Leclerc, N. (2014). Starvation and inhibition of lysosomal function increased tau secretion by primary cortical neurons. Sci Rep *4*, 5715.

Moscou, M.J., and Bogdanove, A.J. (2009). A Simple Cipher Governs DNA Recognition by TAL Effectors. Science *326*, 1501–1501.

Mucke, L., Masliah, E., Yu, G.-Q., Mallory, M., Rockenstein, E.M., Tatsuno, G., Hu, K., Kholodenko, D., Johnson-Wood, K., and McConlogue, L. (2000). High-Level Neuronal Expression of Aβ_{1–42} in Wild-Type Human Amyloid Protein Precursor Transgenic Mice: Synaptotoxicity without Plaque Formation. Journal of Neuroscience *20*, 4050–4058.

Mullan, M., Crawford, F., Axelman, K., Houlden, H., Lilius, L., Winblad, B., and Lannfelt, L. (1992). A Pathogenic Mutation for Probable Alzheimers-Disease in the App Gene at the N-Terminus of Beta-Amyloid. Nat Genet *1*, 345–347.

Muratore, C.R., Rice, H.C., Srikanth, P., Callahan, D.G., Shin, T., Benjamin, L.N.P., Walsh, D.M., Selkoe, D.J., and Young-Pearse, T.L. (2014). The familial Alzheimer's disease APPV717I mutation alters APP processing and Tau expression in iPSC-derived neurons. Human Molecular Genetics *23*, 3523–3536.

Nieweg, K., Andreyeva, A., van Stegen, B., ver, G.T.O., and Gottmann, K. (2015). Alzheimer's disease-related amyloid-beta induces synaptotoxicity in human iPS cell-derived neurons. Cell Death Dis *6*, e1709–e1713.

Oddo, S., Caccamo, A., Shepherd, J.D., Murphy, M.P., Golde, T.E., Kayed, R., Metherate, R., Mattson, M.P., Akbari, Y., and LaFerla, F.M. (2003). Triple-Transgenic Model of Alzheimer's Disease with Plaques and Tangles. Neuron *39*, 409–421.

Panchuk-Voloshina, N., Haugland, R.P., Bishop-Stewart, J., Bhalgat, M.K., Millard, P.J., Mao, F., and Leung, W.Y. (1999). Alexa dyes, a series of new fluorescent dyes that yield exceptionally bright, photostable conjugates. J. Histochem. Cytochem. *47*, 1179–1188.

Paquet, D., Kwart, D., Chen, A., Sproul, A., Jacob, S., Teo, S., Olsen, K.M., Gregg, A., Noggle, S., and Tessier-Lavigne, M. (2016). Efficient introduction of specific homozygous and heterozygous mutations using CRISPR/Cas9. Nature *533*, 125–129.

Paresce, D.M., Ghosh, R.N., and Maxfield, F.R. (1996). Microglial cells internalize aggregates of the Alzheimer's disease amyloid beta-protein via a scavenger receptor. Neuron *17*, 553–565.

Peacock, M.L., James T Warren, J., Roses, A.D., and Fink, J.K. (1993). Novel polymorphism in the A4 region of the amyloid precursor protein gene in a patient without Alzheimer's disease. Neurology *43*, 1254–1254.

Pecho-Vrieseling, E., Rieker, C., Fuchs, S., Bleckmann, D., Esposito, M.S., Botta, P., Goldstein, C., Bernhard, M., Galimberti, I., Müller, M., et al. (2014). Transneuronal propagation of mutant huntingtin contributes to non–cell autonomous pathology in neurons. Nat Neurosci *17*, 1064–1072.

Perez-tur, J., Froelich, S., Prihar, G., Crook, R., Baker, M., Duff, K., Wragg, M., Busfield, F., Lendon, C., Clark, R.F., et al. (1995). A mutation in Alzheimer's disease destroying a splice acceptor site in the presenilin-1 gene. Neuroreport *7*, 297.

Platt, R.J., Chen, S., Zhou, Y., Yim, M.J., Swiech, L., Kempton, H.R., Dahlman, J.E., Parnas, O., Eisenhaure, T.M., Jovanovic, M., et al. (2014). CRISPR-Cas9 Knockin Mice for Genome Editing and Cancer Modeling. Cell *159*, 440–455.

Pooler, A.M., Phillips, E.C., Lau, D.H.W., Noble, W., and Hanger, D.P. (2013). scientific report. Nature Publishing Group *14*, 389–394.

Qian, S., Jiang, P., Guan, X.M., Singh, G., Trumbauer, M.E., Yu, H., Chen, H.Y., Van der Ploeg, L., and Zheng, H. (1998). Mutant human presenilin 1 protects presenilin 1 null mouse against embryonic lethality and elevates A beta 1-42/43 expression. Neuron *20*, 611–617.

Rapoport, M., Dawson, H.N., Binder, L.I., Vitek, M.P., and Ferreira, A. (2002). Tau is essential to beta -amyloid-induced neurotoxicity. Proc Natl Acad Sci U S A *99*, 6364–6369.

Robakis, N.K., Ramakrishna, N., Wolfe, G., and Wisniewski, H.M. (1987). Molecular

cloning and characterization of a cDNA encoding the cerebrovascular and the neuritic plaque amyloid peptides. Proc Natl Acad Sci U S A *84*, 4190–4194.

Roberson, E.D., Scearce-Levie, K., Palop, J.J., Yan, F., Cheng, I.H., Wu, T., Gerstein, H., Yu, G.-Q., and Mucke, L. (2007). Reducing endogenous tau ameliorates amyloid beta-induced deficits in an Alzheimer's disease mouse model. Science *316*, 750–754.

Rogaev, E.I., Sherrington, R., Rogaeva, E.A., Levesque, G., Ikeda, M., Liang, Y., Chi, H., Lin, C., Holman, K., Tsuda, T., et al. (1995). Familial Alzheimer“s disease in kindreds with missense mutations in a gene on chromosome 1 related to the Alzheimer”s disease type 3 gene. Nature *376*, 775–778.

Roher, A., Wolfe, D., Palutke, M., and Kukuruga, D. (1986). Purification, Ultrastructure, and Chemical-Analysis of Alzheimer-Disease Amyloid Plaque Core Protein. Proc Natl Acad Sci U S A *83*, 2662–2666.

Römer, P., Hahn, S., Jordan, T., Strauß, T., Bonas, U., and Lahaye, T. (2007). Plant Pathogen Recognition Mediated by Promoter Activation of the Pepper Bs3 Resistance Gene. Science *318*, 645–648.

Ryman, D.C., Acosta-Baena, N., Aisen, P.S., Bird, T., Danek, A., Fox, N.C., Goate, A., Frommelt, P., Ghetti, B., Langbaum, J.B.S., et al. (2014). Symptom onset in autosomal dominant Alzheimer disease: a systematic review and meta-analysis. Neurology *83*, 253–260.

Saman, S., Kim, W., Raya, M., Visnick, Y., Miro, S., Saman, S., Jackson, B., McKee, A.C., Alvarez, V.E., Lee, N.C.Y., et al. (2012). Exosome-associated tau is secreted in tauopathy models and is selectively phosphorylated in cerebrospinal fluid in early Alzheimer disease. J Biol Chem *287*, 3842–3849.

Saman, S., Lee, N.C.Y., Inoyo, I., Jin, J., Li, Z., Doyle, T., McKee, A.C., and Hall, G.F. (2014). Proteins recruited to exosomes by tau overexpression implicate novel cellular mechanisms linking tau secretion with Alzheimer's disease. J Alzheimers Dis *40 Suppl 1*, S47–S70.

Sanders, D.W., Kaufman, S.K., DeVos, S.L., Sharma, A.M., Mirbaha, H., Li, A., Barker, S.J., Foley, A.C., Thorpe, J.R., Serpell, L.C., et al. (2014). Distinct tau prion strains propagate in cells and mice and define different tauopathies. Neuron *82*, 1271–1288.

Santa-Maria, I., Varghese, M., Ksiezak-Reding, H., Dzhun, A., Wang, J., and Pasinetti, G.M. (2012). Paired Helical Filaments from Alzheimer Disease Brain Induce Intracellular Accumulation of Tau Protein in Aggresomes. J Biol Chem *287*,

20522–20533.

Schellenberg, G.D., Bird, T.D., Wijsman, E.M., ORR, H.T., ANDERSON, L., Nemens, E., WHITE, J.A., BONNYCASTLE, L., WEBER, J.L., ALONSO, M.E., et al. (1992). Genetic-Linkage Evidence for a Familial Alzheimers-Disease Locus on Chromosome-14. Science *258*, 668–671.

Scheltens, P., Blennow, K., Breteler, M.M.B., De Strooper, B., Frisoni, G.B., Salloway, S., and Van der Flier, W.M. (2016). Alzheimer's disease. Lancet *388*, 505–517.

Scheuner, D., Eckman, C., Jensen, M., Song, X., Citron, M., Suzuki, N., Bird, T.D., HARDY, J., Hutton, M., Kukull, W., et al. (1996). Secreted amyloid beta-protein similar to that in the senile plaques of Alzheimer“s disease is increased in vivo by the presenilin 1 and 2 and APP mutations linked to familial Alzheimer”s disease. Nature Medicine *2*, 864–870.

Selkoe, D.J. (1996). Amyloid -Protein and the Genetics of Alzheimer's Disease. J Biol Chem *271*, 18295–18298.

Selkoe, D.J. (2000). Toward a comprehensive theory for Alzheimer“s disease. Hypothesis: Alzheimer”s disease is caused by the cerebral accumulation and cytotoxicity of amyloid beta-protein. Ann. N. Y. Acad. Sci. *924*, 17–25.

Selkoe, D.J., and Hardy, J. (2016). The amyloid hypothesis of Alzheimer's disease at 25 years. EMBO Mol Med. *8*, 595–608.

Shen, J., Bronson, R.T., Chen, D.F., Xia, W., Selkoe, D.J., and Tonegawa, S. (1997). Skeletal and CNS Defects in Presenilin-1-Deficient Mice. Cell *89*, 629–639.

Shi, Y., Kirwan, P., Smith, J., MacLean, G., Orkin, S.H., and Livesey, F.J. (2012a). A Human Stem Cell Model of Early Alzheimer's Disease Pathology in Down Syndrome. Science Translational Medicine *4*, 124ra29–124ra29.

Shi, Y., Kirwan, P., and Livesey, F.J. (2012b). Directed differentiation of human pluripotent stem cells to cerebral cortex neurons and neural networks. Nat Protoc *7*, 1836–1846.

Song, W., Nadeau, P., Yuan, M., Yang, X., Shen, J., and Yankner, B.A. (1999). Proteolytic release and nuclear translocation of Notch-1 are induced by presenilin-1 and impaired by pathogenic presenilin-1 mutations. Proc Natl Acad Sci U S A *96*, 6959–6963.

Southern, E. (2006). Southern blotting. Nat Protoc *1*, 518–525.

Spires-Jones, T.L., and Hyman, B.T. (2014). The Intersection of Amyloid Beta and Tau at Synapses in Alzheimer's Disease. Neuron *82*, 756–771.

Sproul, A.A., Jacob, S., Pre, D., Kim, S.H., Nestor, M.W., Navarro-Sobrino, M., Santa-Maria, I., Zimmer, M., Aubry, S., Steele, J.W., et al. (2014). Characterization and Molecular Profiling of PSEN1 Familial Alzheimer's Disease iPSC-Derived Neural Progenitors. PLoS ONE *9*, e84547.

St George-Hyslop, P.H., Tanzi, R.E., Polinsky, R.J., Haines, J.L., Nee, L., Watkins, P.C., Myers, R.H., Feldman, R.G., Pollen, D., Drachman, D., et al. (1987). The Genetic-Defect Causing Familial Alzheimers-Disease Maps on Chromosome-21. Science *235*, 885–890.

Stelzmann, R.A., Norman Schnitzlein, H., and Reed Murtagh, F. (1995). An English Translation of Alzheimer's 1907 Uaper, 'Über eine eigenartige Erkankung der Hirnrinde'. Clinical Anatomy *8*, 429–431.

Strittmatter, W.J., Saunders, A.M., Schmechel, D., Pericak-Vance, M., Enghild, J., Salvesen, G.S., and Roses, A.D. (1993). Apolipoprotein E: high-avidity binding to beta-amyloid and increased frequency of type 4 allele in late-onset familial Alzheimer disease. Proc Natl Acad Sci U S A *90*, 1977–1981.

Sturchler-Pierrat, C., Abramowski, D., Duke, M., Wiederhold, K.H., Mistl, C., Rothacher, S., Ledermann, B., Bürki, K., Frey, P., Paganetti, P.A., et al. (1997). Two amyloid precursor protein transgenic mouse models with Alzheimer disease-like pathology. Proc Natl Acad Sci U S A *94*, 13287–13292.

Takahashi, K., and Yamanaka, S. (2006). Induction of pluripotent stem cells from mouse embryonic and adult fibroblast cultures by defined factors. Cell *126*, 663–676.

Takami, M., Nagashima, Y., Sano, Y., Ishihara, S., Morishima-Kawashima, M., Funamoto, S., and Ihara, Y. (2009). gamma-Secretase: Successive Tripeptide and Tetrapeptide Release from the Transmembrane Domain of beta-Carboxyl Terminal Fragment. Journal of Neuroscience *29*, 13042–13052.

Tanzi, R.E., Gusella, J.F., Watkins, P.C., Bruns, G.A., St George-Hyslop, P., Van Keuren, M.L., Patterson, D., Pagan, S., Kurnit, D.M., and Neve, R.L. (1987). Amyloid beta protein gene: cDNA, mRNA distribution, and genetic linkage near the Alzheimer locus. Science *235*, 880–884.

Thinakaran, G., Harris, C.L., Ratovitski, T., Davenport, F., Slunt, H.H., Price, D.L., Borchelt, D.R., and Sisodia, S.S. (1997). Evidence that levels of presenilins (PS1 and PS2) are coordinately regulated by competition for limiting cellular factors. J Biol

Chem *272*, 28415–28422.

Thinakaran, G., Borchelt, D.R., Lee, M.K., Slunt, H.H., Spitzer, L., Kim, G., Ratovitsky, T., Davenport, F., Nordstedt, C., Seeger, M., et al. (1996). Endoproteolysis of Presenilin 1 and Accumulation of Processed Derivatives In Vivo. Neuron *17*, 181–190.

Tischer, E., and Cordell, B. (1996). Beta-amyloid precursor protein. Location of transmembrane domain and specificity of gamma-secretase cleavage. J Biol Chem *271*, 21914–21919.

Van Broeckhoven, C., Backhovens, H., Cruts, M., De Winter, G., Bruyland, M., Cras, P., and Martin, J.-J. (1992). Mapping of a gene predisposing to early–onset Alzheimer's disease to chromosome 14q24.3. Nat Genet *2*, 335–339.

Van Dam, D., and De Deyn, P.P. (2006). Drug discovery in dementia: the role of rodent models. Nat Rev Drug Discov *5*, 956–970.

Walker, E.S., Martinez, M., Brunkan, A.L., and Goate, A. (2005). Presenilin 2 familial Alzheimer's disease mutations result in partial loss of function and dramatic changes in Aβ 42/40 ratios. J Neurochem *92*, 294–301.

Walsh, D.M., Klyubin, I., Fadeeva, J.V., Cullen, W.K., Anwyl, R., Wolfe, M.S., Rowan, M.J., and Selkoe, D.J. (2002). Naturally secreted oligomers of amyloid l[beta]l protein potently inhibit hippocampal long-term potentiation in vivo. Nature *416*, 535–539.

Weggen, S., and Beher, D. (2012). Molecular consequences of amyloid precursor protein and presenilin mutations causing autosomal-dominant Alzheimer's disease. Alzheimers Res Ther *4*, 9.

Weihofen, A., and Martoglio, B. (2003). Intramembrane-cleaving proteases: controlled liberation of proteins and bioactive peptides. Trends in Cell Biology *13*, 71–78.

Weingarten, M.D., Lockwood, A.H., Hwo, S.-Y., and Kirschner, M.W. (1975). A Protein Factor Essential for Microtubule Assembly. pp. 1858–1862.

Wischik, C.M., Edwards, P.C., Lai, R.Y., Roth, M., and Harrington, C.R. (1996). Selective inhibition of Alzheimer disease-like tau aggregation by phenothiazines. Proc Natl Acad Sci U S A *93*, 11213–11218.

Wischik, C.M., Novak, M., Thøgersen, H.C., Edwards, P.C., Runswick, M.J., Jakes, R., Walker, J.E., Milstein, C., Roth, M., and Klug, A. (1988). Isolation of a fragment

of tau derived from the core of the paired helical filament of Alzheimer disease. Proc Natl Acad Sci U S A *85*, 4506–4510.

Woodruff, G., Young, J.E., Martinez, F.J., Buen, F., Gore, A., Kinaga, J., Li, Z., Yuan, S.H., Zhang, K., and Goldstein, L.S.B. (2013). The Presenilin-1 ΔE9 Mutation Results in Reduced γ-Secretase Activity, but Not Total Loss of PS1 Function, in Isogenic Human Stem Cells. CellReports *5*, 974–985.

Wu, J.W., Herman, M., Liu, L., Simoes, S., Acker, C.M., Figueroa, H., Steinberg, J.I., Margittai, M., Kayed, R., Zurzolo, C., et al. (2013). Small Misfolded Tau Species Are Internalized via Bulk Endocytosis and Anterogradely and Retrogradely Transported in Neurons. J Biol Chem *288*, 1856–1870.

Wyss-Coray, T., Loike, J.D., Brionne, T.C., Lu, E., Anankov, R., Yan, F., Silverstein, S.C., and Husemann, J. (2003). Adult mouse astrocytes degrade amyloid-beta in vitro and in situ. Nature Medicine *9*, 453–457.

Yagi, T., Ito, D., Okada, Y., Akamatsu, W., Nihei, Y., Yoshizaki, T., Yamanaka, S., Okano, H., and Suzuki, N. (2011). Modeling familial Alzheimer's disease with induced pluripotent stem cells. Human Molecular Genetics *20*, 4530–4539.

Yahata, N., Asai, M., Kitaoka, S., Takahashi, K., Asaka, I., Hioki, H., Kaneko, T., Maruyama, K., Saido, T.C., Nakahata, T., et al. (2011). Anti-Aβ drug screening platform using human iPS cell-derived neurons for the treatment of Alzheimer's disease. PLoS ONE *6*, e25788.

Yanamandra, K., Kfoury, N., Jiang, H., Mahan, T.E., Ma, S., Maloney, S.E., Wozniak, D.F., Diamond, M.I., and Holtzman, D.M. (2013). Anti-tau antibodies that block tau aggregate seeding in vitro markedly decrease pathology and improve cognition in vivo. Neuron *80*, 402–414.

Yang, H., Wang, H., Shivalila, C.S., Cheng, A.W., Shi, L., and Jaenisch, R. (2013). One-Step Generation of Mice Carrying Reporter and Conditional Alleles by CRISPR/Cas-Mediated Genome Engineering. Cell 1–10.

Yetman, M.J., Lillehaug, S., Bjaalie, J.G., Leergaard, T.B., and Jankowsky, J.L. (2015). Transgene expression in the Nop-tTA driver line is not inherently restricted to the entorhinal cortex. Brain Structure and Function *221*, 1–19.

Zhang, D., Pekkanen-Mattila, M., Shahsavani, M., Falk, A., Teixeira, A.I., and Herland, A. (2014). A 3D Alzheimer's disease culture model and the induction of P21-activated kinase mediated sensing in iPSC derived neurons. Biomaterials *35*, 1420–1428.

Zhu, F., Gamboa, M., Farruggio, A.P., Hippenmeyer, S., Tasic, B., Schüle, B., Chen-Tsai, Y., and Calos, M.P. (2013). DICE, an efficient system for iterative genomic editing in human pluripotent stem cells. Nucleic Acids Res.